Titre: Title:	Axial Compressor Gas Path Design for Desensitization of Aerodynamic Performance and Stability to Tip Clearance
Auteur: Author:	Mert Cevik
Date:	2013
Type:	Mémoire ou thèse / Dissertation or Thesis
Référence: Citation:	Cevik, M. (2013). Axial Compressor Gas Path Design for Desensitization of Aerodynamic Performance and Stability to Tip Clearance [Thèse de doctorat, École Polytechnique de Montréal]. PolyPublie. https://publications.polymtl.ca/1302/

Document en libre accès dans PolyPublie
Open Access document in PolyPublie

URL de PolyPublie: PolyPublie URL:	https://publications.polymtl.ca/1302/
Directeurs de recherche: Advisors:	Huu Duc Vo
Programme: Program:	Génie mécanique

UNIVERSITÉ DE MONTRÉAL

AXIAL COMPRESSOR GAS PATH DESIGN FOR DESENSITIZATION OF
AERODYNAMIC PERFORMANCE AND STABILITY TO TIP CLEARANCE

MERT CEVIK

DÉPARTEMENT DE GÉNIE MÉCANIQUE

ÉCOLE POLYTECHNIQUE DE MONTRÉAL

THÈSE PRÉSENTÉE EN VUE DE L'OBTENTION

DU DIPLÔME DE PHILOSOPHIAE DOCTOR

(GÉNIE MÉCANIQUE)

DÉCEMBRE 2013

UNIVERSITÉ DE MONTRÉAL

ÉCOLE POLYTECHNIQUE DE MONTRÉAL

Cette thèse intitulée:

AXIAL COMPRESSOR GAS PATH DESIGN FOR DESENSITIZATION OF
AEROSYNAMIC PERFORMANCE AND STABILITY TO TIP CLEARANCE

présentée par : CEVIK Mert

 en vue de l'obtention du diplôme de : Philosophiae Doctor

a été dûment accepté par le jury d'examen constitué de :

M. MUREITHI Njuki W., Ph.D., président

M. VO Huu Duc, Ph.D., membre et directeur de recherche

M. TRÉPANIER Jean-Yves, Ph.D., membre

M. GHALY Wahid, Ph.D., membre

DEDICATION

To my lovely wife and my family...

ACKNOWLEDGEMENTS

RESUME

Le jeu d'aube est l'espace entre le bout du rotor en mouvement et le carter stationnaire d'une turbomachine. Dans un compresseur l'écoulement qui traverse ce jeu, dû à la différence de pression entre l'intrados et l'extrados de l'aube, a un impact majeur et généralement négatif sur la performance (rapport de pression et rendement) et la stabilité aérodynamique (marge contre le décrochage) du compresseur. Une augmentation du jeu d`aube, soit temporaire durant les phases d'opération transitoires, soit permanente due à l'usure, entraîne une perte de la performance et stabilité aérodynamique du compresseur et par conséquent une augmentation de la consommation de carburant et une diminution de l'enveloppe d'opération de la turbine à gaz. Bien que beaucoup de recherche a été fait pour améliorer la performance et stabilité aérodynamique des compresseurs à la valeur de design (minimale ou nominale) du jeu d'aube, très peu a été fait sur la réduction de la sensibilité de ces paramètres à l'augmentation de ce jeu. Le développement de technologies permettant de contrer cet effet mènera à des moteurs d'avion dont la performance et l'enveloppe d'opération seront plus robustes aux demandes opérationnelles et à l'usure.

Ce projet est la seconde phase d'un programme de recherche pour développer des stratégies de conception pour réduire la sensibilité de la performance et stabilité aérodynamique des compresseurs axiaux au jeu d'aube. La première phase avait porté sur des stratégies de conception d'aubes et avait mené à la découverte et l'explication de deux caractéristiques de l'écoulement permettant de réduire cette sensibilité, soit une augmentation de la quantité de mouvement méridionale entrant au bout du rotor et la réduction ou l'élimination du double écoulement de jeu. Le double écoulement de jeu est l'écoulement qui sort d'un jeu d'aube et entre dans le jeu de l'aube adjacente au lieu de convecter en aval hors du passage d'aube. Cet écoulement a un effet très négatif sur la performance et la stabilité aérodynamique du compresseur. Deux stratégies de conception impliquant le fléchissement et l'angle de décalage des aubes avaient été proposées et démontrées par simulations numériques pour exploiter ces deux caractéristiques de l'écoulement afin de réduire la sensibilité.

En tant que deuxième phase du programme de recherche, les objectifs de ce projet sont de développer des stratégies de conception de la veine gazeuse pour les compresseurs axiaux pour arriver à ce même objectif, pour évaluer la possibilité de les combiner avec les stratégies de conception d'aubes de compresseurs axiaux pour une meilleure désensibilisation et la possibilité

de les appliquer à des compresseurs non-axiaux. La recherche des stratégies de conception de la veine gazeuses reposait sur l'exploitation des deux caractéristiques d'écoulement mentionnées précédemment. Deux stratégies de conception ont été proposées. La première est la courbure de la veine gazeuse à une forme concave pour augmenter la quantité de mouvement méridionale entrant au bout du rotor. La seconde est un traitement de carter qui est composé de fentes circonférentielles en dent de scie de très faible profondeur placées sur le carter au-dessus du rotor pour réduire le double écoulement de jeu.

Une évaluation par simulations numériques de l'écoulement des deux stratégies sur le rotor axial en régime haut-subsonique utilisé comme référence dans la première phase a révélé que les fentes en dents de scie réduisaient de façon beaucoup plus significative la sensibilité ainsi que la perte de performance nominale. Une analyse détaillée du champ d'écoulement a montré que ce traitement de carter fonctionne essentiellement en améliorant le transfert de quantité de mouvement de l'écoulement du passage d'aube vers le fluide de haute entropie du double écoulement de jeu près du carter, tournant ce fluide dans le sens du courant principal, l'empêchant ainsi d'entrer dans le jeu de l'aube adjacent. Cette amélioration se fait par l'aspiration du fluide de haute entropie du double écoulement de jeu dans les fentes qui les réinjecte radialement pour se mélanger avec l'écoulement aspiré du passage d'aube du côté de l'intrados qui a pris la place de ce fluide dans le jeu d'aube.

Une étude paramétrique par simulations numériques de l'écoulement a été ensuite réalisée pour minimiser la sensibilité de la performance et stabilité aérodynamique ainsi que la perte de performance nominale. Cette étude à révélé que l'étendue axial et la position du traitement de carter ont le plus d'influence sur la réduction de la sensibilité mais aussi sur la perte de performance nominale, alors que la profondeur et le nombre de fentes ont plus d'impact sur la perte de performance nominale et la forme des fentes ont un impact modéré sur les deux. Un design amélioré du traitement de carter a été produit pour lequel les simulations numériques ont démontré une désensibilisation complète du rapport de pression et de la marge contre le décrochage et une réduction importante de la sensibilité du rendement avec seulement une très petite perte de rapport de pression nominale.

L'application du traitement de carter amélioré à la géométrie d'une aube moins sensible au jeu d`aube de la première phase du programme de recherche a démontré que ce traitement de

carter peut être combiné avec les stratégies de conception d'aubes pour diminuer d'avantage la sensibilité tout en réduisant/éliminant/renversant la perte de performance nominale.

L'efficacité de cette stratégie de traitement de carter par fentes très peu profondes a finalement été évaluée avec des simulations numériques préliminaires pour montrer qu'elle fonctionne aussi pour un étage de compresseur axial, un rotor de compresseur à écoulement mixte et un impulseur de compresseur centrifuge.

ABSTRACT

Tip clearance is the necessary small gap left between the moving rotor tip and stationary shroud of a turbomachine. In a compressor, the pressure driven flow through this gap, called tip clearance flow, has a major and generally detrimental impact on compressor performance (pressure ratio and efficiency) and aerodynamic stability (stall margin). The increase in tip clearance, either temporary during transient engine operations or permanent from wear, leads to a drop in compressor performance and aerodynamic stability which results in a fuel consumption increase and a reduced operating envelope for a gas turbine engine. While much research has looked into increasing compressor performance and stall margin at the design (minimum or nominal) tip clearance, very little attention has been paid for reducing the sensitivity of these parameters to tip clearance size increase. The development of technologies that address this issue will lead to aircraft engines whose performance and operating envelope are more robust to operational demands and wear.

The current research is the second phase of a research programme to develop design strategies to reduce the sensitivity of axial compressor performance and aerodynamic stability to tip clearance. The first phase had focused on blade design strategies and had led to the discovery and explanation of two flow features that reduces tip sensitivity, namely increased incoming meridional momentum in the rotor tip region and reduction/elimination of double leakage. Double leakage is the flow that exits one tip clearance and enters the tip clearance of the adjacent blade instead of convecting downstream out of the rotor passage. This flow was shown to be very detrimental to compressor performance and stall margin. Two rotor design strategies involving sweep and tip stagger reduction were proposed and shown by CFD simulations to exploit these features to reduce sensitivity.

As the second phase, the objectives of the current research project are to develop gas path design strategies for axial compressors to achieve the same goal, to assess their ability to be combined with desensitizing axial compressor blade design strategies and to be applied to non-axial compressors. The search for gas path design strategies was based on the exploitation of the two flow desensitizing features listed above. Two gas path design strategies were proposed and analyzed. The first was gas path contouring in the form of a concave gas path to increase incoming tip meridional momentum. The second was a casing treatment consisting of very

shallow sawtooth shaped circumferential indentations placed on the shroud over the rotor to reduce double leakage.

An assessment through CFD simulations of the two strategies on the high subsonic axial reference compressor rotor of the first phase showed that the sawtooth casing indentation provided much larger sensitivity reduction and much lower performance penalty. A detailed flow field analysis showed that this casing treatment worked essentially by enhancing the streamwise momentum transfer from the core flow to the high-entropy double leakage flow near the shroud to steer it away from the tip clearance of the adjacent blade. This enhancement involves aspiration of the high-entropy double leakage flow into the indentations and injecting it radially inward to mix with the core flow from the blade pressure side that has taken its place in the tip clearance gap.

A computational parametric study was performed to obtain preliminary design rules for minimizing performance and stall margin sensitivity to tip clearance as well as nominal performance loss. It revealed that the axial extent and location of the casing treatment have the highest impact on sensitivity reduction but also on nominal performance penalty, while groove depth and groove number impact mostly nominal performance and groove shape has only a moderate impact on both. An improved casing indentation design was produced for which CFD simulations showed a complete desensitization of pressure ratio and stall margin while reducing efficiency sensitivity significantly with only a very small penalty in nominal pressure ratio.

The application of the optimized casing indentation design to a reduced sensitivity blade geometry from the first phase showed that this casing treatment can be combined with desensitizing blade design strategies to further reduce tip sensitivity and reduce/eliminate/reverse nominal performance penalty.

The effectiveness of this shallow groove casing treatment strategy was then evaluated with preliminary CFD simulations and shown to work for an axial compressor stage, a mixed flow rotor and a centrifugal compressor impeller.

TABLE OF CONTENTS

LIST OF FIGURES

LIST OF TABLES

LIST OF APPENDICES

CHAPTER 1   INTRODUCTION

1.1   Background

Axial compressors are one of the central components and a key factor in fuel efficiency and stability of modern aircraft gas turbine engines. An axial compressor consists of a series of successive rotary and stationary blade rows, namely rotors and stators, as illustrated in Figure 1-1. The lower and upper endwalls are called *hub* and *shroud*, respectively, and form the *gas path* of a compressor. Tip clearance flow, which is the flow through the gap between the rotor tip and the stationary casing wall, is a major factor influencing compressor performance and aerodynamic stability. Although a tip clearance gap can also exist at the hub of cantilevered stators, it is a rarely used design configuration in modern compressors. The increase in tip clearance size is a common occurrence at high power regimes such as take-off, during transient operations of an engine, or as a result of rubbing wear during the service life. Such a change in tip clearance size is very detrimental to fuel consumption and stability as a result of amplification of the tip clearance flow. To appreciate the effects of tip clearance flow, this section briefly reviews the axial compressor performance characteristics.
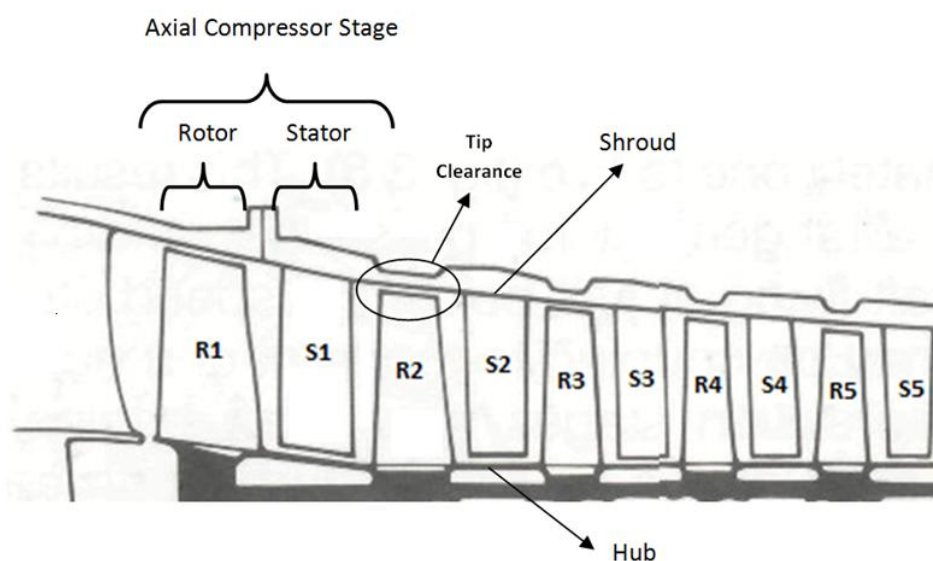
Figure 1-1: Schematic representation of a multi-stage axial compressor
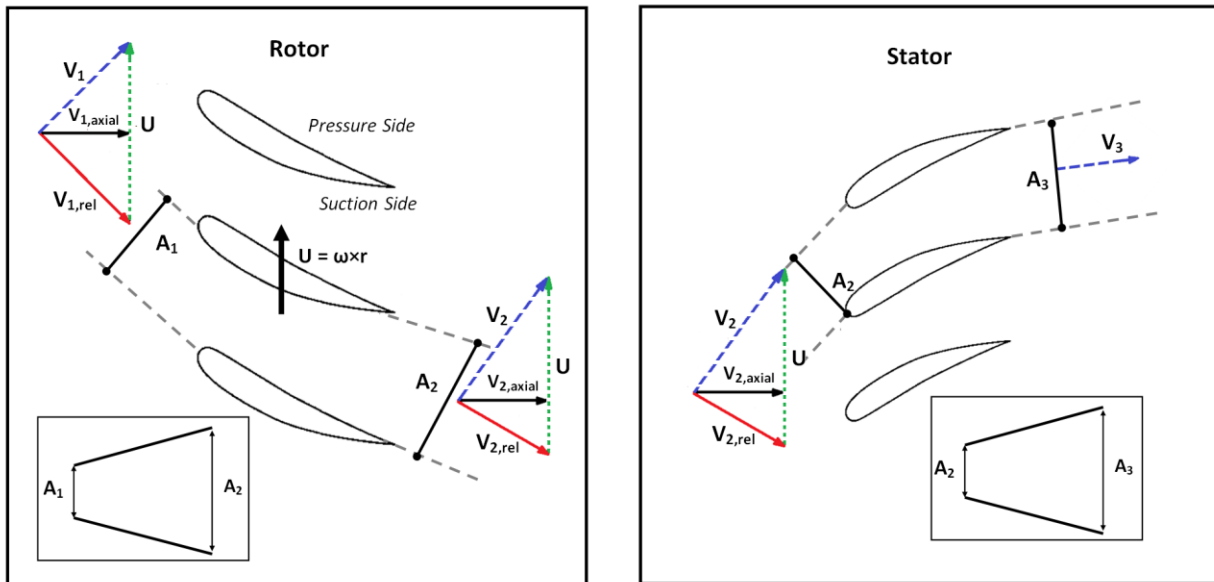
Figure 1-2: Schematic representation of the working principle of an axial compressor stage

The working principle of an axial compressor is illustrated in Figure 1-2 through a constant span cut of a compressor stage with axial inlet and exit flows. The velocity vectors with dashed lines are in the rotating frame of reference of the rotor while those in solid blue line are at the absolute frame of the stator. These two frames are linked by the rotating speed of the compressor (U) and the combination of these three vectors is referred to as a velocity triangle. In the rotating frame of reference, the rotor blade passage acts as a diffuser with an increase in the area normal to the flow thus reducing the relative velocity and increasing the static pressure. At the same time, the flow experiences acceleration in the absolute frame of reference. Its increased kinetic energy is then converted into further static pressure rise by the stator which diffuses the flow by turning it back toward the axial direction.

A consequence of this process is the negative effect of adverse pressure gradient on the growth of blade passage boundary layers. The associated increased displacement thickness near the solid surfaces results in a reduction of effective area increase across the blade passage, thus lowering the pressure rise. Moreover, the viscous losses associated with the boundary layers reduce the pressure rise and hence the adiabatic efficiency, which are the parameters that characterize the

performance of the compressor. These losses are amplified when the compressor operates at off-design conditions, as illustrated by a plot of performance and efficiency versus mass flow at constant speed (U = constant), referred to as a *speedline* and depicted at the top of Figure 1-3. At the design or peak-efficiency mass flow, the angle between the relative incoming flow vector and the rotor leading edge blade angle, known as the *incidence angle (i)*, is at a value giving minimum losses for a particular blade geometry. If the mass flow is reduced, as illustrated in Figure 1-3(a), the normal area the relative incoming flow diminishes and the area ratio across the rotor blade passage increases leading to an increase in pressure ratio. (The same can be deduced for the stator passage). However, the accompanying increase in pressure gradient and thus boundary layer thickness reduces effective area increase and decreases efficiency, which eventually overcomes the physical area increase effect and leads to a peak in pressure rise. A further drop in mass flow would eventually result in a boundary layer separation on the blade suction side and/or aerodynamic instabilities in the form of rotating stall and/or surge. Rotating stall is an aerodynamic instability characterized by the formation of a circumferential cell of axial velocity deficiency that rotates at 50-70% of the rotor speed and is usually accompanied by a sudden drop in pressure rise (Day 1993). This drop often triggers a more severe aerodynamic instability, called *surge.* Surge is an axisymmetric flow oscillation across the entire engine that causes a sudden drop in its power output and physical damage (Greitzer 1976). The instability point is referred to as the stall (or surge) point and its distance (either in terms of mass flow or pressure rise) from the peak efficiency (or design) point is called the *stall margin* or *surge margin*, a parameter that represents the aerodynamic stability of the compressor.

On the other hand, if the mass flow is increased from the design point value, the incoming relative flow normal area increases making the area ratio across the rotor blade passage smaller, thus reducing the pressure rise. In addition, the boundary layer losses increase on the pressure side causing a reduction in pressure rise and efficiency. (The same effect can also be deduced for the stator passage). If the mass flow is further increased, the relative velocity increases and the incoming normal area eventually becomes larger than the passage throat area, resulting in a converging-diverging configuration which chokes when flow velocity reaches Mach 1 at the passage throat as illustrated in Figure 1-3(b), resulting in a rapid increase in loss and thus a prompt drop in pressure rise and efficiency.
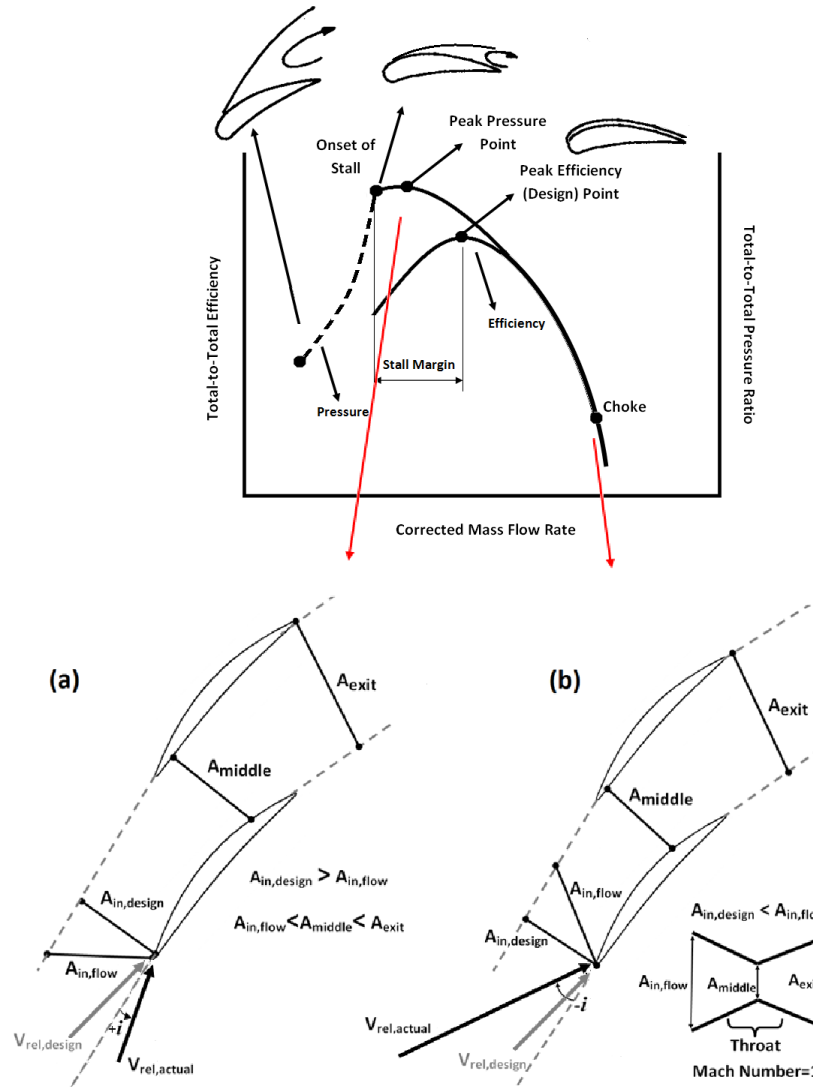
Figure 1-3: Effect of changing mass flow on compressor performance when mass flow is (a) reduced and (b) increased from the design point value

Since the pressure rise for a single axial compressor stage is limited, multiple stages are commonly used to achieve adequate pressure rise. However, the effects of off-design operation are then amplified. A multi-stage compressor is usually designed such that all stages operate at maximum efficiency at its design point, referred to as *stage matching*, mainly through dimensioning the gas path such that the flow at the inlet of each stage correspond to the optimum operation of the stage. However, away from the design point, the change in pressure rise and efficiency of the first stage results in an outlet density change that further alter the inlet flow to

the next stage away from the optimum value making its performance worse than what is should be. This effect, referred to as *stage mismatch*, is propagated through all downstream stages, thus amplifying pressure rise and efficiency drop, which is even more dramatic for off-design conditions involving a change in speed since stage performance is usually more affected by a change in speed than just in mass flow at the same speed.

1.2 The Problem of Tip Clearance

The explanations of performance and stability deterioration, presented at section 1.1, are based on a 2-D perspective. Nevertheless, they serve as a basis to understand the 3-D effects associated with the endwall regions in a real compressor. Figure 1-4 illustrates three dimensional flow structures in an axial compressor rotor passage that are responsible for significant losses in efficiency and pressure rise. One prominent structure is the tip clearance flow which dominates the shroud region of the passage.
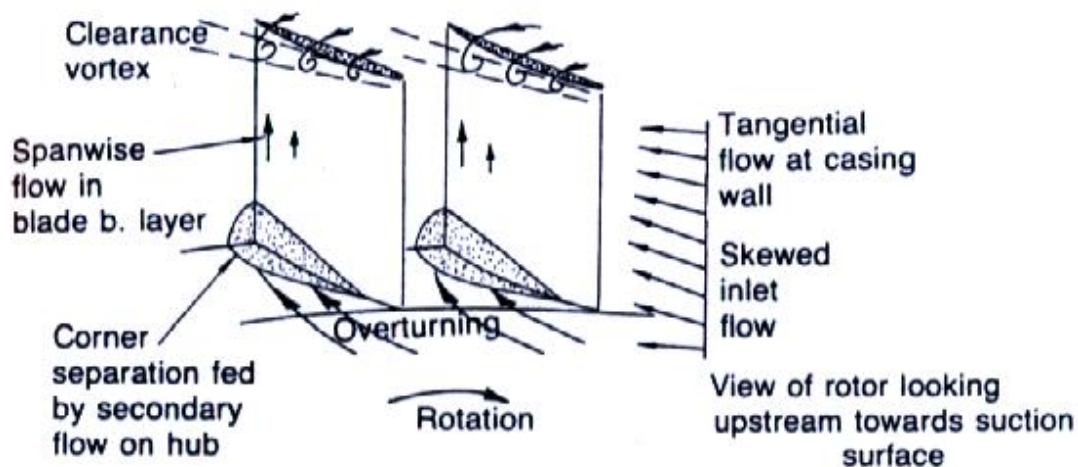
Figure 1-4: Schematic representation of flow phenomena in endwall regions (Cumpsty 1989)

As mentioned previously, tip clearance or tip leakage flow is the fluid migration through the small gap between the tip of the moving rotor and the static shroud. It is driven by the pressure difference between the pressure and suction sides of the blade as illustrated in Figure 1-5. The *leakage jet* exits the gap with a large angle from the blade suction side and thus from the main passage flow. The interaction of the leakage jet with main passage flow generates a tip vortex near the suction side which is a source of performance deterioration through two mechanisms.

The first mechanism is loss of relative stagnation pressure from shear/mixing between the two streams which increases with the difference in flow angle and amplitude between them. This mechanism is directly related to loss in the pressure rise and efficiency. The second mechanism is linked to the low streamwise momentum region at the rotor tip region resulting from this mixing, referred to as tip blockage, which reduces the effective area ratio of the passage, thus directly affecting static pressure rise. Furthermore, the low streamwise velocity in this region causes high incidence on the downstream stator tip region which not only further reduces stage performance but can result in boundary layer and/or corner separation in the rotor passage and induces a premature stator stall.
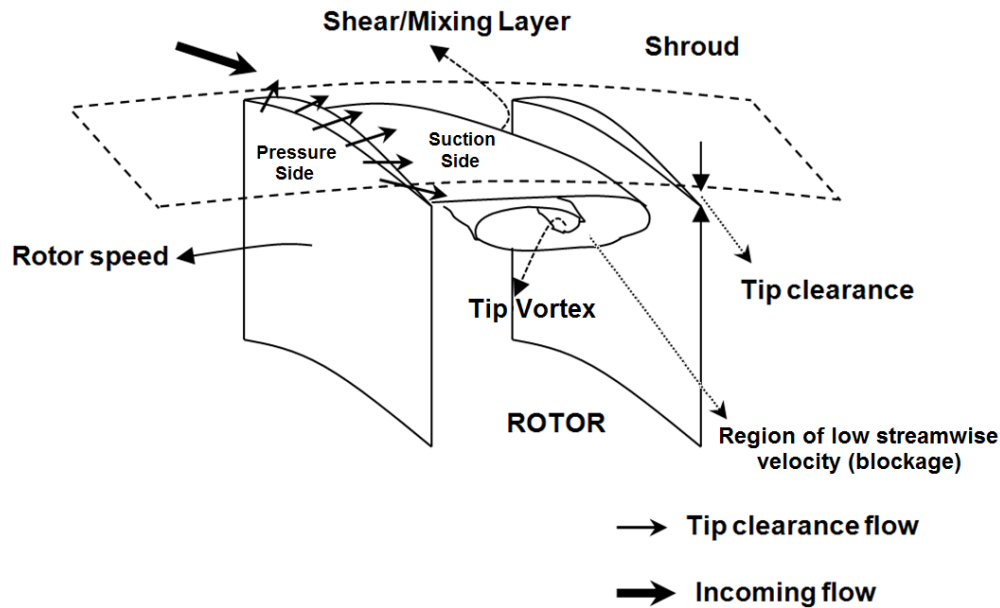
Figure 1-5: Schematic representation of the tip clearance flow (Vo 2001)

In terms of aerodynamic instability, a recent research such as that by Vo et al. (2008) indicates that tip clearance flow has a direct impact on the stall/surge margin through two mechanisms, as will be explained in more details in chapter 2. The first one is associated with the pressure rise reaching the peak value for which tip clearance flow plays a role through its associated loss mechanisms described previously. The second mechanism is linked to the interface formed

between the incoming and tip clearance flows reaching the rotor leading edge plane, which occurs at a higher mass flow if the strength of the tip clearance flow increases.

The amount of tip clearance flow and associated detrimental effect on performance and aerodynamic stability increases with the tip clearance size. The tip clearance loss accounts for approximately 20-40% of total losses in turbomachinery (Lakshminarayana 1996). For axial compressors, this rate is expected to become higher. Hence, the increase in tip clearance size may become the most dominant factor of performance loss in an axial compressor. Moreover, an increase in tip clearance flow reduces the surge margin and therefore reduces the operating range of the compressor and thus the engine envelope. Figure 1-6 shows the substantial effect of increased tip clearance (in percentage of blade chord) on non-dimensional pressure rise, torque efficiency (alternative of total-to-total efficiency measured from torque of compressor shaft) and surge margin for a compressor stage. In this case the doubling of the tip clearance size results in a reduction in peak efficiency by 1.5 percentage points, in peak pressure rise by 9.7% and, in stall margin by 11%.
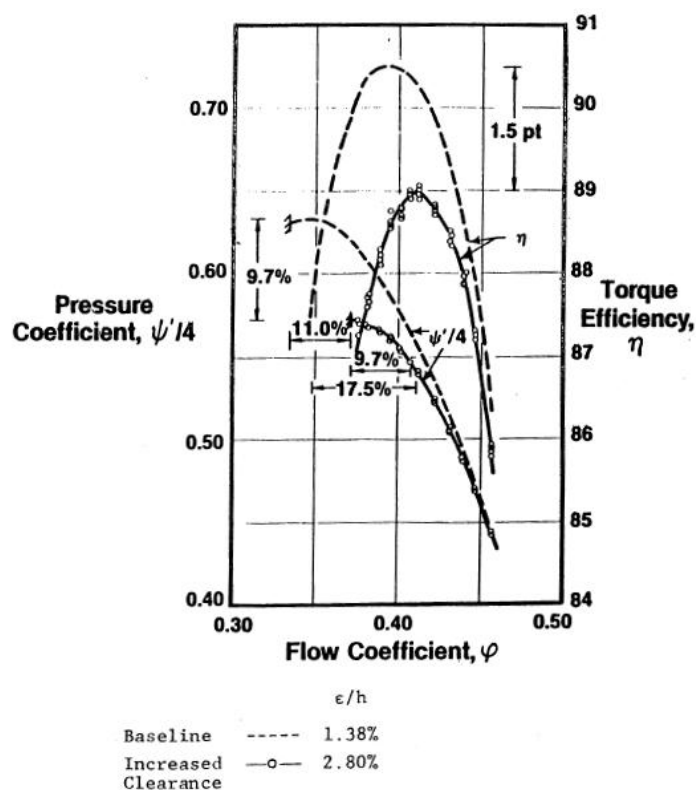
Figure 1-6: Effect of tip clearance size on pressure rise and efficiency (Wisler 1985)

These effects are amplified at higher rotational speed as schematically shown on a compressor map in Figure 1-7 which is made up of multiple speedlines. One can observe in this figure that, at higher speeds the performance drop (shift in speedline) and stall margin drop (shift in surge line) from an increase in tip clearance size are much larger than at the lower rotational speeds.
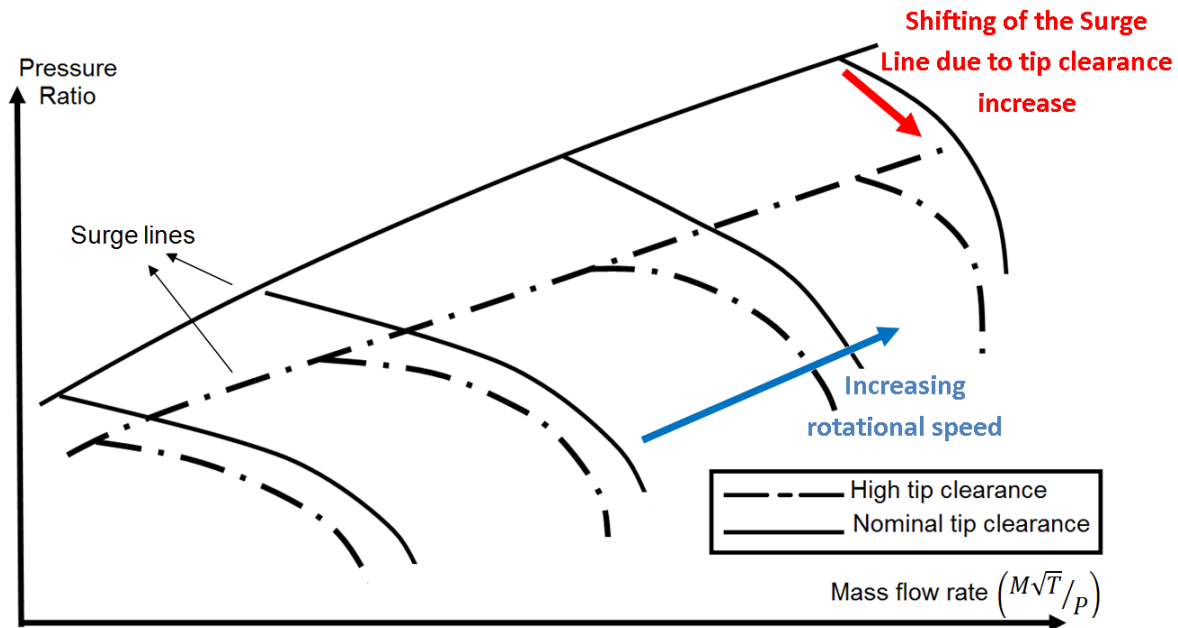
Figure 1-7: Schematic of the effect of tip clearance size on a compressor map

In a multi-stage environment, the detrimental effect of tip clearance variation is magnified. A change in stage pressure rise and efficiency accompanying a change in tip clearance size, causes mismatching between stages similar to the effect of off-design operation described in section 1.1.

Tip clearance increase could occur on a temporary basis due to differential thermal expansion between rotor and shroud during transient engine operation such as rapid engine acceleration/deceleration and maximum power operation, resulting in possible surge during critical aircraft maneuvers and take-off. On the other hand, operational wear tend to increase nominal tip clearances throughout the engine lifecycle that leads to a permanent performance degradation and increased fuel consumption. Cumpsty (1989) states that for tip clearances greater than 1% of chord in size, increasing tip clearance induces mismatching and performance deterioration inevitably. Since the current gas turbine engine technology is moving towards more

compact engine cores with smaller compressor blades, it becomes mechanically impractical to manufacture rotor blades with tip clearance below this criterion. The above arguments substantiate the need to make the compressor performance and aerodynamic stability *less sensitive to the change in tip clearance size* for the next generation of aircraft engine.

1.3 Desensitizing Design Features

Erler (2012) carried out the first phase of this research programme with the objective of identifying blade design strategies to desensitize performance and stall margin to tip clearance for axial compressors. The results of her study showed that two flow features reduce the sensitivity of performance and stability to tip clearance size for an axial compressor rotor, namely an increase in incoming meridional momentum in the tip region and a reduction/elimination of double leakage flow.

Double leakage flow is tip clearance fluid that enters the tip clearance of the adjacent blade instead of convecting downstream out of the local blade passage. The double leakage was shown to have a detrimental effect on the performance and aerodynamic stability and its intensity increases with tip clearance, thus explaining the drop in pressure rise, efficiency and stall margin with tip clearance increase. Its elimination was predicted and shown to have a desensitizing effect on rotor performance and stability. On the other hand, the increasing incoming meridional momentum in the tip region reduces sensitivity to tip clearance through its reduction of double leakage as well as through improved mixing with tip clearance flow. These results imply that any blade design strategy that exploits these two desensitizing features would reduce the performance and stability sensitivity to tip clearance size. Erler (2012) showed that a forward chordwise swept blade design has a desensitization effect through an increase in incoming meridional momentum at the blade tip, while reducing blade stagger in the tip region achieves desensitization through reduced double leakage.

1.4 Research Questions

To build upon and complement the research carried out by Erler (2012) which focused on to desensitization through blade design strategies for axial compressor rotors, this study investigated the following research questions:

1- Can gas path design strategies be elaborated to desensitize axial compressor rotor performance and aerodynamic stability to tip clearance increase?

2- Can such strategies be combined with axial rotor blade desensitizing strategies to further reduce performance and stability sensitivity to tip clearance size?

3- Can such gas path desensitization design strategies work in a stage (rotor-stator) environment and for non-axial compressors?

1.5 Motivation and Objectives

The objectives of this research are:

1. Develop gas path design features to render the performance and aerodynamic stability of axial compressor rotors less sensitive to change in tip clearance size.

2. Evaluate the effect of gas path desensitization design features when combined with blade desensitization design strategies for an axial compressor rotor.

3. Preliminarily assessment of the gas path desensitization features in an axial compressor stage as well as for centrifugal and mixed flow compressors.

1.6 Outline of the Thesis

This thesis consists of five chapters. This introductory chapter is followed by Chapter 2 which presents a literature review of the physics of tip clearance flow and design features to reduce the tip clearance losses as well as a review of the little existing work on performance and stability desensitization to tip clearance size. Chapter 3 outlines the methodology of the current study, followed by the results in Chapter 4. Chapter 5 gives the conclusions and future work.

CHAPTER 2   LITERATURE REVIEW

While there are very few studies in the open literature about the desensitization of compressor performance to tip clearance size, there has been a significant research since the 1980s on tip clearance flow and its effects on loss and aerodynamic stability, and on alternative compressor designs to reduce these effects. This chapter will begin by highlighting the main results from the research on tip clearance flow physics which can provide clues for this research. This review is followed by a summary of past research on tip clearance flow management for nominal performance/stability improvement and performance/stability desensitization to tip clearance size.

2.1 Tip Clearance Flow Physics

The detrimental effects of tip clearance on compressor performance had been known since the 1970s, as demonstrated in the study by Smith (1970), which showed the sensitivity of peak pressure rise to tip clearance. However the nature of tip clearance flow has only been investigated closely during the mid-1980s with advancements in computational and experimental capabilities.

The studies by Inoue et al. (1986) and Inoue and Koroumaru (1989) involved hot-wire measurements on a low-speed axial-flow rotor. The former study covers the measurements at the rotor inlet and exit and the latter study performed measurements in the tip clearance region. Inoue et al. (1986) showed the existence of the tip vortex and resulting tip blockage at the rotor exit plane as well as the decrease in efficiency with increased tip clearance. Inoue and Koroumaru (1989) showed the distribution of the leakage jet along the chord and its interaction with the main flow as well as the resulting development of the tip vortex and its evolution through the blade passage.

Storer and Cumpsty (1991) carried out a detailed investigation of the flow through the tip gap using cascade tests and 3-D Reynolds-Averaged Navier Stokes (RANS) CFD simulations. They decomposed the tip clearance flow into components that are normal and parallel to the local blade camber. As illustrated in Figure 2-1, their results indicated that the normal component (V_L) is

essentially a pressure driven inviscid flow while the tangential component (V_S) comes from the blade passage flow closest to the blade tip gap at the local chord position. Thus, the magnitude and the direction of the tip clearance flow can be predicted from the chordwise distribution of pressure difference across the gap and from the incoming axial velocity and chordwise blade camber angle distribution. The study also showed that the tip leakage flow and tip vortex strength obviously increases with the increase in tip clearance size.
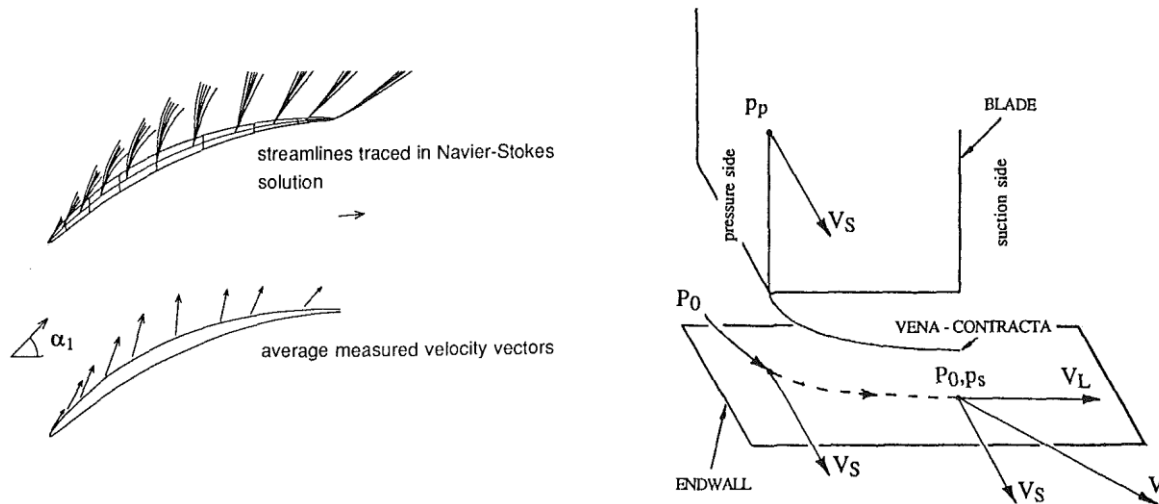
Figure 2-1: Source of tip clearance flow vector magnitude & direction (Storer and Cumpsty 1991)

Storer and Cumpsty (1994) carried out further research to investigate the losses associated with tip clearance flow. They showed that tip leakage losses occur through two mechanisms. The first mechanism is associated with the shear/mixing layer between the main flow and the tip clearance flow, which have different velocity magnitudes and directions. As illustrated at the left side of Figure 2-2, the tip shear layer loss is generated by the mixing of the tip clearance flow with the incoming flow and the driving factor behind the loss generation is that these two flows have different velocity magnitudes and directions. The contour plot of viscous dissipation presented in the right plot of this figure shows the shear/mixing layer. Most of the loss in total pressure associated with tip clearance is a result of this shear/mixing layer while the loss inside the gap is comparatively very small. The second loss mechanism is the tip blockage from the

momentum deficit generated by the shear/mixing loss, which causes a reduction in effective area increase and thus in static pressure rise.
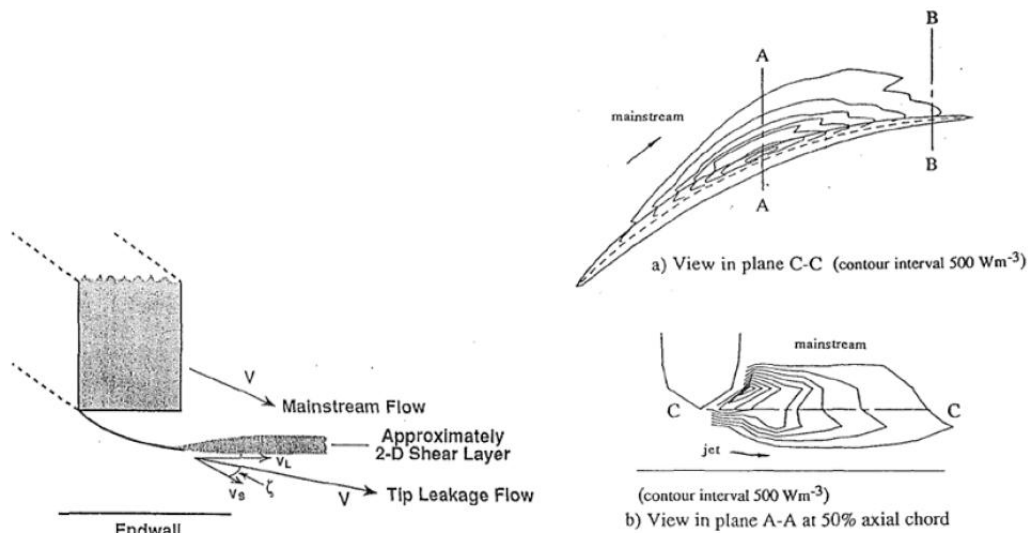
Figure 2-2: Shear/mixing layer representation (Storer and Cumpsty 1994)

Khalid et al. (1999) proposed a method to quantify the compressor endwall blockage in the three-dimensional flow field at the exit of a blade passage, which is similar to calculating a displacement thickness in a 1-D boundary layer with the mainstream velocity taken at the nearest passage core flow point to the local point in the tip blockage region. As illustrated in Figure 2-3, they also proposed a model to explain the blockage formation and growth in a compressor blade passage. This model consists of a 1-D wake generated by mixing between incoming and tip clearance flow that then grows as it convects up a positive pressure gradient to the passage exit plane. Figure 2-3(a) shows a basic illustration of the model. The leakage fluid exits the tip gap at a certain angle and total pressure (state 1) and moves through a straight line (state 2) until it meets the free stream (state 3) where it mixes with the incoming flow. The size and direction of the blockage or velocity deficit could be determined by a control volume analysis of the mixing between the two streams with mass and momentum balance. The growth of blockage from the mixing point to the exit plane (state 4) is modelled as a wake moving up a pressure gradient, as illustrated in Figure 2-3(b). The growth of the blockage could be computed by a 2D integral wake analysis. The results of blockage calculations from this model were shown to be consistent with the trends determined from numerical simulation and experimental results.
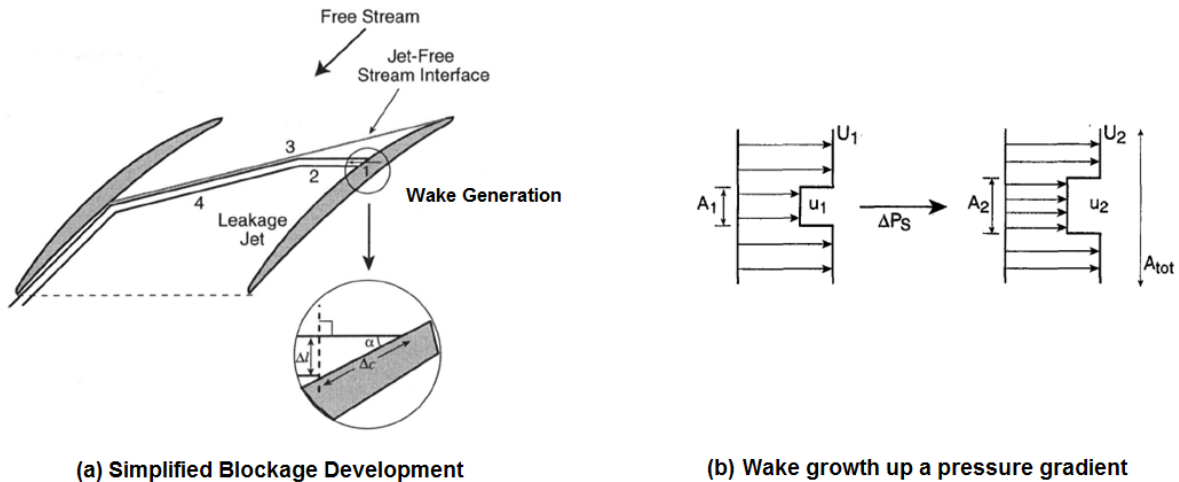
Figure 2-3: The model of blockage development (Khalid, et al. 1999)

Suder (1998) carried out an experimental study to investigate the tip blockage development in a transonic axial compressor at various rotational speeds. The study shows that the pressure and temperature rise near the end-wall region is directly related to tip clearance flow. Its results identify the blockage as the primary source for the performance and operating range drop. It was determined from the data shown in Figure 2-4 that the blockage in the shroud region is two to three times greater than the boundary layer blockage in the rest of the passage. Finally, the author analyzed the losses associated with the shock/tip leakage vortex and shock/boundary layer interactions and concluded that the strength and location of the shock has no direct relation with the tip blockage.
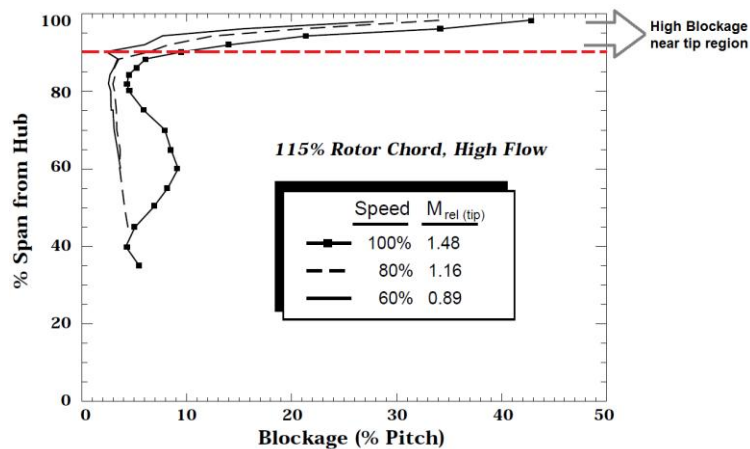
Figure 2-4: Radial distribution of blockage for the design speed and part speeds (Suder 1998)

As mentioned earlier, tip clearance flow has also a significant impact on the aerodynamic instabilities of a compressor, particulary on rotating stall. Most of the modern compressors are tip critical which means that rotating stall originates in the rotor tip region, mainly due to tip clearance flow, rather than from blade/hub boundary layer separation.

There are two known rotating stall inception mechanisms, namely long-length scale (modal) stall inception and short-length scale (spike) stall inception. Modal stall inception is characterized by the evolution of small amplitude disturbances into a fully developed rotating stall cell. Modal stall inception occurs when the total-to-static pressure rise reaches or goes slightly beyond the peak (zero-slope) value (Camp and Day 1998). Moore and Greitzer (1986) had shown analytically that a positive slope of the total-to-static pressure rise curve corresponds to negative damping of naturally occurring circumferential perturbations which then grow into a fully-developed rotating stall cell. In this context, there is a link between tip clearance flow and modal stall inception as the tip clearance flow associated loss and blockage could cause the speedline to reach the zero-slope peak earlier than with blade and endwall boundary layers alone, as indicated by Vo et al. (2008).

Spike stall inception is the other known and most common route to rotating stall in modern compressors. It is characterized by the formation of a high amplitude perturbation localized in the rotor tip region that covers only two to three blade pitches (Day 1993). It grows into a fully-developed rotating stall cell much more rapidly than modal stall disturbances. Spike stall inception is encountered at operating conditions where the total-to-static pressure rise characteristic has a negative slope (Moore and Greitzer 1986), i.e. prior to reaching the condition for modal stall inception. Camp and Day (1998) showed by an experimental study that, spike stall inception occurs at a critical rotor tip incidence but a reduction of rotor tip incidence or increase in tip clearance could cause a change from spike to modal stall inception. Nonetheless a definitive physical explanation about its mechanism has not yet been found.

Vo et al. (2008) proposed a mechanism and two associated predictive criteria for spike stall inception. The first criterion involves the spillage of tip clearance fluid below the leading edge of the adjacent blade's tip as depicted in Figure 2-5(a). As shown in Figure 2-5(b), there is an interface marked by high entropy gradient between the low-entropy incoming flow and high-entropy tip clearance flow whose position is determined by the momentum balance between these

two streams. Originally in the blade passage, this interface moves upstream as the mass flow is reduced due to the strengthening of the tip clearance flow combined with the weakening of the incoming flow. Its position at the leading edge plane signals the onset of leading edge spillage. The second criterion is the axially reversed tip clearance flow at the trailing edge, which impinges to the pressure surface of the adjacent blade. This criterion was referred to as "tip clearance backflow" and is illustrated in Figure 2-6(a). It can be detected by the radial distribution of mass flow reaching zero at the trailing edge blade tip as shown by point 4 in Figure 2-6(b). The mechanism proposed by Vo et al. (2008) is based on the fact that the impinging tip clearance fluid tends to go upstream from the postive pressure gradient but is forced to convect downstream by the incoming flow or to leak through the adjacent blade's tip clearance. The advent of the leading edge spillage criterion provides a low resistance path for the continued upstream movement of the impinging tip clearance fluid leading to an unstoppable tip blockage increase associated with the formation and growth of a spike perturbation. In this context, the authors state that both of the criteria should be satisfied for the occurence of spike stall inception.

An experimental study by Deppe et al. (2005) on three low-speed single-stage axial compressors and a numerical study by Hah et al. (2006) on a transonic axial compressor stage seem to confirm these two criteria. Deppe et al. (2005) also showed that tip injection directed in the tip region aimed to push the interface back into the blade passage does delay rotating stall. Nevertheless, aside from these two studies, the backflow criterion remains controversial while the leading edge criterion seems to be a common feature associated with spike stall inception.
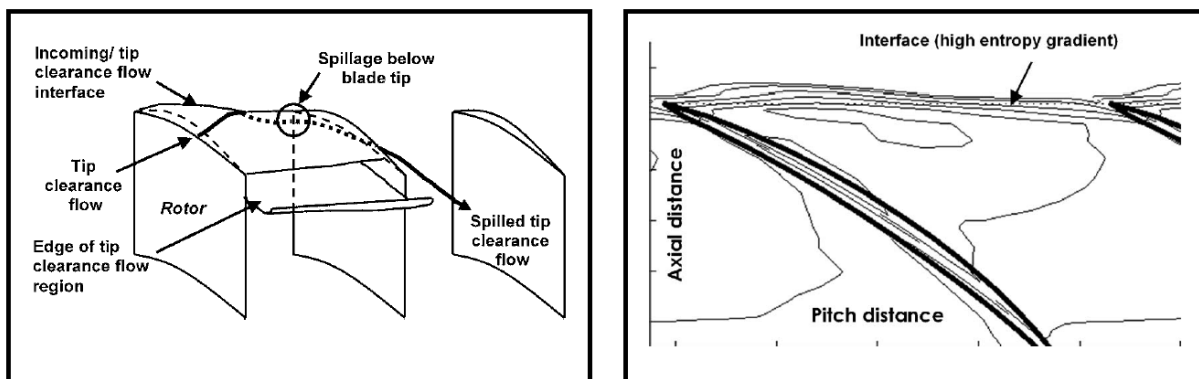
(a) Leading Edge Spillage   **(b)** Entropy contours in the passage

Figure 2-5: Leading edge spillage spike stall inception criterion (Vo, et al. 2008)
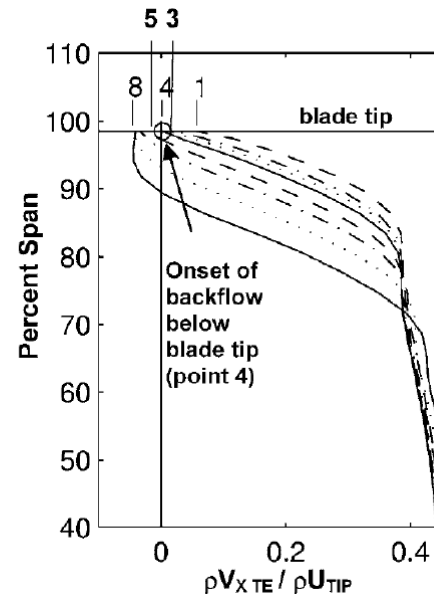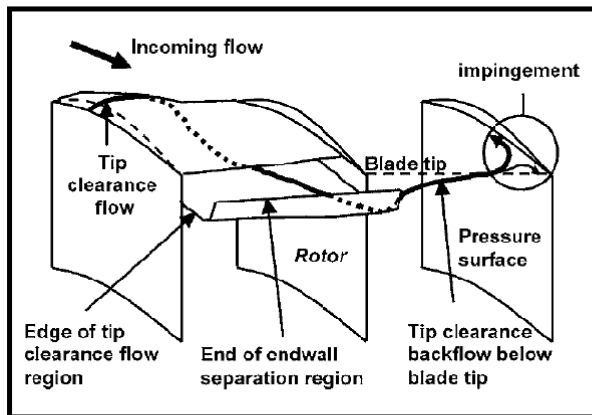
(a) Tip Clearance Backflow   **(b)** Spanwise distribution of mass flow at the trailing edge plane

Figure 2-6: Tip clearance backflow spike stall inception criterion (Vo, et al. 2008)

2.2 Tip Region Flow Management Strategies

The studies available in the open literature related with the tip clearance flow mostly focus on nominal performance and/or stability improvement by reducing the tip leakage effects with very few works covering desensitization to tip clearance change. A review of these studies will be presented in this section by classifying the related design modifications under two groups, namely blade design strategies and gas path design strategies. In the first group, the studies are further subdivided into nominal performance/stability improvement versus tip desensitization. Nevertheless, the same classification could not be made on the second group due to lack of studies focusing on desensitization.

2.2.1   Blade Design Strategies for Tip Flow Management

The descriptions of blade design strategies could be classified under two main approaches, namely modification to the blade sections (camber line, thickness distribution) and modification to the stacking line. The stacking line is a reference line passing through the aerodynamic centers of the blade profiles where the pitching moment coefficient does not vary with angle of attack, as

illustrated at Figure 2-7(a). Blade sweep (Figure 2-7(b)) involves bending the stacking line axially while blade lean (Figure 2-7(c)) means that it is bent circumferentially. As a variation/combination of these bending directions, chordwise sweep and dihedral refer to bending of the stacking line in the direction parallel and perpendicular to the chord, respectively. The dihedral in direction of rotation is known as positive dihedral and the chordwise sweep is referred to as forward when pointing in the upstream direction, as illustrated in Figure 2-8.

Nominal Performance and Stability Improvement

The numerical and experimental study of Gallimore et al. (2002) on low and high-speed axial compressors, and the numerical study of Shao et al. (2007) on axial transonic compressors by modifying the chordwise loading distribution through camber line change, both emphasized the favourable effects of aft-loaded blades on performance. The latter study concluded that an aft-loaded blade creates less tip losses compared to its mid-loaded and front-loaded counterparts. Both studies attributed the observed improvements to the reduction in tip leakage losses.
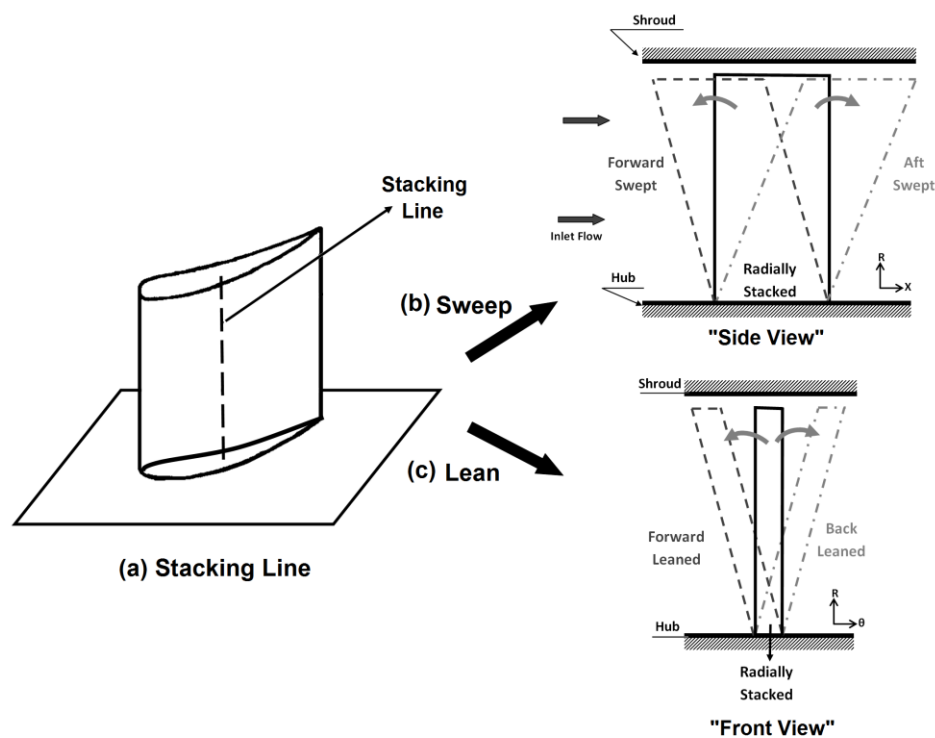
Figure 2-7: Schematic View of (a) Stacking Line, (b) Sweep, and (c) Lean
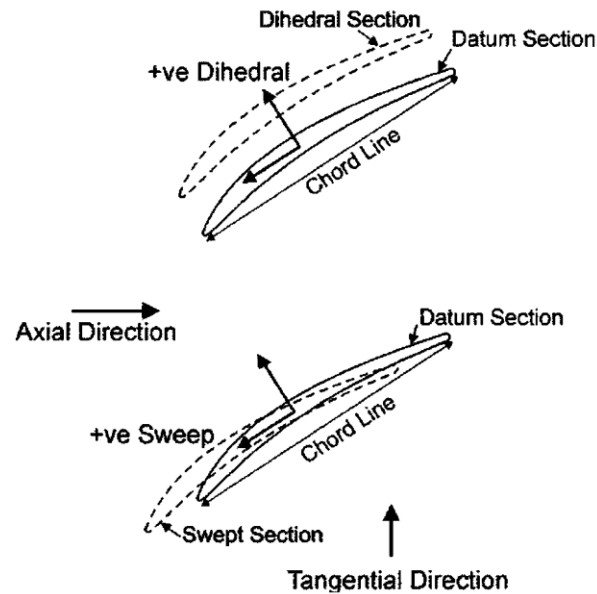
Figure 2-8: Schematic representations of Dihedral and Chordwise Sweep (Gallimore, et al. 2002)

The studies involving stacking line modification mostly point out either forward swept or forward leaned blade design as promising designs to improve nominal performance. Denton and Xu (1998) proposed an explanation on the effects of forward-lean through an analytical study. They hypothesized that forward lean would not have a spanwise distribution in meridional velocity like in a radially stacked blade. The passage of a forward-leaned blade would conserve parallel constant slope isobars that would create a positive pressure gradient normal to the shroud and negative pressure gradient normal to the hub, as illustrated in Figure 2-9(a). The authors concluded that, a spanwise force (F_r) is induced by the blade to balance two pressure gradients, as shown in Figure 2-9(b). This spanwise force creates a radial flow curvature in meridional flow (Δr) that redistributes the spanwise pressure and decreases pressure at tip region. Denton and Xu (1998) also proposed a physical explanation for the effect of sweep. They stated that at each endwall the pressure gradients normal to walls are supposed to be low as no flow could penetrate the wall. Hence for a case with aft-sweep, the blade loading should be low at the blade tip near the trailing edge since there is no blade section under that location, as illustrated in Figure 2-10(a). At the leading edge side of the blade tip, the loading should be higher as there are loaded blade sections at lower spans. Thus, an aft-swept rotor blade should be front-loaded in the tip region, while conversely a forward swept blade should have an aft-loaded tip. Passrucker et al.

(2003) later investigated blade sweep on a transonic axial rotor analytically, computationally and experimentally. The authors confirmed the explanation of Denton and Xu (1998), and pointed out the effect of sweep on repositioning the shock and reducing the accumulation of radially migrating blade boundary layer fluid, as illustrated in Figure 2-10(b) and (c). They also reported that forward swept blade increases both efficiency and stall margin.
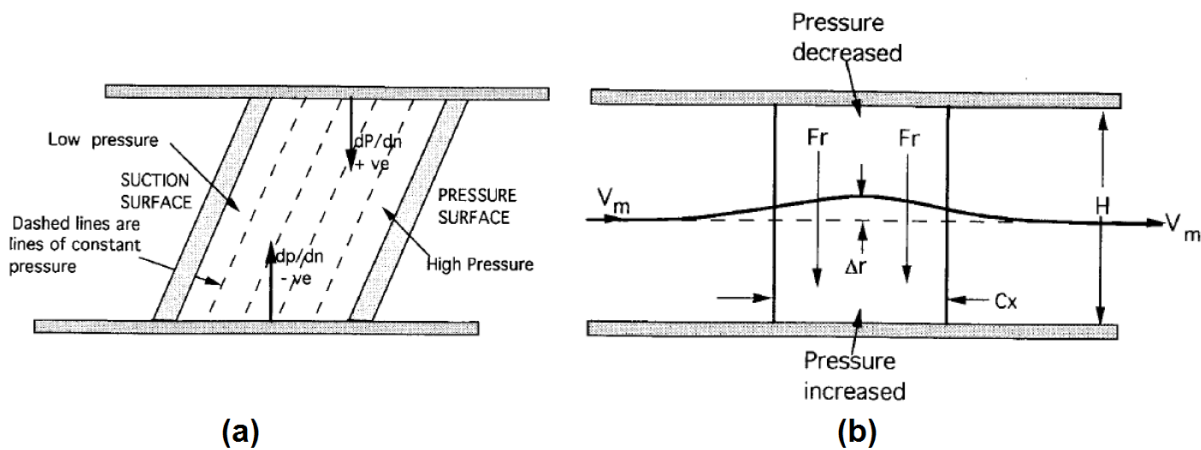
Figure 2-9: Illustration of effect of forward-lean on passage pressure distribution (a) Front view (b) Side view (Denton and Xu 1998)
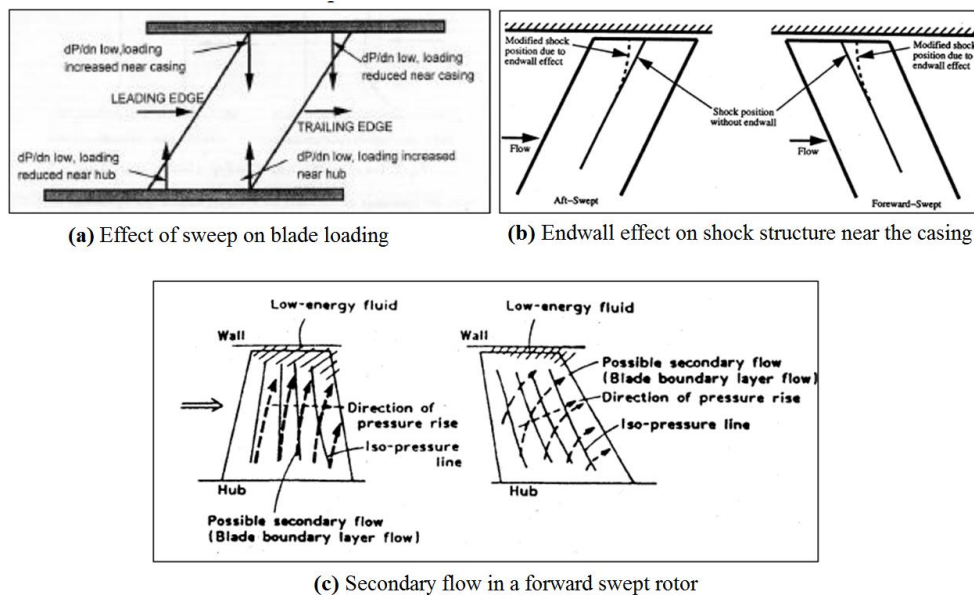
Figure 2-10: Illustration of effect of sweep on design characteristics (Passrucker, et al. 2003)

McNulty et al. (2004) and Goller et al. (2005) presented studies on low-speed axial compressor rotor, numerically and experimentally. They both reached a similar conclusion on the effect of blade sweep with Passrucker et al. (2003), as their results show performance and stall margin improvement achieved by forward sweep design. The numerical and experimental study of Benini and Biollo (2007) on transonic compressors showed the improving effect of both sweep and lean on performance and mass flow range (choking mass flow). Nonetheless, the backward sweep is noted to give slightly better performance than forward sweep which is attributed to modification of passage shock structure near tip. On the other hand, the forward lean was determined to increase the efficiency substantially by again reshaping the shock structure and reducing the shock intensity in the passage. The optimization study presented by Lee et al. (2008) based on thickness and lean modification, came up with a forward leaned blade design which achieves an improvement of 1.5 percentage points in efficiency. Nonetheless, the authors noted that the modification of blade lean had a dominant effect on the improvement of efficiency when compared to the effect of changes in blade profile.

The numerical study presented by Gallimore et al. (2002) about the effects of chordwise sweep and dihedral on a low-speed compressor stage, showed improving effects of both modifications. While chordwise swept designs were shown to improve efficiency and stall margin based on reducing shock losses, positive dihedral was shown to decrease tip loading and reduce tip leakage losses.

Desensitization to Tip Clearance Change

McNulty et al. (2004) presented a numerical and analytical study on the impact of forward swept rotors on low-speed multistage axial compressors with high and moderate tip clearances. Two rotor models were tested, with different tip loading levels achieved through modification of tip stagger and solidity. The tip loading difference causes the first rotor to have a stronger tip flow and the other a moderate tip flow, relative to each other. The forward swept rotor was shown to decrease the sensitivity of nominal performance and stall margin to tip clearance size compared to a radially stacked rotor regardless of the tip flow strength, as presented in Figure 2-11. The authors showed that forward sweep increases the streamwise momentum in the tip region and reduces the tip blockage at the rotor passage exit plane which are beneficial for performance and aerodynamic stability. Furthermore, the study pointed out double leakage

phenomena as a major factor that increases tip leakage loss. It was proposed that forward sweep creates a tip vortex with less radial extent and higher axial velocity at the downstream part of the tip vortex leading edge by reducing the local static pressure in the tip region, which is claimed to reduce tip losses associated with double leakage. The authors also remarked upon the detrimental effect of tip blockage on stage performance making the stator operate at higher tip incidence.
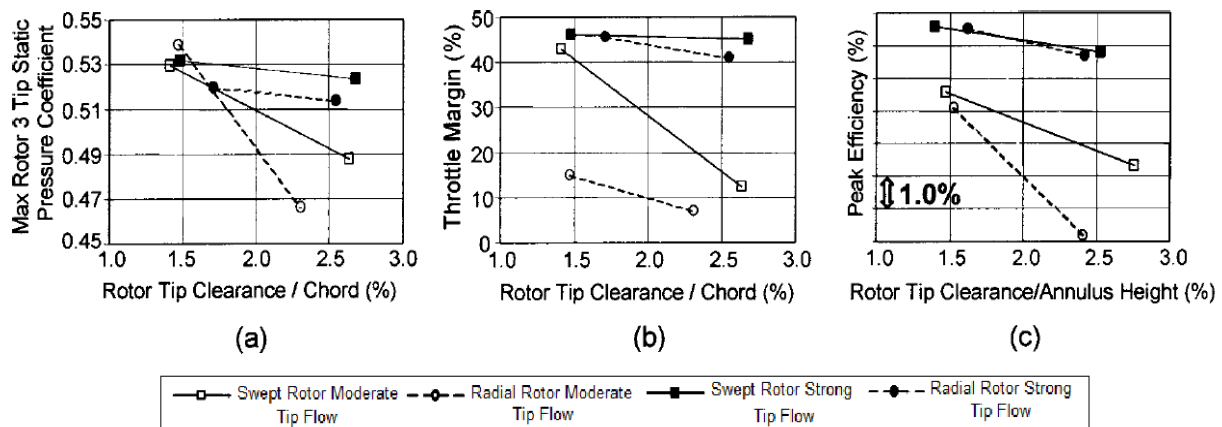
Figure 2-11: Measured rotor tip clearance sensitivities (a) maximum tip static pressure coefficient, (b) throttle margin, and (c) peak efficiency (McNulty, et al. 2004)

Wadia et al. (2004) investigated the effect of forward sweep on tip clearance flow for a transonic axial compressor rotor. Their study was based on numerical simulations for both radially stacked and forward swept rotors at three different tip clearance sizes. The authors reported that although the forward swept rotor has higher nominal peak efficiency, they showed that its peak efficiency is more sensitive to tip clearance size, as shown in Figure 2-12. On the other hand, they observed that the forward swept design`s nominal stall margin is improved by 5.5% and is less sensitive to tip clearance size at the intermediate tip clearance gap range. The authors concluded that forward swept blade design is in general advantageous due to higher nominal performance and lower stall margin sensitivity to tip clearance.
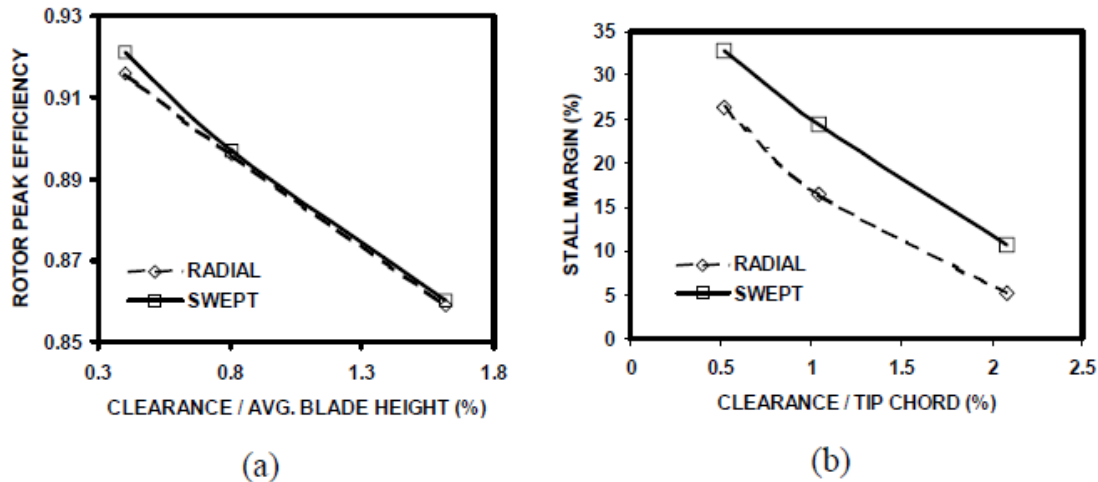
Figure 2-12: Rotor Tip Clearance Sensitivity of efficiency (a) and stall margin (b) (Wadia, et al. 2004)

Ramakrishna and Govardhan (2010) numerically investigated the effects of axial and chordwise sweep on tip clearance flow for a low-speed axial compressor at different tip clearance sizes. Their results showed that both axial and chordwise forward swept designs have lower sensitivity compared to an unswept blade. Lower blade tip incidence was observed for both forward swept designs relative to radially stacked rotor, but the axial sweep is shown to have a lower tip incidence, particularly at low mass flow rates which was concluded to be a more beneficial tendency for the aerodynamic stability in terms of reducing the severity of flow separations at the blade suction surface. The reduction in tip incidence is inferred to have a limiting effect on tip loss and blockage which is attributed as the source of desensitization in forward sweep.

Erler (2012) carried out an extended numerical study on the desensitization of axial compressor performance and stability via blade design strategies. The study was based on a high-subsonic, tip critical, double-circular arc, radially stacked, axial compressor rotor which was designed for the study and referred to as the BASE rotor. The author first carried out a computational parametric study on the effects of various modifications, including axial and chordwise sweep, lean, dihedral, and on camber line. The first major finding of the research was that shifting the chordwise distribution of blade tip loading is not a desensitizing feature. The results of the study confirmed that only forward chordwise swept and axial swept blade designs

are promising in reducing the sensitivity of performance and stability to the tip clearance size. However, the most important outcome of Erler`s research was the identification and explanation of two desensitizing flow features, namely the elimination/reduction of double leakage and the increase in incoming meridional momentum in tip region.

Double leakage is the flow that exits one tip clearance and proceeds to enter the tip clearance of the adjacent blade instead of convecting downtream out of the blade passage. The reason for its negative effect is illustrated in Figure 2-13, which shows the difference in streamwise and normal momentum components of flow exiting the tip clearance between the absence and presence of double leakage. When double leakage is absent, all the fluid entering the tip clearance comes from the low-entropy core flow on the blade pressure side and accelerated by the pressure difference across the blade from zero normal velocity to a final value V_L while maintaining the initial streamwise velocity V_S of the core flow, as discovered by Storer and Cumpsty (1991). When double leakage is present, the double leakage fluid which always lies next to the shroud (by having least interaction with core flow) enters the tip clearance with a non-zero normal velocity $V_{N,DL}$ and a low streamwise velocity component $V_{S,DL}$ lower than V_S. Then it exits the tip clearance with higher normal ($V_{L,DL}$) and lower streamwise ($V_{S,DL}$) velocity components than the standard tip leakage fluid. The higher the proportion of double leakage, the higher the average normal velocity component and the lower the average streamwise velocity component of the tip clearance flow. The resulting 'stronger' tip clearance flow leads to higher velocity vector difference with the core flow and thus higher shear mixing loss and tip blockage and by extension higher performance loss. In addition, the stronger tip clearance flow also pushes the incoming/tip clearance flow interface (whose position depends on the momentum balance between the two streams) closer to the leading edge plane, hence reduces stall margin according to the interface criterion proposed by Vo et al. (2008). Thus any increase in double leakage proportion with tip clearance size increase results in a drop of performance and stall margin and leads to increase in sensitivity of these parameters to tip clearance.

Figure 2-13: Effect of the double leakage on tip leakage flow velocity components illustrated on chordwise cut of the blade (Erler 2012)

With its high normal velocity and low streamwise velocity components, the double leakage fluid tends to move across the blade passage and proceed to double leak again in the adjacent blade's tip clearance. Thus, the presence of double leakage tends to promote more double leakage. Double leakage fluid lies next to the shroud. By its relative movement to the rotor, the shroud drags this fluid circumferentially across the blade passage. Hence, an increase in tip clearance tends to increase double leakage proportion as this fluid takes over the additional height, as illustrated at the top of Figure 2-14. The resulting larger double leakage proportion tends to promote more double leakage in the next blade as illustrated by the increase chordwise extent of double leakage at the bottom streamline plot of Figure 2-14. Thus, the increase in tip clearance promotes the increase in double leakage proportion and thus reduced performance and stall margin, i.e. sensitivity.

Numerical experiments were carried out to isolate, validate and explain each desensitizing flow feature. The isolated effect of double leakage was assessed by reducing the blade pitch through blade number increase so as to increase double leakage proportion of tip clearance flow without altering the inlet meridional velocity profile. The results from the simulations plotted in Figure 2-15(a) did indeed show that double leakage proportion increases with tip clearance. Furthermore, the rate of increase of double leakage rise with the amount of initial (minimum tip

clearance) double leakage, which proved that double leakage promotes more double leakage, and by extension that a larger amount of initial blockage increases the performance sensitivity of the compressor rotor, as shown in Figure 2-15(b). It was thus concluded that a reduction or removal of double leakage would partially or totally desensitize the compressor performance and stability to tip clearance.

To isolate and explain the effect of high incoming meridional momentum in the tip region, the spanwise distribution of inlet total pressure was altered to increase (or in one case decrease) the inlet meridional velocity at the tip of BASE rotor as shown in Figure 2-16. The blade geometry was adjusted to maintain the tip loading the same in the presence of higher incoming flow momentum in the tip region so as not to reduce sensitivity by simply unloading the tip through incidence reduction. As shown in Figure 2-17, the rotor design with high incoming meridional momentum near tip boundary condition has lower performance and stability sensitivity. The author concluded that this flow feature affects the flow field in two ways. First, the increased meridional momentum reduced double leakage by increasing the streamwise meridional velocity component of the leakage flow ($V_{str,tc}$) by increasing the streamwise velocity of the core flow entering the tip gap ($V_{below-tip}$), as illustrated in Figure 2-18. Second, the author showed through the blockage development model of Khalid as shown in Figure 2-3 that an increase in incoming meridional momentum in the tip region desensitizes the performance and aerodynamic stability to tip clearance even in the absence of double leakage.
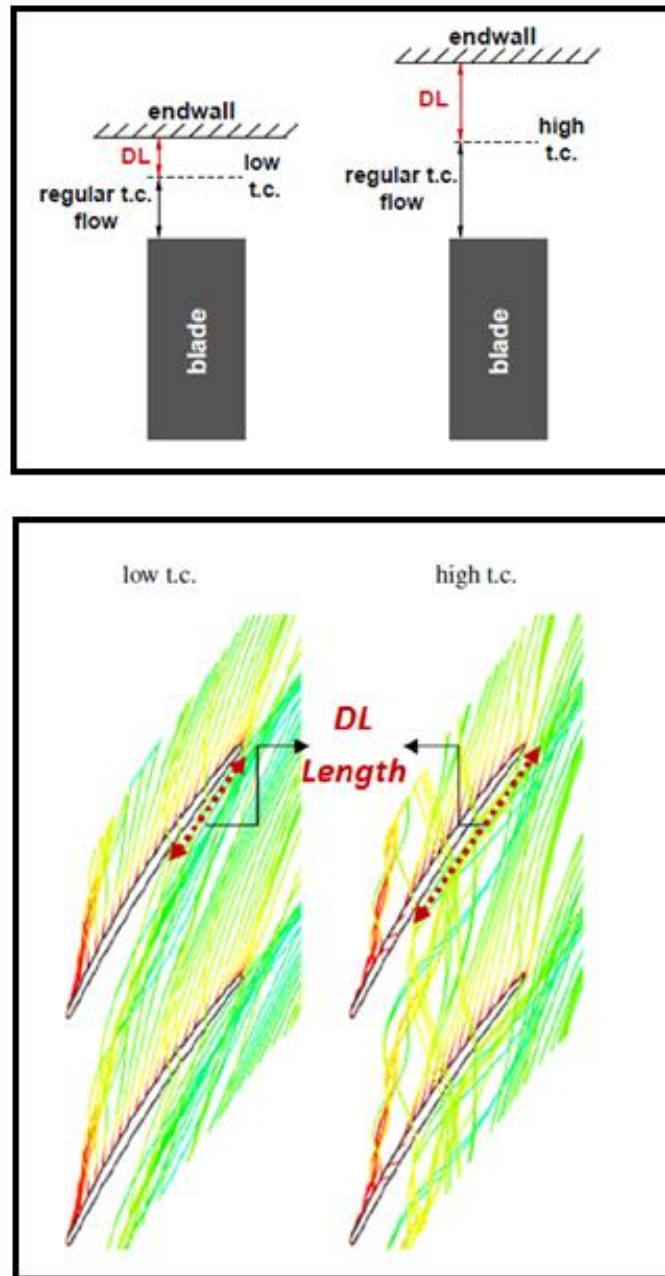
Figure 2-14: Effect of tip clearance increase on radial extent (top) and circumferential extent (bottom) of double leakage (Erler 2012)

(a)

(b)
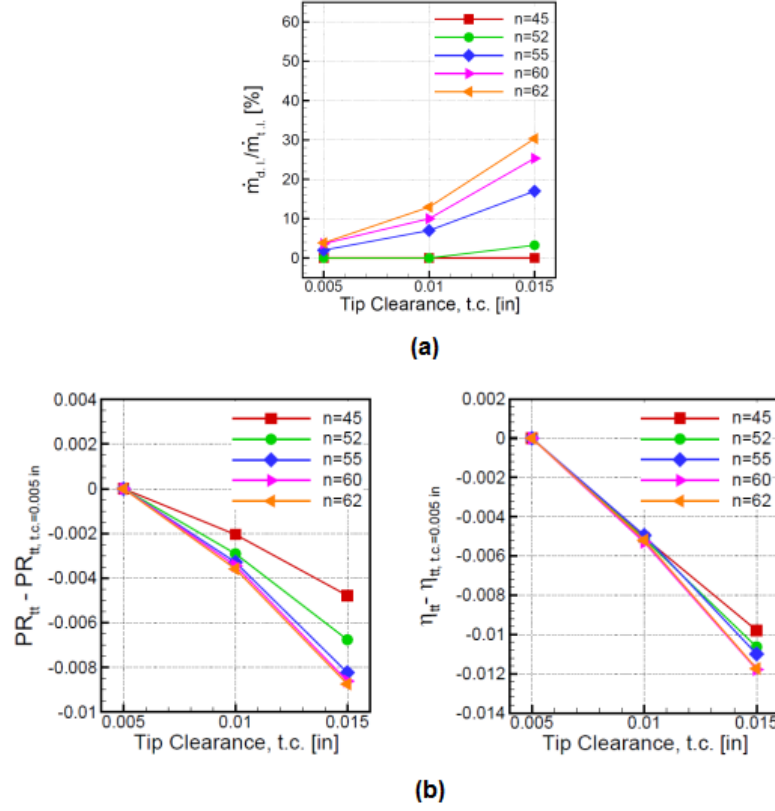
Figure 2-15: Variation of double leakage proportion with (a) tip clearance and (b) performance for the BASE rotor with different number of blades (Erler 2012)

(a) Total pressure profiles

(b) Incoming meridional momentums
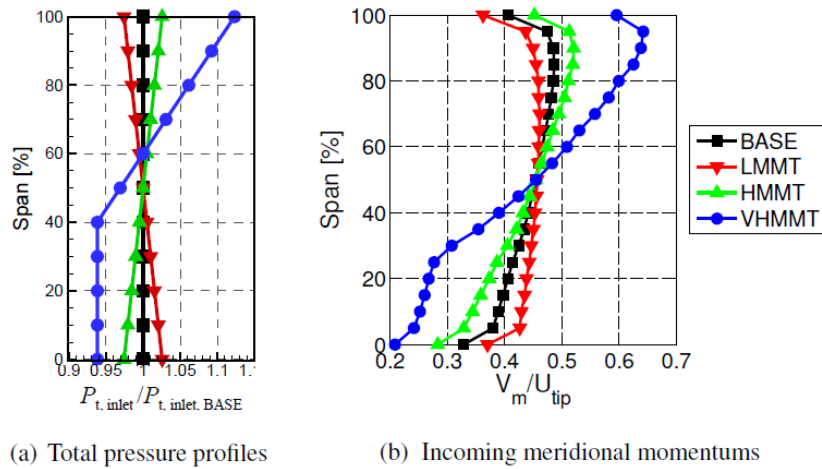
Figure 2-16: Spanwise distributions of inlet total pressure profiles and resulting incoming meridional momentum applied to BASE rotor geometry (Erler 2012)
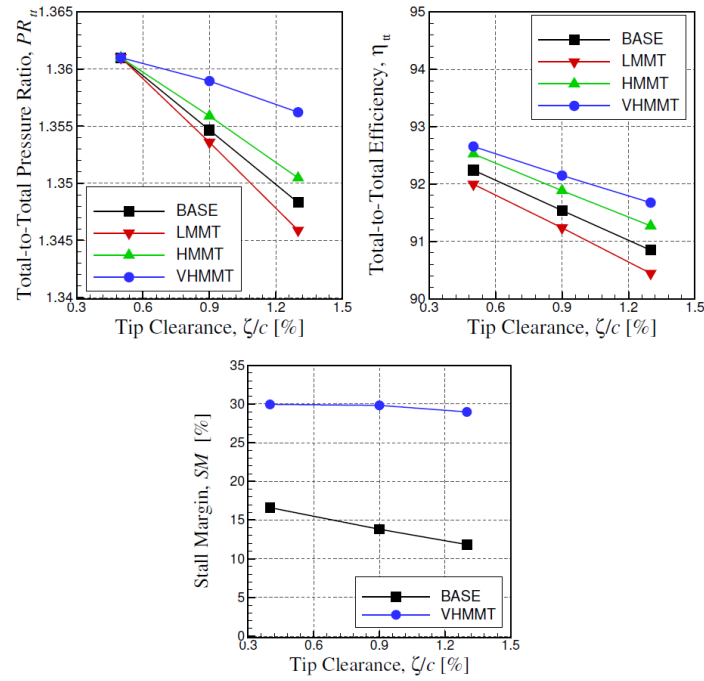
Figure 2-17: Performance and stall margin sensitivity associated with incoming meridional momentum profiles of Figure 2-15 (Erler 2012)
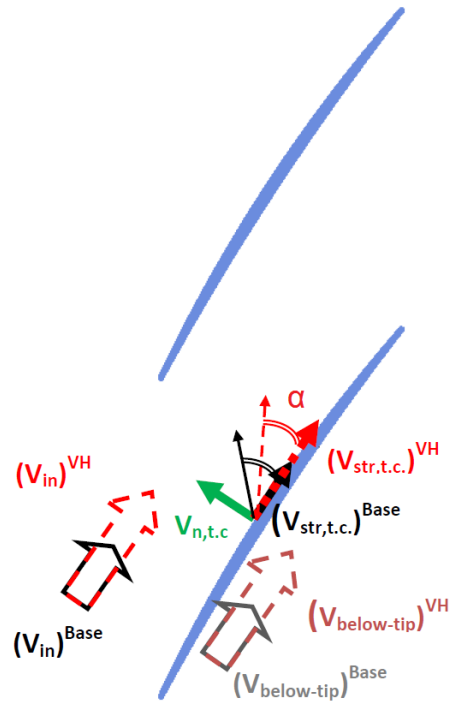
Figure 2-18: Illustration of the effect of increased incoming tip meridional momentum on the tip leakage flow velocity components (Erler 2012)

Finally, Erler (2012) also proposed two rotor blade designs that exploit the desensitizing flow features, namely full forward chordwise sweep (FFCS) and partially low stagger (PLS). The FFCS rotor, shown in Figure 2-19, improved both the incoming meridional momentum in the tip region and reduced double leakage as intended (see Figure 2-20). As a result, it was able to decrease the sensitivity of total pressure ratio, efficiency and stall margin by 23.9%, 24.6% and 90%, respectively. The PLS rotor geometry shown in Figure 2-21 is generated by decreasing the stagger of the blade at upper half of the span while increasing at the lower half in order to keep the design mass flow constant. Figure 2-22 indicate that the PLS design reduced double leakage even more than the FFCS design without relying on any change in meridional momentum profile. Although the PLS design was not as successful as the FFCS design, it still reduced the sensitivity of total pressure ratio, efficiency and stall margin by 15.9%, 29.1% and 33%, respectively, to prove Erler's hypothesis.

(a) BASE   (b) FFCS
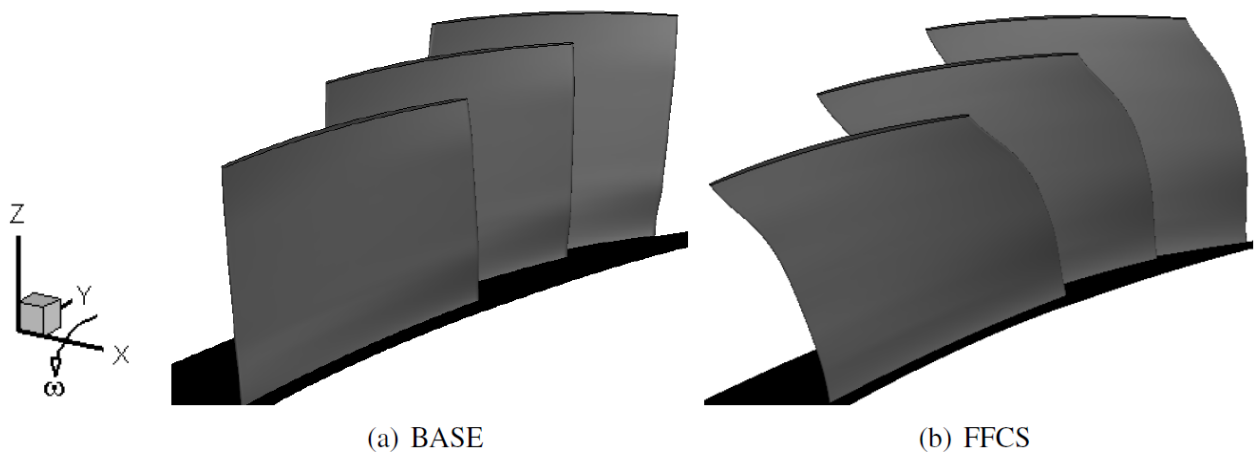
Figure 2-19: 3-D views of Baseline (BASE) and FFCS rotor blade geometry (Erler 2012)
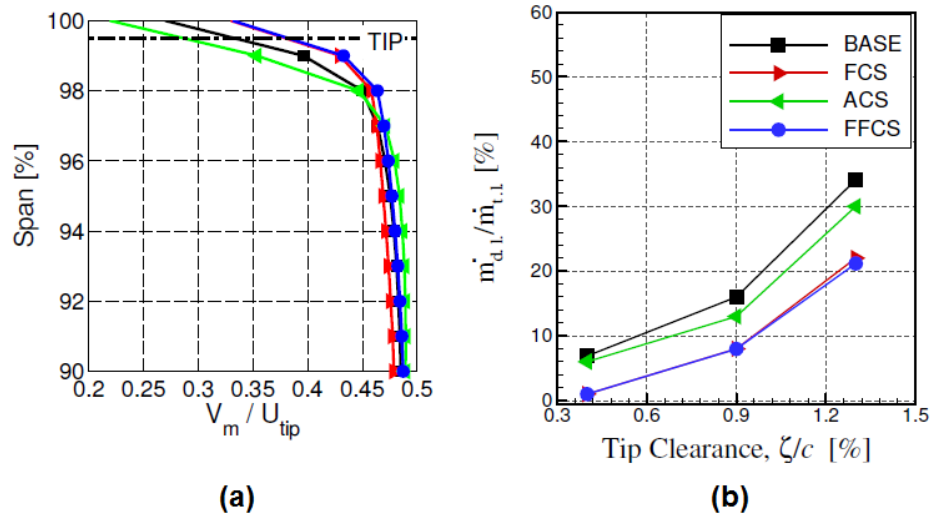
Figure 2-20: Effect of FFCS rotor blade on desensitizing flow features (Erler 2012)
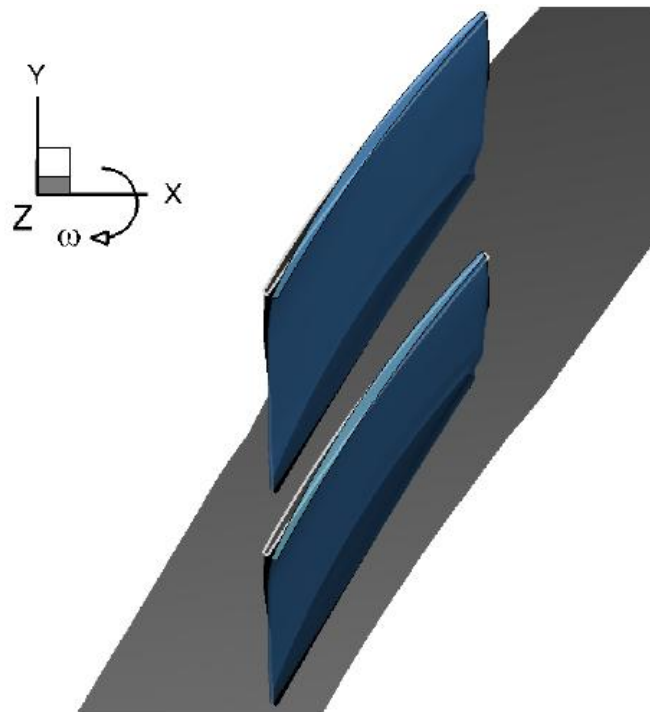
Figure 2-21: 3-D views of PLS (gray) and BASE (blue) blades (Erler 2012)
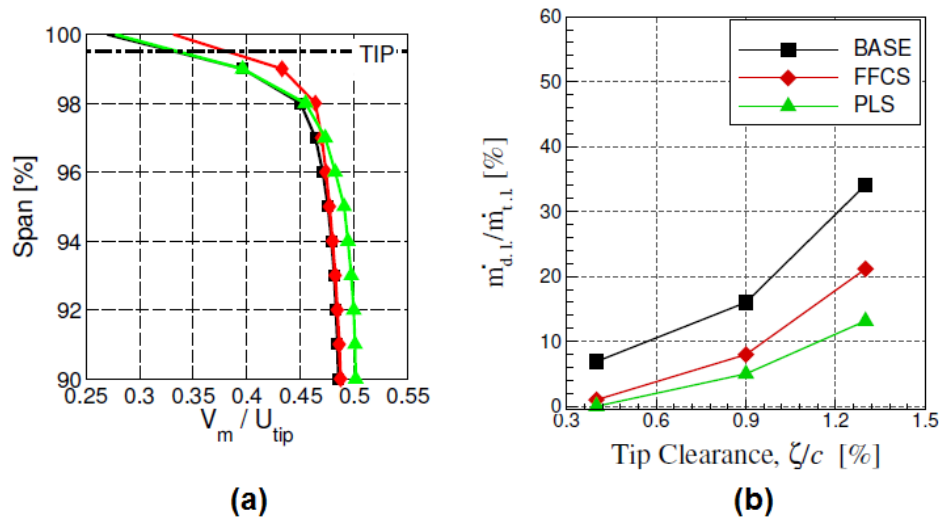
Figure 2-22: Effect of PLS rotor blade on desensitizing flow features (Erler 2012)

2.2.2 Gas Path Design Strategies and Their Effects on Desensitization

The studies in the open literature related with gas path modifications for reducing tip clearance losses or sensitivity are relatively limited. Gas path based design strategies could be grouped under two categories, casing treatment and gas path contouring. Casing treatment consists of integrating circumferential grooves or slots on the shroud above the rotor, generally to improve stall margin. As a second category, gas path contouring is the modification of gas path shape to redistribute the passage flow near the shroud. While casing treatment has not been used for tip desensitization yet, it is a proven and widely used method for stall margin improvement. On the other hand gas path contouring is a rarely used method, generally to improve nominal performance of a compressor, and there is no example in the open literature showing its use for tip desensitization.

Casing Treatment

Takata and Tsukuda (1977) presented an experimental study involving seven casing treatment configurations tested on a low-speed axial compressor stage with different tip clearance sizes. They found that the best three configurations in terms of stall margin improvement were skewed slots, axial slots and circumferential grooves as illustrated in Figure 2-23. However, their results also showed that skewed and axial slot type casing treatment desensitizes the stall margin to tip

clearance size change. However, the authors neither mentioned this desensitization as a particular feature, nor gave any explanation about it. They proposed that, the casing treatment, particularly the axial slots, work by suctioning the low momentum fluid near the shroud near the rotor outlet and re-injecting it near the leading edge as a high-speed jet. This process was shown to improve flow condition in the upper half span by means of momentum interchange between endwall flow and high-speed jet, which reduces tip blockage and tip loss.

(a) Axial Skewed Slots   **(b) Axial Slots**   **(c) Circumferential Grooves**
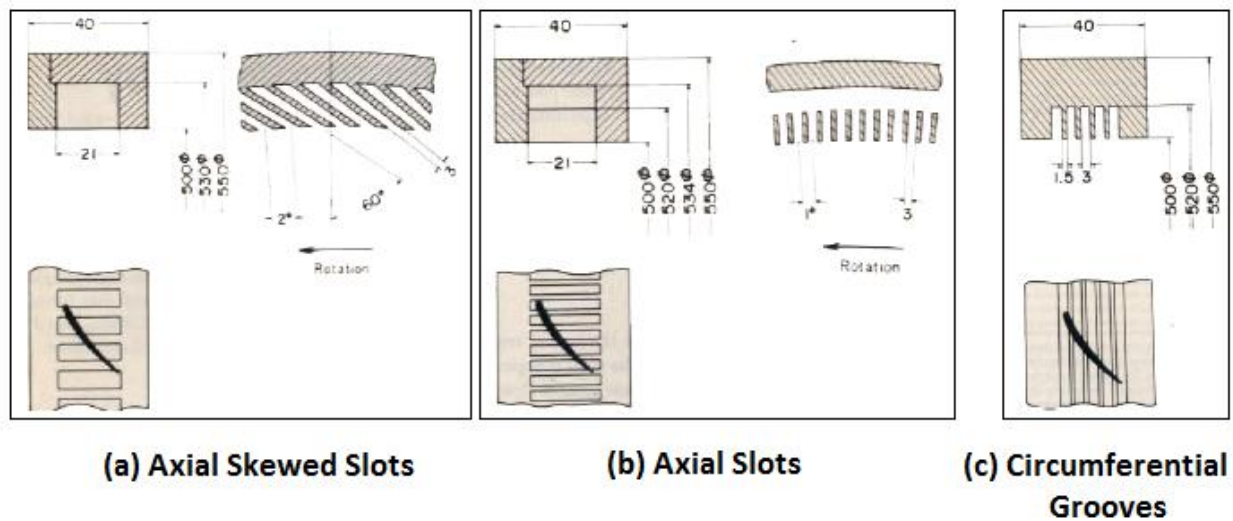
Figure 2-23: Best casing treatment configurations examined by Takata and Tsukuda (1977)

.

Fujita and Takata (1984) carried out another experimental study on a subsonic axial compressor rotor and tested the effect of various casing treatment types on performance and stall margin. Their results showed that, there is a trade-off between nominal efficiency and stall margin improvement. Their data in Figure 2-24 showed that the axial skewed slots casing treatment is the most promising configuration for stall margin improvement, which is consistent with the findings of Takata and Tsukuda (1977), but also incurs the largest nominal efficiency penalty, while circumferential grooves have more limited stall margin improvements but are better at preserving nominal efficiency.
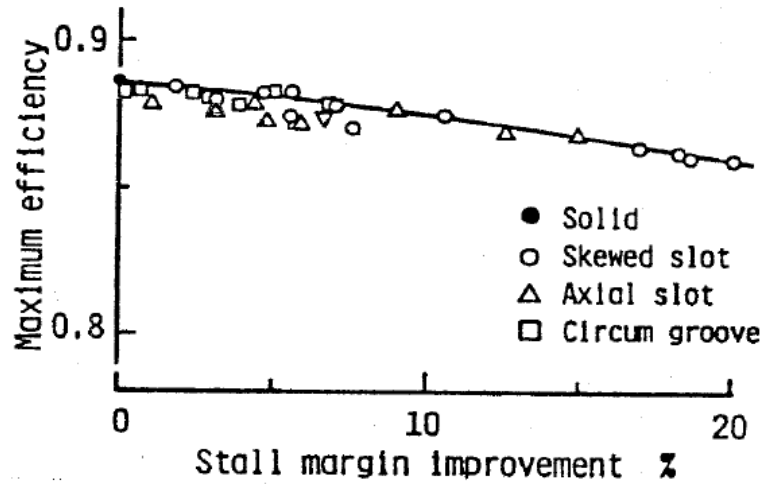
Figure 2-24: Rotor maximum efficiency versus stall margin improvement
(Fujita and Takata 1984)
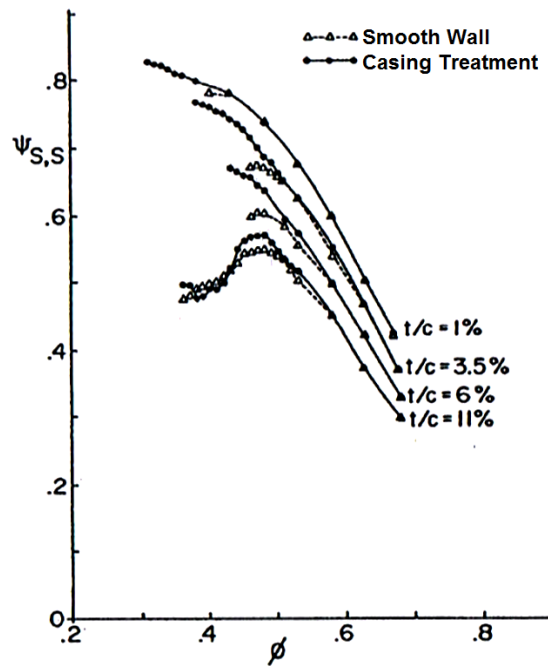
Figure 2-25: Nondimensional static pressure rise across rotor versus flow coefficient at various
tip clearances for the smooth and treated casings (Smith and Cumpsty 1984)

Smith and Cumpsty (1984) presented an experimental study covering tests of a low-speed
axial compressor rotor with a skewed slots casing treatment, similar to that used by Takata and

Tsukuda (1977), at different tip clearance sizes. The authors reported that nominal stability margin is increased by the casing treatment at each tip clearance size, as presented in Figure 2-25. Although it was not shown by the measurements, the authors concluded that a similar improvement could be seen for the pressure rise and efficiency as the casing treatment was found to reduce the detrimental effects of tip clearance flow. Based on this conclusion, authors also claimed that casing treatment could potentially be used for the desensitization of rotor performance to tip clearance change.

A more recent comparison of axial slots and circumferential grooves was made by Lu et al. (2006) with a numerical study on a subsonic axial compressor rotor. Both casing treatment configurations cover the entire axial chord of rotor. The results showed that while the axial skewed slot has almost four times the stall margin improvement of the circumferential grooves, it has ten times more loss in peak efficiency (5.01 versus 0.54 percent). These results agree with the trend shown by Fujita and Takata (1984).

A computational study carried out by Wilke and Kau (2003) on a transonic axial compressor rotor showed that, the performance-stall margin trade-off in axial slots could be eliminated by changing their axial location. They shifted the location of a casing treatment composed of axial slots with semi-circular a cross section from the reference location in the middle of the blade passage to a more upstream location where only a downstream part of axial slot lay in the blade passage as illustrated in Figure 2-26. The results showed that axial slots located in the middle of the passage improve stall margin by 20% while decreasing the peak efficiency by 4%. The relocated axial slot designs were shown to achieve the same stall margin improvement with only a 0.2% drop in peak efficiency. The performance improvement was attributed to the shock position, which moves downstream of the passage due to suppression of the tip vortex for the reference slot location and remains unchanged for the upstream slot location. They concluded that the shift in shock position for the reference slot location eliminates the pressure ratio gain that comes from the shock mechanism.
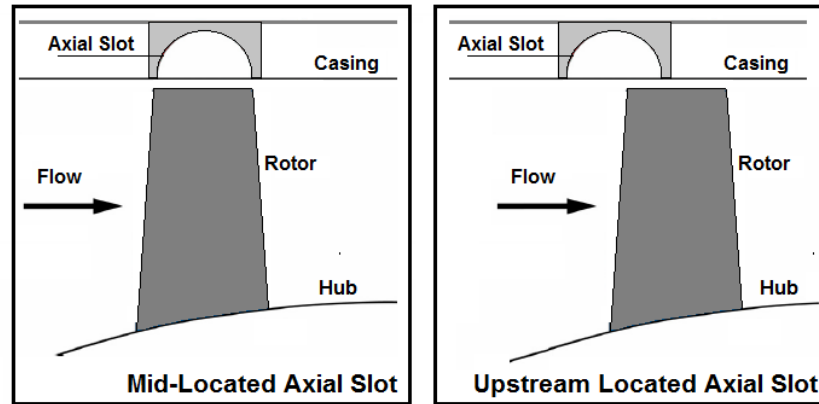
Figure 2-26: Cross sectional view of axial slot locations (Wilke and Kau 2003)

Danner et al. (2009) investigated skewed axial slots computationally and experimentally on a transonic compressor stage. The authors investigated the effect of slot position by changing the overlapped portion of axial slots located at the upstream of the passage as illustrated in Figure 2-27. They achieved a rise of up to 4.9% in total pressure ratio and 1% in efficiency while improving stall margin by up to 63% with the small overlap configuration. The authors explained this improvement with the changing shock characteristics in the flow field and concluded that achieving the same improvement is not possible in subsonic compressors due to the absence of shocks.
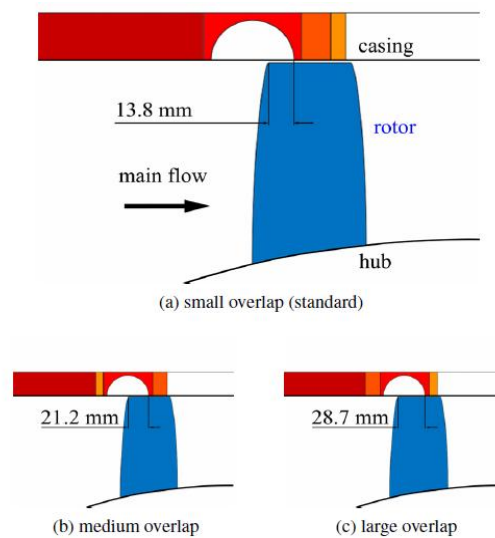
Figure 2-27: Cross sectional views of axial slots with different overlapped portions (Danner, et al. 2009)

An experimental study by Thompson et al. (1998) on a transonic compressor rotor showed the effect on performance of a shallow casing treatment in the form of a stepped tip gap. A stepped tip gap shape is generated by increasing the tip gap size near the aft of the passage, as shown in Figure 2-28. Two stepped gap designs with different axial extents were generated which were referred to as forward step and aft step, covering 42% and 14% of axial chord, respectively, from the rotor trailing edge. These designs were tested at three different tip clearance sizes. The results showed that while the forward stepped gap improves the performance and flow range (i.e. choke mass flow) at the smallest tip clearance size, the aft stepped gap makes a similar improvement at medium tip clearance size. Nonetheless no stall margin improvement was detected at any of the tested tip clearance sizes. Since the improvement in aft-stepped tip gap was more promising, only this configuration was tested at large tip clearance, and the results showed that it degrades the performance.
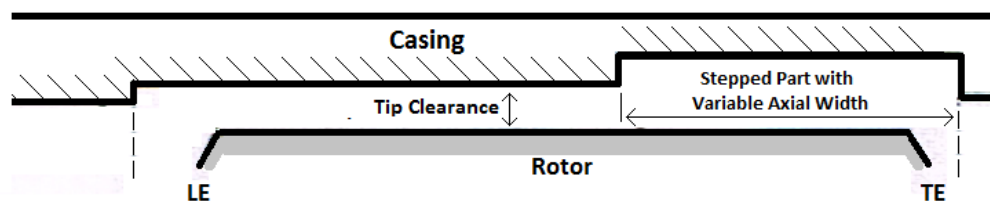
Figure 2-28: Schematic representation of the stepped tip gap design (Thompson, et al. 1998)

Wilke and Kau (2002) presented a computational study on effects of circumferential groove and axial slots on a transonic compressor stage. However since their simulations were all performed in steady state, the results related to the axial slots is not considered for review due to questionable reliability and accuracy. For the circumferential grooves the authors compared two types, shown in Figure 2-29, namely configuration 1 and configuration 2. The authors stated that the grooves mainly have a reducing effect on the radial extent of the tip vortex and the loss intensity by reducing the strength of velocity components of tip leakage perpendicular to the blade. They explained that the tip vortex modification results from the transfer of high relative total pressure fluid at the blade tip pressure side to the suction side where relative total pressure is comparatively low. The fluid transfer modifies the tip leakage velocity components and reduces the quantity of the fluid attending to tip vortex formation, which results in a weaker and smaller

tip vortex. As a result, the tip vortex breakdown is delayed, leading to better aerodynamic stability. However, the authors also concluded that the tip leakage flow that enters and expands through the groove has a risk of creating recirculation zones when re-entering the passage and increase tip blockage. The comparison of two configurations showed that configuration 1 improves stall margin better with relatively lower peak efficiency loss (almost 5 times less) than configuration 2. The proposed reason for this difference is related to the close placement of too many grooves on the passage. It is explained that as high energy main flow are deflected radially inwards by the upstream grooves, the low-energy fluid radially re-entering the passage from the downstream grooves could easily be transported in the upstream direction by the pressure-gradient that results in a critical blockage area even near peak efficiency point.

Additionally the authors simulated the first two and the last two grooves of configuration 1 separately to observe the effect of groove location. They stated that the downstream located grooves are determined to be completely ineffective since the tip leakage vortex was observed to be fully developed like in the smooth casing configuration. On the other hand, the upstream located grooves are determined to be less effective than the four-groove configuration about modifying the tip leakage flow.
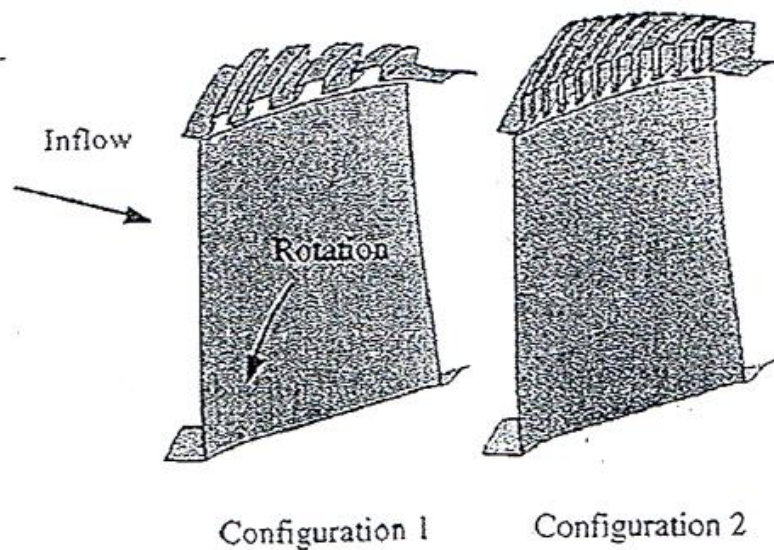
Figure 2-29: Casing treatment configurations investigated by Wilke and Kau (2002)

Shabbir and Adamczyk (2005) analytically and numerically examined the flow mechanism associated with circumferential grooves on a low-speed axial compressor. The authors hypothesized that the stall margin improvement comes from the transport of axial momentum between the grooves and the main flow. They claimed that the axial momentum transport is generated by the impingement of the exiting flow from the grooves to the mainstream flow near the shroud. The net axial pressure force in the passage is only balanced by the axial shear stress force of the mainstream flow near the shroud in a smooth casing configuration. The addition of the grooves results in additional axial force which helps to sustain a balance with the pressure force, as illustrated in Figure 2-30, resulting in the extension of the mass flow range. The authors also showed that the effectiveness of each individual groove depends upon its axial location. The grooves closer to the leading edge are found to be more effective in terms of momentum exchange compared to the grooves located close to the trailing edge. As shown in Figure 2-31, the contribution of each groove to radial momentum transport drops as they located further downstream from the leading edge, with the last groove located near the trailing edge presenting almost a negligible contribution. While the hypothesis stated by the authors is disputable as it does not bring an explicit explanation on the mechanism behind the momentum exchange, the study shows that effectiveness of a groove is directly related to its location.
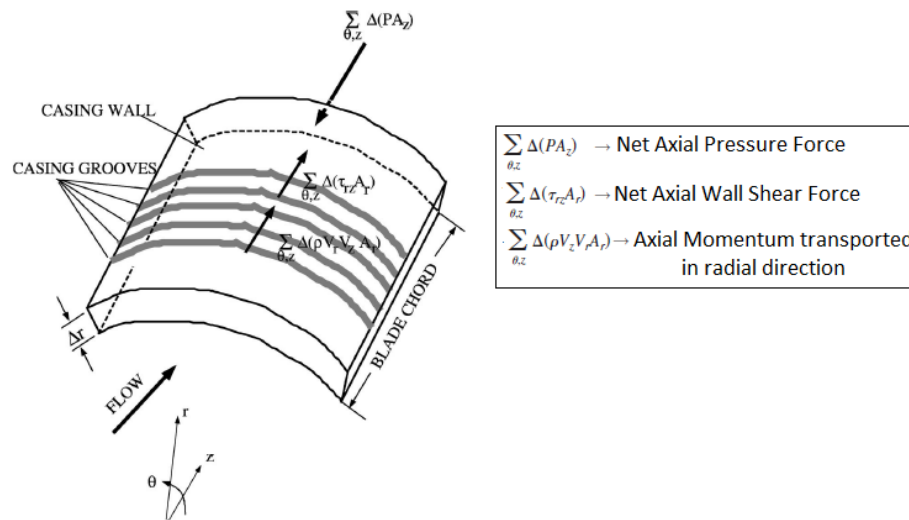
Figure 2-30: Schematic representation of axial momentum balance near the casing in the presence of circumferential grooves (Shabbir and Adamczyk 2005)
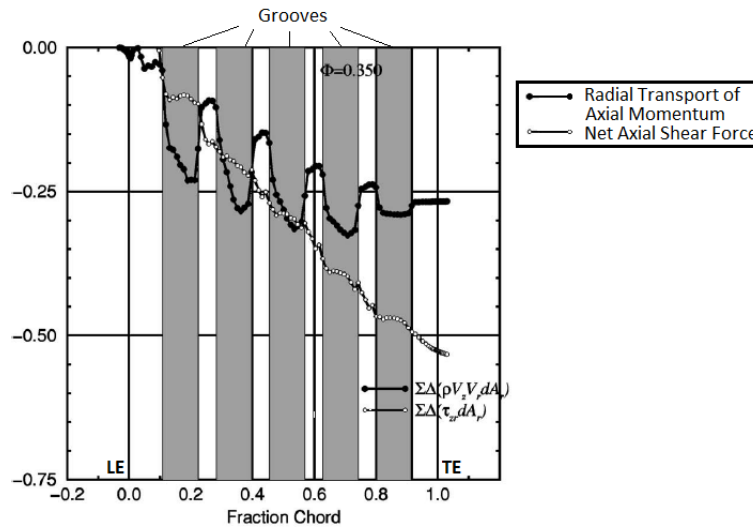
Figure 2-31: Contribution of each groove to the next axial force which is composed of net axial shear force and radially transported axial momentum (Shabbir and Adamczyk 2005)

Muller et al. (2007) investigated the effect of variation of the depth and axial extent of circumferential grooves both numerically and experimentally on a transonic axial compressor stage. Groove depths of 3 mm (shallow) and 12 mm (deep) from and groove axial extents of 39% and 82% of axial chord length were investigated. The axial width of each groove was kept constant and the number of grooves increased to change the total axial extent of the casing treatment. Thus the 39% axial chord extent configuration had three grooves while the 82% axial chord extent had six grooves. The grooves started at 15.25% axial chord length distance from the rotor leading edge. In total, four configurations were tested. While all configurations were found to be effective in increasing the stall margin, the 82% axial chord extent deep-groove configuration increased it the most. However, the axial extent seemed to have significantly more effect on this improvement than the groove depth. The authors also noted that deep grooves have a detrimental effect on the performance, particularly on the efficiency. Nevertheless, their experimental results indicated that shallow grooves located towards the aft could increase the maximum stage efficiency more than 1 percentage point while also improving the pressure ratio. The authors attributed the favourable effect on performance to the improvement in stator inlet flow rather than a direct effect on the rotor. They stated that corner separation in the stator passage is suppressed by the generation of higher turbulence level near the tip region of the rotor

by the presence of the grooves. Numerical simulations showed that the effect of grooves on the flow field is associated with the change in loading and the modification of tip leakage flow. The loading at the tip is reduced which significantly reduces the leakage jet normal flow velocity at the exit of the tip clearance. The interaction of the flow in and out of the grooves with the slower tip leakage flow results in the inclination of tip leakage vortex towards the blade which weakens the tip vortex intensity. This study showed that shallow grooves are more preferable than deep grooves if preserving the nominal performance level is a design consideration.

Zhang and Ma (2007) presented the results of a computational study on the effect of a trench shaped casing treatment on the NASA Rotor 37 transonic axial rotor. The authors modified the shape of the casing and the rotor tip by giving them a radial inclination towards the trailing edge while keeping the tip clearance size constant, as shown in Figure 2-32. They showed that this modification improved the stall margin of the compressor. However they could not improve pressure ratio and efficiency parameters nor provide a clear explanation on the physical effects of this modification.
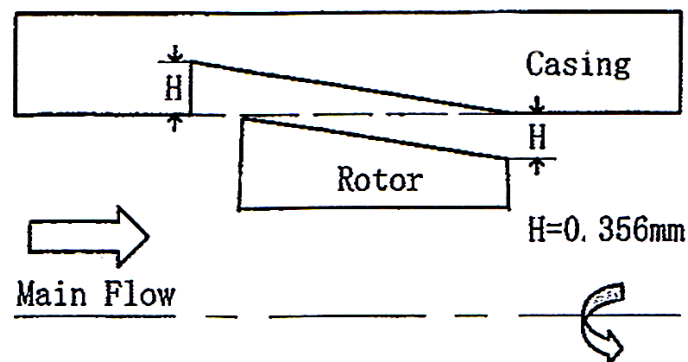
Figure 2-32: Schematic representation of the casing modification of Zhang and Ma (2007)

Mileshin, et al. (2008) experimentally and numerically studied the effectiveness of circumferential grooves, shown in Figure 2-33, on a transonic compressor stage. They investigated the effects of grooves at two different tip clearance sizes namely 0.76% and 2.66% of blade span size. A total of eight 6 mm-deep circumferential grooves with rectangular cross-section shape are placed on the casing covering 82% of the rotor axial chord starting from the leading edge. The authors cited that 16% of the observed pressure ratio drop due to the increase of tip clearance size on a solid casing is recovered by the presence of grooves, as presented in

Figure 2-34. Moreover the surge margin was shown to be increased by the grooves at large tip clearance. From the numerical simulation the authors observed that the mass flow transfer from rotor passage to grooves is the highest in the front grooves at design point while being highest in the central grooves close to the stall point. On the other hand the grooves located downstream had no significant mass flow transfer which is consistent with the results of Shabbir and Adamzyck (2005).
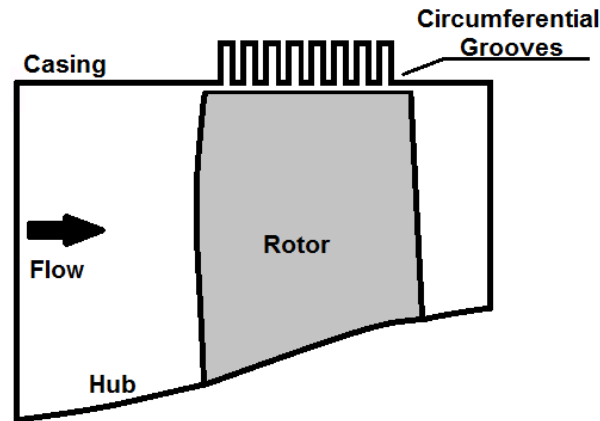
Figure 2-33: Circumferential grooves investigated by Mileshin et al. (2008)
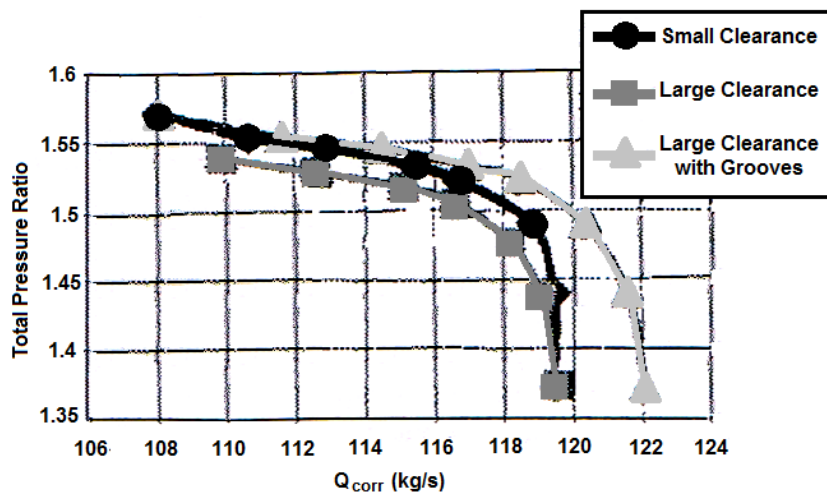
Figure 2-34: Total pressure ratio map obtained from the experiments on transonic compressor stage with smooth casing and casing treatment by Mileshin et al. (2008)

Legras et al. (2010) conducted a numerical study related to the effects of circumferential grooves on the NASA Rotor 37 transonic axial rotor. A total of six grooves covering 81.5% of the rotor tip axial chord starting from 5% of tip chord upstream of the rotor leading edge. The analyses focused on a detailed investigation of the flow field near the tip region, particularly tip leakage vortex-shock interaction, rather than the effects on the rotor performance. The authors cited that the principal effect of circumferential grooves is in limiting the expansion of the tip leakage vortex in the passage towards the adjacent blade. They stated that the reduction of the pressure difference across the blade tip, significantly reduces (by almost 25%) tip leakage mass flow and limits the rolling-up mechanism of tip vortex, as shown in Figure 2-35. Nonetheless the authors also emphasized the existence of secondary vortices in passage which are generated by the interaction of the grooves and tip leakage flow.
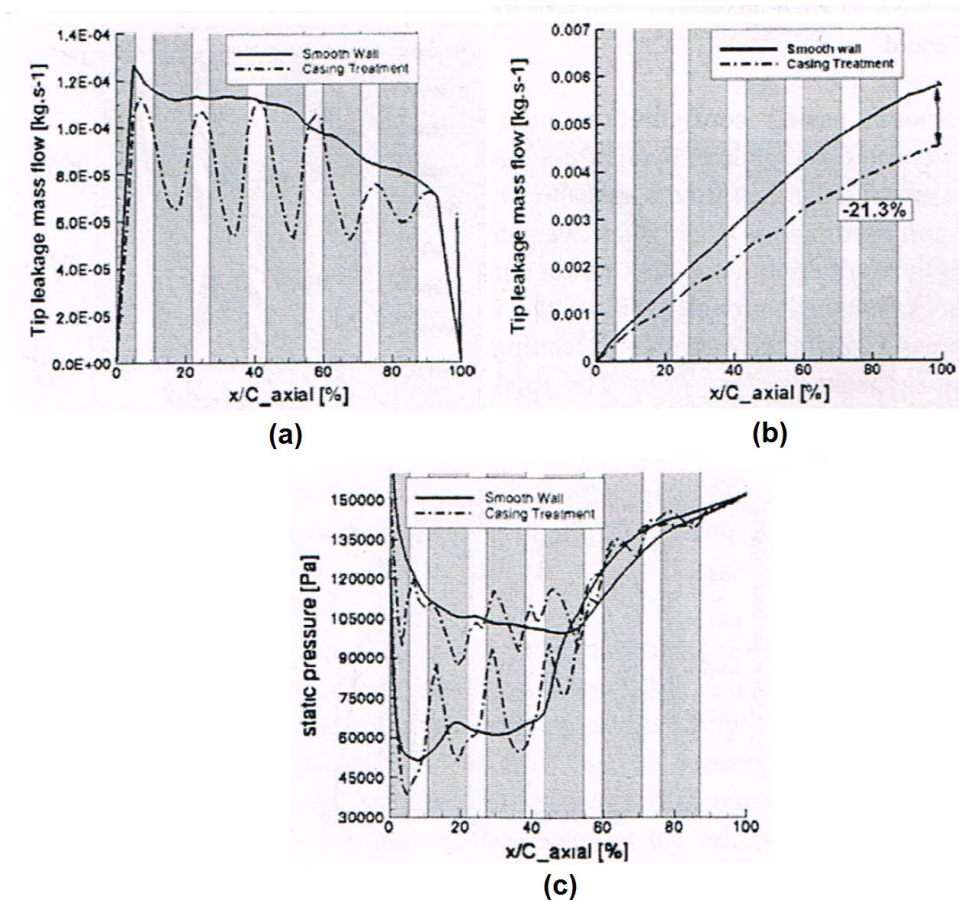
Figure 2-35: Distribution of flow features at mid-gap over the tip axial chord (a) Local tip mass flow, (b) Chordwise evolution of total tip mass flow, (c) Tip blade static pressure distribution on pressure and suction sides (Legras, et al. 2010)

Gas Path Contouring

There are very few studies published on gas path design strategies for tip clearance flow management. One study that could be placed under this category is that of Wang et al. (2002) who carried out numerical simulations of various modifications to a stator hub clearance shape. As presented in Figure 2-36, the hub clearance configurations studied were two uniform profiles (2 and 4% of tip axial chord), an expanding profile (from 1 to 3% tip axial chord) and a shrinking profile (from 3 to 1% tip axial chord) towards the trailing edge. The analyses were held with both stationary and rotating hub to observe the effect of hub rotation on the flow field. The authors found that the expanding shape improved the peak efficiency in the static hub case through a weakened leakage vortex. On the other hand, the shrinking configuration was found to have even a deteriorating effect on performance. However, the improvement associated with the expanding shape is found to be reduced when the hub rotates due to the dominant effect of the circumferential velocity component induced by the hub. Hence, the authors claimed that the expanding gap configuration can not be applied to rotors, due to the dominant effect of rotation.

(a) small tip clearance   (b) large tip clearance   (c) expanding tip clearance   (d) shrinking tip clearance
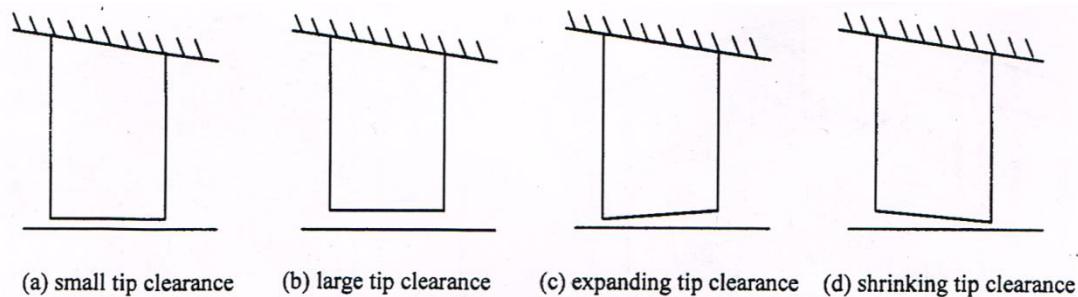
Figure 2-36: Tip clearance shapes examined by Wang et al. (2002)

Ma and Li (2008) numerically studied the effects of non-uniform tip clearance distributions on a compressor rotor performance. They examined three different tip clearance distributions, as shown in Figure 2-37. They found that configuration "x1" has the highest efficiency and static pressure rise and stated that the performance increase is associated with the decreasing tip blockage at the passage exit. However the operating range was found to be lower than that of the uniform tip clearance, which is somewhat counter-intuitive because a decrease in tip blockage usually results in an increase in operating range. The authors concluded that the larger clearance

size near the trailing edge weakens the tip vortex and delay blade boundary layer separation by sweeping low energy fluid parts away from the blade tip region at the suction side.
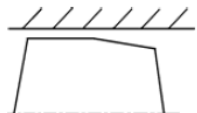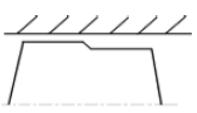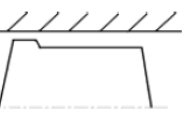
case	x1	x2	x3	t 1	t 2	t 3	q1	q 2	q 3
tip clearance at trailing edge(mm)	0.712	1.424	1.068	0.712	1.068	0.89	0.712	0.89	1.068
profile of the tip clearance									

Figure 2-37: Tip clearance contours examined by Ma and Li (2008)

Shao et al. (2007) analytically studied the effects of chordwise tip loading and tip clearance distribution on the tip leakage mixing loss, by using an extended version of a loss model previously presented by Denton (1993). Their results showed that the leakage mixing loss is directly proportional to the level and the chordwise distribution of blade loading. Furthermore the effects of various non-uniform tip clearance configurations presented in Figure 2-38, on mixing loss are demonstrated by using the same loss model. The study showed that higher clearance at the leading edge (Gap 3 and 7) for a front loaded blade and higher clearance at the trailing edge for an aft loaded blade (Gap 2 and 6) creates less tip loss than a blade with uniform tip loading and tip clearance.

Distribution of Tip Clearance		Tip Clearance/Blade Span (Average Level of 2%)		
		Leading edge	Middle of chord	Trailing edge
Gap-1		2.0%	2.0%	2.0%
Gap-2		0.8%	2.0%	3.2%
Gap-3		3.2%	2.0%	0.8%
Gap-4		3.6%	1.2%	3.6%
Gap-5		0.4%	2.8%	0.4%
Gap-6		2.0%	1.2%	5.2%
Gap-7		5.2%	1.2%	2.0%

Figure 2-38: Types of tip clearance distribution studied by Shao, et al. (2007)

Kroger et al. (2009) showed with a computational study that it is possible to increase the efficiency of an axial flow compressor up to 0.35 percentage point by modifying the casing contour of the rotor. The authors used an in-house three-dimensional optimization code to reshape the casing and blade tip contours of a subsonic axial compressor rotor. The optimization problem was setup based on six geometrical parameters that define the shape of rotor blade tip in meridional plane and the objective was to minimize the isentropic efficiency and endwall blockage. The resulting blade tip and casing shape obtained from the optimization study is shown in Figure 2-39. The authors showed that, the optimized tip rotor increased the meridional velocity near the tip, modified the tip vortex trajectory, and lowered the overall tip leakage mass flow rate by 2.5%, as presented in Figure 2-40. The authors stated that, the tip leakage mass flow between 10% and 30% chord length position of the tip gap region is augmented which strengthened the tip vortex and caused a rapid dissipation of the intensity of the vortex compared to the baseline design.
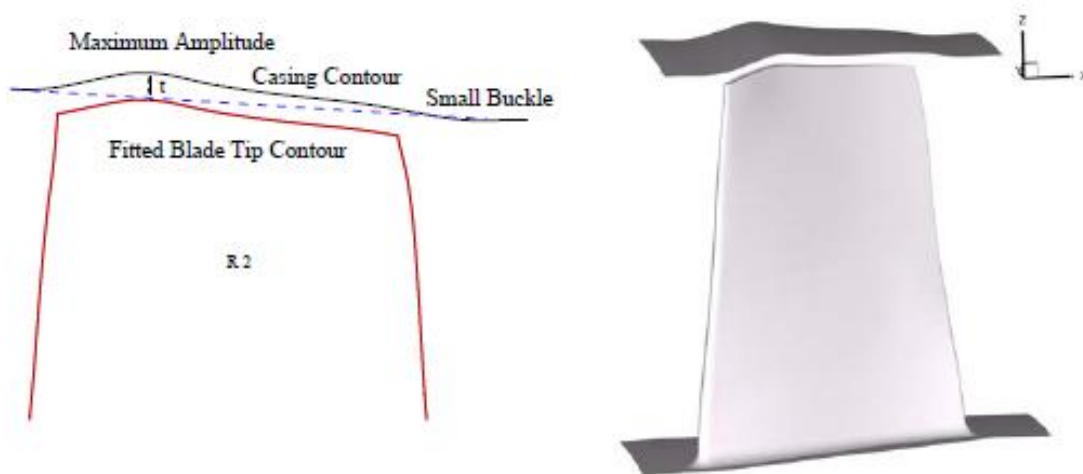
Figure 2-39: Side and three-dimensional views of the contoured casing of Kroger et al. (2009)
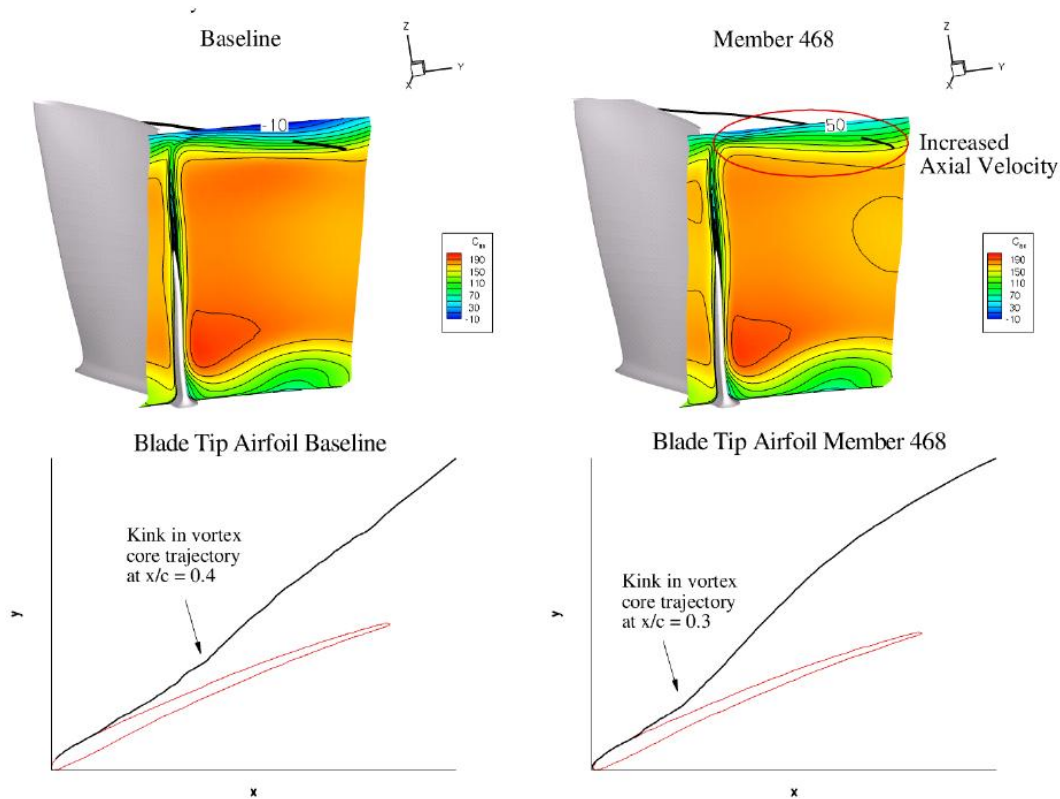
Figure 2-40: Vortex core trajectory and axial velocity contours for the baseline and optimized (Member 468) designs of Kroger et al. (2009)

2.3 Summary

The information from the literature review that is pertinent to the present research can be summarized as follows:

- The effects of tip clearance can be summarized based on three parameters: tip loss, tip blockage and, the position of the interface between the incoming and tip clearance flows. The first two parameters are related to performance, i.e. pressure rise and efficiency, while the third parameter is an indicator of stall margin.

- Blade design strategies such as forward-sweep and forward-lean seem to be effective in reducing the sensitivity of performance and aerodynamic stability of an axial compressor to tip clearance increase.

- Two flow features are associated with desensitization to tip clearance size, namely increase incoming meridional velocity near the shroud and reduction/elimination of

double leakage. These features can also improve nominal performance and stall margin. Forward chordwise sweep can exploit the first feature, and by extension the second, while a low tip stagger rotor design exploits exclusively the second feature.

- Both axial slots and circumferential grooves casing treatments seem to have a potential for desensitization. Although the axial slots can provide much larger improvement in stall margin than circumferential grooves, they can cause a substantially larger nominal performance penalty. This penalty could only be eliminated by shifting much of the slots' axial extend upstream of the rotor leading edge, which can interfere with upstream stators in a multi-stage environment.

- Circumferential grooves and casing indentations seem to be effective in improving performance at various tip clearance sizes and may provide a solution to desensitize the rotor performance and stall margin to tip clearance size without large nominal performance penalties.

- No explicit work on desensitization with casing treatment, neither with slots nor grooves, has been carried out in the open literature nor any explicit associated flow mechanism proposed for desensitization using casing treatment.

- The studies on circumferential grooves indicate that the geometric parameters such as depth, axial extent, groove number and axial location can have an important effect on performance and aerodynamic stability as well as their sensitivity to tip clearance increase. While a decrease in groove depth does not change the stall margin improvement significantly, it reduces nominal performance loss. On the other hand the increase in axial width was shown to increase the effectiveness of the grooves on tip leakage flow and increase the stall margin improvement. The axial location of the grove is an important factor in stall margin improvement with the upstream location being more effective.

- Gas path contouring has been shown to have an effect on nominal performance and aerodynamic stability without any investigation on sensitivity to tip clearance size. However, it can increase meridional velocity in the tip region, which is one of the two desensitizing flow features.

2.4 Hypothesis on Tip Desensitization of a Compressor Through Gas Path Design Strategies

Erler's study (2012) showed that two flow features are effective in desensitization of performance and stall margin to tip clearance, namely high incoming meridional momentum near tip region and the elimination/reduction of double leakage flow, and also presented that blade design characteristics such as sweep and stagger can exploit these features. The present research proposed that:

- Gas path design strategies such as casing treatment and gas path contouring could be used to exploit either or both of these flow features for tip desensitization.
- Blade desensitization design characteristics can be combined to gas path design strategies to enhance desensitization effects and/or counter any nominal performance penalties associated with strategies such as casing treatment.

CHAPTER 3   METHODOLOGY

This chapter describes the chosen methodology to address the research questions and reach the objectives of this study. A computational approach is chosen because it allows for a low-cost rapid evaluation of various gas path design strategies and a detailed analysis of the flow field to evaluate and understand their effect. The first part of this chapter presents an overview of the approach taken to come up with promising gas path design strategies and to select, analyze, and refine the most promising strategy. The second part describes the computational setup chosen to carry out this approach.

3.1 Roadmap of the study

3.1.1 Development of Gas Path Design Strategies for Desensitization

Two desensitizing flow features defined by Erler (2012) are higher incoming meridional momentum in the blade tip region and elimination/reduction of double leakage. The flow mechanisms associated with these features in reducing performance and aerodynamic sensitivity to tip clearance were summarized in chapter 2. The implication is that any design strategy that can exploit these flow features should reduce sensitivity to tip clearance. Erler (2012) demonstrated this fact with blade design strategies, namely forward sweep to increase incoming momentum in the tip region and lowering tip stagger to reduce double leakage. The question is what gas path design strategies can achieve the same effects. From the literature review, gas path contouring and casing treatment are promising avenues to explore. In keeping the same philosophy as in the study by Erler (2012), blade loading at the tip must not be decreased so as to avoid prejudicing the results from potential desensitization effects due to a drop in tip loading.

The reference rotor geometry used to compare the change in performance and stall margin sensitivity to tip clearance is the baseline axial rotor design of Erler (2012) (henceforth referred to as BASE rotor), since much of the desensitization work so far has been based on this geometry. The BASE rotor is a high subsonic, tip critical rotor with double circular arc (DCA) blade profiles with an almost constant spanwise loading distribution. The design features of the BASE rotor and its geometry are presented in Table 3-1 and Figure 3-1, respectively. The detailed

information on design specifications and performance data of this design are given in Appendix A.

Table 3-1: Design parameters and Boundary Conditions for the BASE rotor blade

Property	Value	Property	Value
Inlet Total Pressure	195.218 kPa	Shroud Radius	0.141277 m
Inlet Total Temperature	483.35 K	Mean Solidity	0.8
Tip Mach Number	0.9	Mean Chord	0.0273 m
Rotation Speed	26286	Hub-to-Shroud Ratio	0.806738
Inlet Flow Direction	Axial	Hub Thickness	7% chord
Nominal Tip Clearance	0.4% chord	Tip Thickness	3% chord
Flow Coefficient	0.5	Stacking Line Location	0.5 chord
Blade Number	45	Profile Type	DCA

(a) Radially Stacked Blade, 3D View   (b) Tip Profile
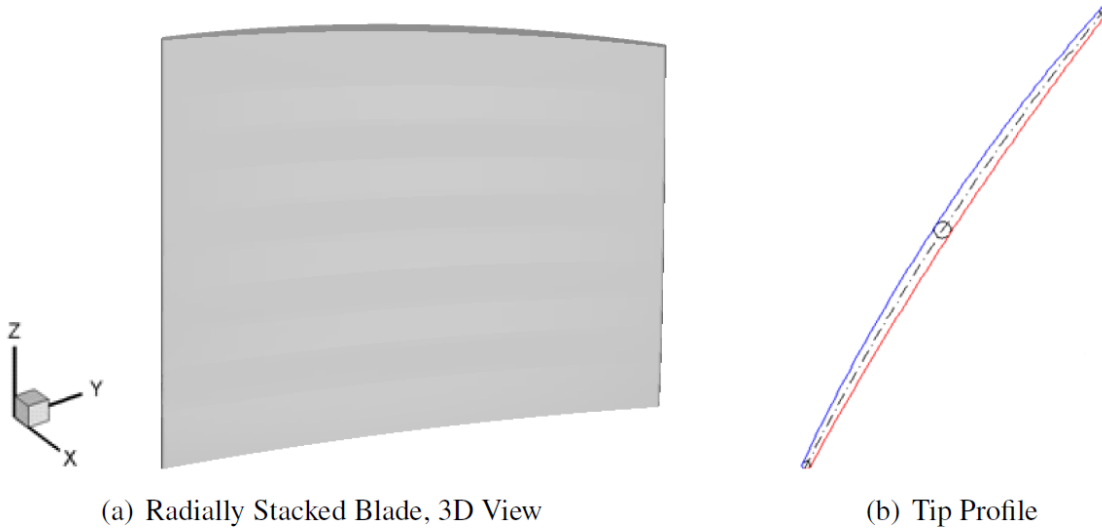
Figure 3-1: Geometry of the BASE rotor in 3D view and blade profile at tip (Erler 2012)

Gas Path Contouring

Kroger et al. (2009) mentioned that their local casing contouring through an optimization scheme resulted in increased meridional velocity near the tip. With this inspiration, one can consider using gas path curvature to significantly alter the spanwise meridional velocity distribution. If one assumes a constant spanwise total pressure distribution, skewing the meridonal velocity in favour of the tip region is possible with a concave gas path at the inlet of the rotor combined with irrotational flow upstream of the rotor as illustrated in Figure 3-2.
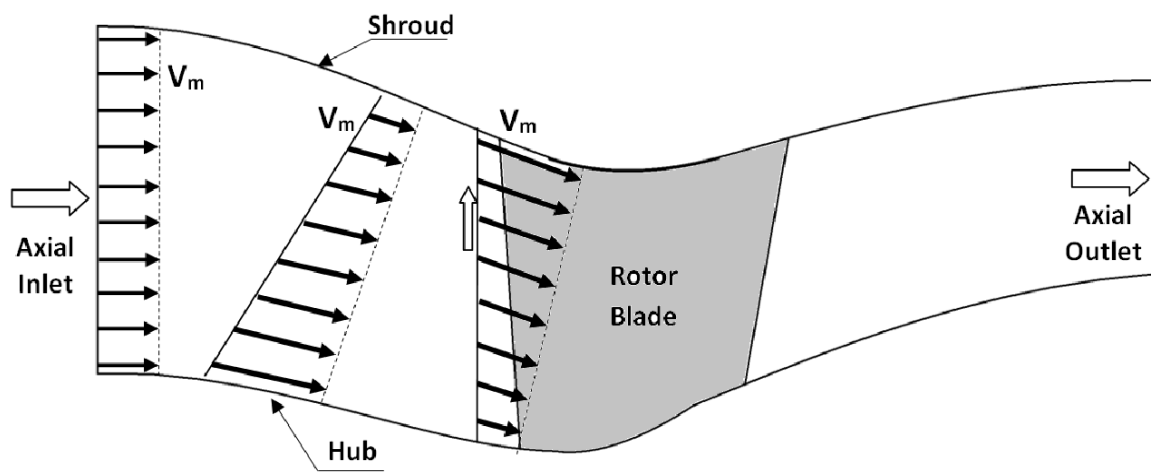
Figure 3-2: Predicted effect of concave gas path on rotor inlet meridional velocity

The amount of curvature is an important consideration when implementing this strategy. While a larger curvature would, from an inviscid flow perspective, greatly increase the meridional velocity in the tip region and thus the tip desensitization effect, in reality it could also create substantial boundary layer separation at the endwall and diminish or annul any increase in tip meridional velocity. In this case, the curvature of the gas path is limited with 10 degrees of average slope between leading edge and mid-chord, a value chosen to be on the edge of endwall boundary layer separation. Another consideration is isolating the effect of meridional momentum change on desensitization. A change in blade loading distribution, particularly in the tip region, as a result of gas path curvature would have a significant impact on sensitivity on its own. This effect should thus be eliminated for an accurate assessment of the desensitization effect of gas

path curvature through increased incoming tip meridional velocity. Thus, the rotor geometry itself was also altered from the BASE geometry through changes in camber and stagger to preserve as closely as possible the spanwise loading distribution of the BASE rotor. Figure 3-3 shows the concave gas path design in comparison to that of the BASE rotor geometry.

Conventional Gas Path   **Concave Gas Path**
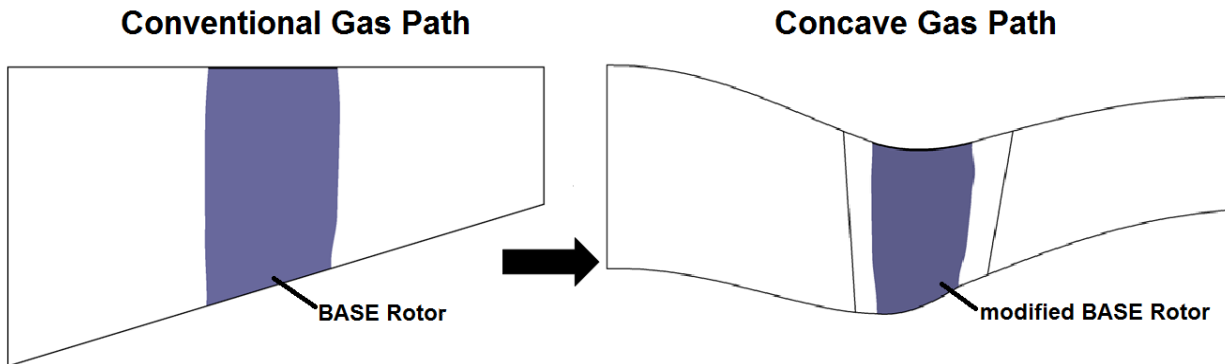
Figure 3-3: Side views of the BASE rotor gas path versus concave gas path design

Casing Treatment

    As mentioned in chapter 2, some of the data from past research indicates that casing treatment in the form of slots and circumferential grooves can reduce performance and aerodynamic stability sensitivity to tip clearance. However, the authors of these studies did not explain the flow mechanism associated with this effect. Based on the conclusions of the recent work by Erler (2012), one can hypothesize that this effect is linked to the reduction of double leakage, especially in cases when the axial extent of the casing treatment is confined to the blade passage, which is the majority of cases studied, and thus has little influence on the incoming meridional momentum upstream of the rotor leading edge. For axial slots, this mechanism may be associated with the flow recirculation from the rear of the blade passage which is re-injected at the front of the blade passage to increase the streamwise momentum of the tip clearance flow, resulting in a decrease of tip clearance fluid reaching the adjacent blade pressure side and thus reducing double leakage. In the case of circumferential groves, the hypothesis proposed in the current study is that the circumferential ridges created by the grooves block the upstream motion of the fluid exiting

the tip clearance and deflecting the flow toward the downstream direction so that it would be less likely to reach the adjacent blade and become double leakage. The proposed mechanism is illustrated in Figure 3-4.
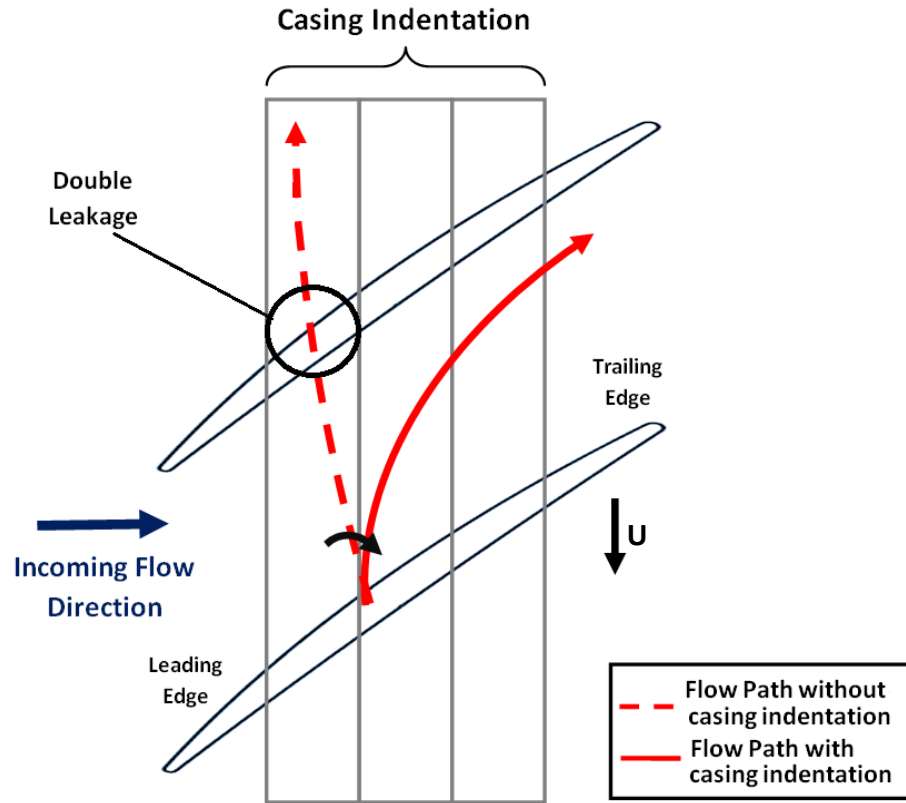
Figure 3-4: Proposed mechanism for tip desensitization by circumferential grooves casing treatment through double leakage prevention/reduction

While the literature review shows that slot type casing treatments are superior to grooves in terms of stall margin improvement, they generally come with significantly higher loss in nominal efficiency. However, the goal of tip desensitization is to reduce the change in stall margin with tip clearance rather than to improve its nominal value, which should already be sufficient for a working design. Consequently, a circumferential grooves casing treatment is a better choice as its application on an existing rotor design entails a much lower performance penalty than axial slots. In addition, according to the literature, geometrical design parameters such as groove depth, axial extent, axial location and groove numbers seem to have important effect on nominal performance and sensitivity to tip clearance. Past research, such as that of Muller et al. (2007), showed that the

nominal efficiency penalty increases with groove depth. For desensitization, these conclusions would point to restricting the depth of the groove. For axial location, the results of Wilke and Kau (2002), Shabbir and Adamczyk (2005) and Mileshin et al. (2008) point to groove location nearer the leading edge as being more effective in terms of mass interactions with the passage flow. Given the proposed mechanism for reducing double leakage as shown in Figure 3-4 and the fact that the tip clearance fluid leading to double leakage (see high-entropy - red- streamlines in Figure 3-5(a)) emanates from the central region of the blade chord, the grooves should be placed in the mid-chord region.
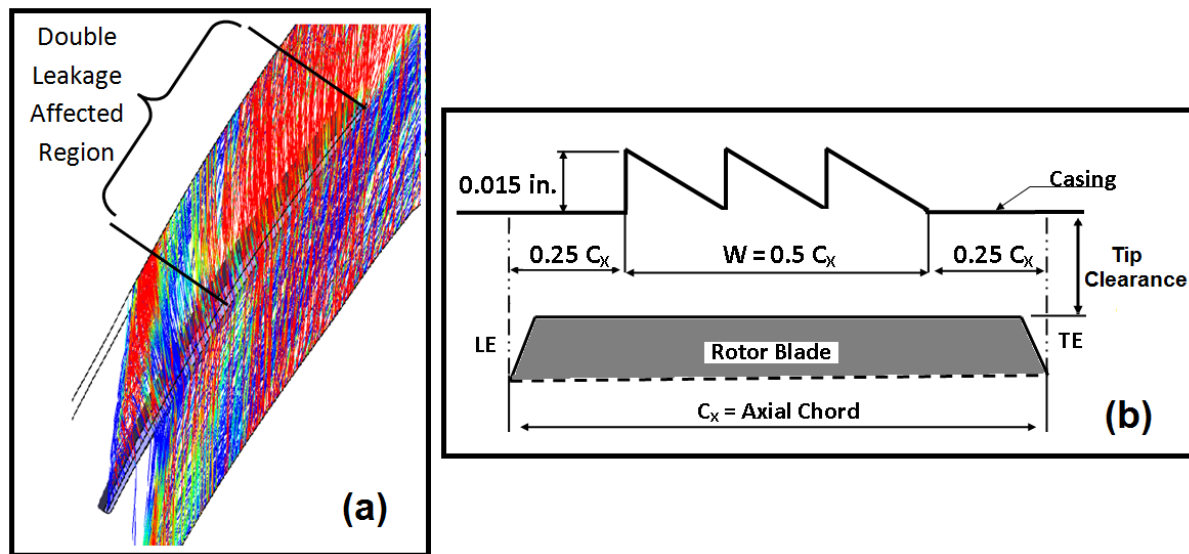
Figure 3-5: (a) Location of double leakage flow detected through entropy of streamlines emanating from tip clearance for BASE rotor at minimum tip clearance and (b) cross-sectional view of proposed nominal casing treatment design for tip desensitization

Based on the above reasoning, the proposed casing treatment for desensitization, illustrated in Figure 3-5(b), consists of very shallow (depth on the order of tip clearance size) triangular cross-sectioned circumferential indentations located in the mid-chord region of the blade passage. The three triangular saw tooth shape indentations are meant to provide enough ridges in the central chord region to deflect the tip clearance flow that would otherwise lead to double leakage. The shallow depth and lack of back steps (as would exists in rectangular grooves) for upstream flowing tip clearance fluid should minimize nominal performance loss. Table 3-2 gives

quantitative details of this nominal casing treatment configuration whose indentation shape is henceforth referred to as negative sawtooth.

Table 3-2: Design parameters for the nominal desensitizing casing treatment design

Parameter	Nominal Design
Shape	Negative Sawtooth
Depth	15×10^{-3} inch
Indentation Width	½ Axial Chord
Groove Number	3 Groove
Location	Mid-Located

Assessment of Desensitization and Selection of Strategy

The next step is to validate the effectiveness of each of the two proposed gas path strategies in reducing the sensitivity of performance and aerodynamic stability to tip clearance increase. The sensitivity analysis involves simulating a configuration involving the gas path and rotor at nominal (0.005 in.), medium (0.010 in.) and large (0.015 in.) tip clearance through shroud radius increase, as recommended by the project industrial sponsor (Pratt & Whitney Canada) at the same corrected mass flow, whose value is taken here as that of the BASE rotor maximum efficiency point. For the performance sensitivity, plots of total pressure ratio and total-to-total efficiency versus tip clearance size are produced for both the BASE rotor and the studied gas path desensitization design. The slope of each curve represents the sensitivity of each parameter to tip clearance. For aerodynamic stability, the leading edge spillage criterion of Vo et al. (2008) is employed, by plotting the axial position of the incoming/tip clearance flow interface (taken at a pitch location close to the pressure side, as detailed in Appendix B) with respect to the rotor leading edge plane versus tip clearance size. The stability sensitivity is the slope of this curve. The comparison of the slopes of these curves for the a gas path desensitization strategy with the cooresponding slopes for the BASE rotor gives the change in the sensitivity to tip clearance of

performance of stall margin, while the comparison of the values at minimum tip clearance gives the change in nominal performance and an indication of the change in nominal stall margin.

In addition, the spanwise distribution of incoming meridional momentum or velocity and the variation of double tip leakage (see Appendix B) with tip clearance size are produced to analyze the flow mechanism associated with the observed desensitization effect.

Given the time limitation of the current project, only the most effective of the two proposed gas path desensitization strategies will be studied in detail to develop preliminary design rules and assessment for real compressor application. The selection is primarily based on the reduction in sensitivity but will also include practical considerations involving cost and integration into a multi-stage aeronautical compressor environment.

3.2 Parametric Study and Optimization
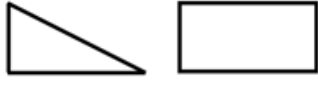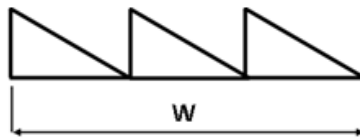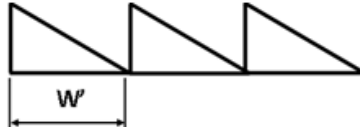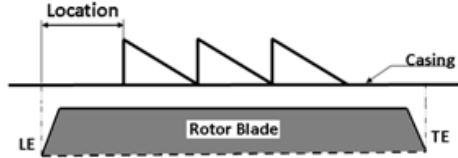
A parametric study is subsequently carried out for the most promising one of the two proposed gas path design strategies by individually varying each geometric design parameter and carrying out the CFD simulations to assess its effect on desensitization and nominal performance. This parametric study serves to optimize, on a very preliminary basis, the design in terms of maximizing the desensitization effect and minimizing penalty in nominal (minimum tip clearance) performance and stall margin. In addition, a detail analysis of the simulations in the parametric study should also reveal the effect of each parameter on the desensitizing flow mechanism and help to determine the preliminary design rules in terms of the trends associated with the variation of each geometric design parameters.

For the gas path contouring strategy, the main geometric design parameter is the radius of curvature. For the circumferential groove casing treatment strategy, the geometrical design parameters are illustrated in Table 3-3 and described below:

- Shape: The cross sectional shape of the indentation.
- Depth: Depth of the groove which lays between the nominal rotor casing radius and the highest radius point of the indentation geometry.
- Indentation width: Total axial length of the casing indentation (W).
- Groove number: Number of grooves at a certain indentation width which is also the measure of width of each single groove (W').

- <u>Location</u>: Axial distance between the rotor blade leading edge and the front of the indentation.

Table 3-3: Design parameters of a casing indentation

An improved gas path design configuration will be produced from the parametric study and will be applied to the BASE rotor design. Simulations will be carried out to determine the change in sensitivity and nominal performance compared to the nominal gas path design configuration and the BASE rotor configuration.

3.2.1 Integration with Blade Design Strategies

The improved gas path design configuration from the parametric study will then be combined with the best blade desensitization strategy to see if the desensitizing effects for gas path and blade design strategies can be added to further reduce performance and stall margin sensitivity to tip clearance. This combination could also serve to remove any nominal performance penalty brought by the gas path design strategy. For the BASE rotor geometry used in this study, Erler

(2012) had applied blade geometry desensitizing strategy to produce the least tip sensitive rotor with the same spanwise loading in the form of the full forward chordwise swept (FFCS) rotor, shown in Figure 3-6. The improved gas path design strategy for desensitization will thus be applied to this rotor and simulations carried out to evaluate the change in sensitivity and nominal performance/stall margin from the combination of versus individual gas path and blade desensitizing design strategies.

(a) BASE   (b) FFCS
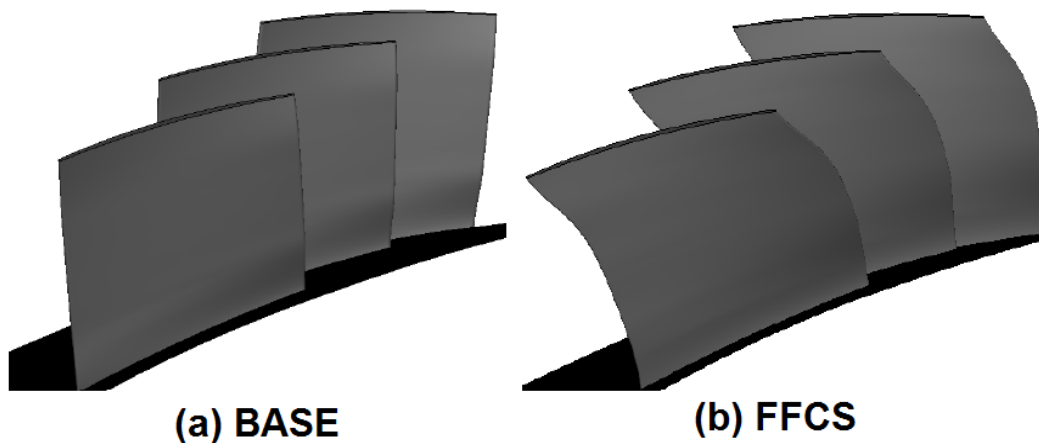
Figure 3-6: 3D view of (a) BASE and (b) FFCS blade designs (Erler 2012)

3.2.2 Preliminary Assessment for Real Compressors

Up to this point, the study is limited to an isolated axial compressor rotor. The final step for this study is a preliminary assessment of whether the chosen desensitizing gas path design strategy would work in a real aeronautical compressor environment. First, a stator is designed for and added to the optimized configuration of section 3.1.2 to determine if and how much of the desensitization effect for the rotor carries into an axial stage environment. Finally, the chosen desensitizing gas path design strategy is applied to non-axial compressor rotors in the form of a mixed flow rotor and a centrifugal compressor impeller, which are described in section 4.4.2 and 4.4.3 to see if it brings about any reduction in performance and stall margin sensitivity through one of the two desensitizing flow features.

3.3 Computational Setup

3.3.1 Computational Tool Selection

ANSYS CFX version 13.0 is chosen as the computational tool to carry on this study. ANSYS CFX is a Computational Fluid Dynamics (CFD) code that solves the Reynolds-Averaged-Navier-Stokes (RANS) equations with a pressure based, coupled implicit algorithm. It is able to solve the flow field with structured or unstructured mesh grids. It has a robust convergence characteristic that gives the ability to get a steady state convergence typically within a few hundred iterations. The more accurate computational techniques such as Large Eddy Simulation (LES) and Direct Numerical Simulation (DNS) are not employed for this research due to their excessive computational time and resource requirement compared to the current technique. Moreover, current software is commonly used and recommended by Pratt & Whitney Canada (P&WC).

The computational tool validation for ANSYS CFX version 13.0 was carried out by Erler (2012) with the NASA Rotor 37 transonic compressor geometry. The design of this blade is explained by Reid and Moore (1978) in detail and used as the validation case for numerous studies. Its tip leakage flow is demonstrated experimentally by Suder et al. (1996) and numerically by Chima (1998). According to this knowledge, the previously described computational settings were validated by comparing blade passage flow fields at 70% and 95% span locations and the total pressure ratio at the design point.

3.3.2 Computational domain

A single rotor blade passage is solved in steady state with the rotational frame used as the reference frame and periodic condition assigned to the circumferential boundaries, as shown in Figure 3-7. The inlet boundary condition is defined with spanwise distributions of stagnation (total) pressure (P_t), stagnation temperature (T_t) and flow swirl angle (α). An average static pressure (P_s) value is specified for the outlet condition. For the turbulence settings at the inlet boundary, a medium turbulence intensity (Tu=5%) and local length (l=0.5 span) are used. The inlet and exit axial planes are placed more than one pitch away from the blade leading and trailing edges. Given that the amplitudes of circumferential perturbations takes about one wavelength to attenuate to zero and the use of circumferentially uniform pressure inlet and exit

boundary conditions, the chosen upstream and downstream duct length ensures that perturbation up to one pitch in wavelength in the blade passage can be captured by the simulation. A no-slip boundary condition is applied at all solid surfaces and the shroud is assigned as counter rotating wall in the frame of reference of the rotor.

As high speed flow is simulated, the flow is defined in CFX as an ideal gas for compressibility to be taken into account. In order to calculate the temperature variation accurately at high speed flow conditions, the total energy equation is solved by including the viscous work term. Due to the high Reynolds number ($5\times10^5 - 7\times10^5$ based on axial chord) and the overall positive pressure gradient through the blade passage, the boundary layers can be assumed fully turbulent such as a boundary layer transition model is not used. ANSYS CFX includes many two-equation models such as the $k - \omega$, $k - \varepsilon$ and Shear Stress Transport (SST) models. The SST is a model which combines the $k - \omega$ model near the wall regions and the $k - \varepsilon$ model in the bulk flow (ANSYS 2006). This model is chosen as it has been shown by Liu et al. (2008) to best predict the tip vortices associated with the flow field in the rotor blade tip region. (However, later simulations of the chosen gas path design strategies were carried out for selected cases with both the SST and $k - \varepsilon$ turbulence models to evaluate the effect of the turbulence model on the results. The results of these simulations are presented in Appendix C and indicated that the choice of turbulence model did not affect the observed sensitivity reduction.)

The curved endwall regions of contoured gas path designs caused severe boundary layer separations on the blade suction surface near the tip and at the endwall region near the hub. In order to overcome this problem hub walls at the inlet and exit of the rotor passage are set as free-slip wall by dividing the flow domain into three parts referred to as inlet, rotor passage and, exit zones, as shown in Figure 3-8.

(a) Spanwise cut   (b) Meridional cut
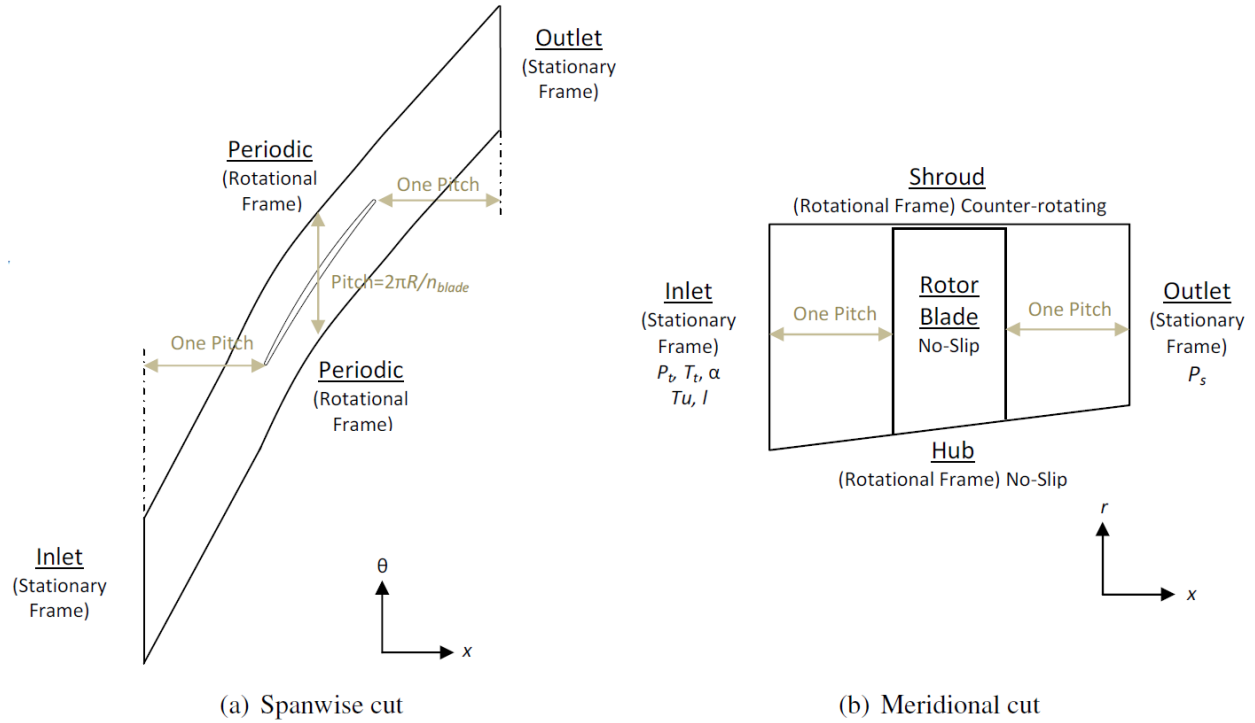
Figure 3-7: Definition of the computation domain of the baseline rotor blade (Erler 2012)
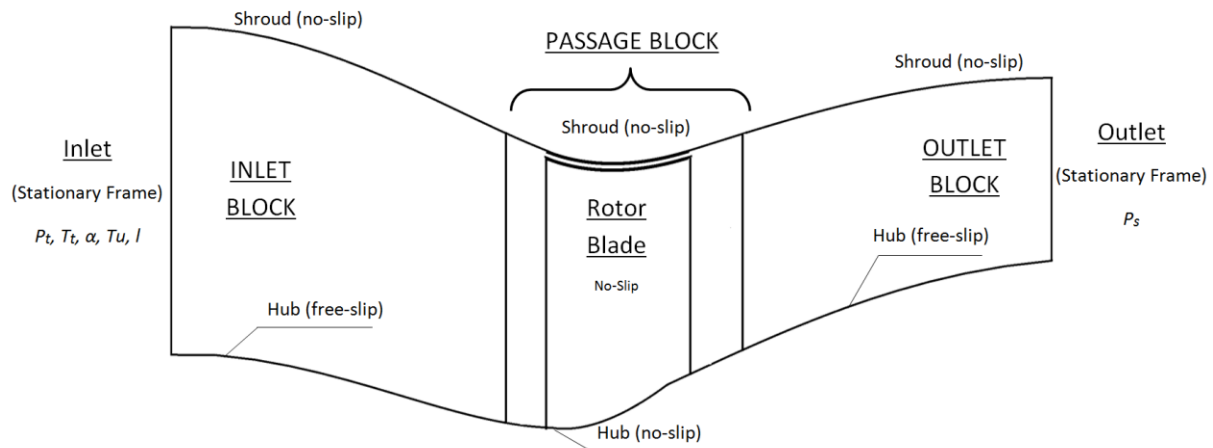
Figure 3-8: Definition of the computation domain of a gas path contoured rotor

For the configurations with casing treatment, the casing indentation has to be modeled in a separate domain adjacent to the rotor domain shown in Figure 3-9. The rotor domain is meshed exactly in the same manner and with the same software (ANSYS TurboGrid) as Erler (2012) to

maintain commonality for ease of comparison. The choice of two domains is then necessary because the mesh generation software does not allow for generating a single structured mesh for the blade flow domain in combination with the casing indentation. The rotor domain is defined as rotating and the casing treatment as stationary. The asymmetric nature of the casing indentation lends itself to fast and efficient steady simulations. However, these simulations would only be physically meaningful if the circumferential variation in flow properties at the interface between the groove and blade domains can be captured. Thus, instead of a mixing plane interface commonly used in steady CFD simulations, the frozen-rotor interface in CFX is used between the two domains. This interface option is made for simulating adjacent rotating and stationary domains assuming a fixed relative position to allow the flow field information to be transferred between them without any circumferential averaging. This interface is perfectly suitable for axisymmetric grooves since the interaction between two domains is independent of relative position. Past studies such as those of Muller et al. (2007), Wilke et al. (2002) and Mileshin et al. (2008) used a similar setup to simulate circumferential grooves. Finally, as a consequence of setting the casing treatment domain stationary, the shroud wall of this domain is defined as no-slip, stationary wall as shown in Figure 3-9. (For verification, later simulations were carried out for selected cases in unsteady mode using a sliding plane interface between the rotor and casing indentation domain. The results and analysis presented in Appendix E show that unsteady simulations affect the absolute value of nominal performance and sensitivity reduction but not the observed trends nor the proposed mechanism behind the desensitization effect.)
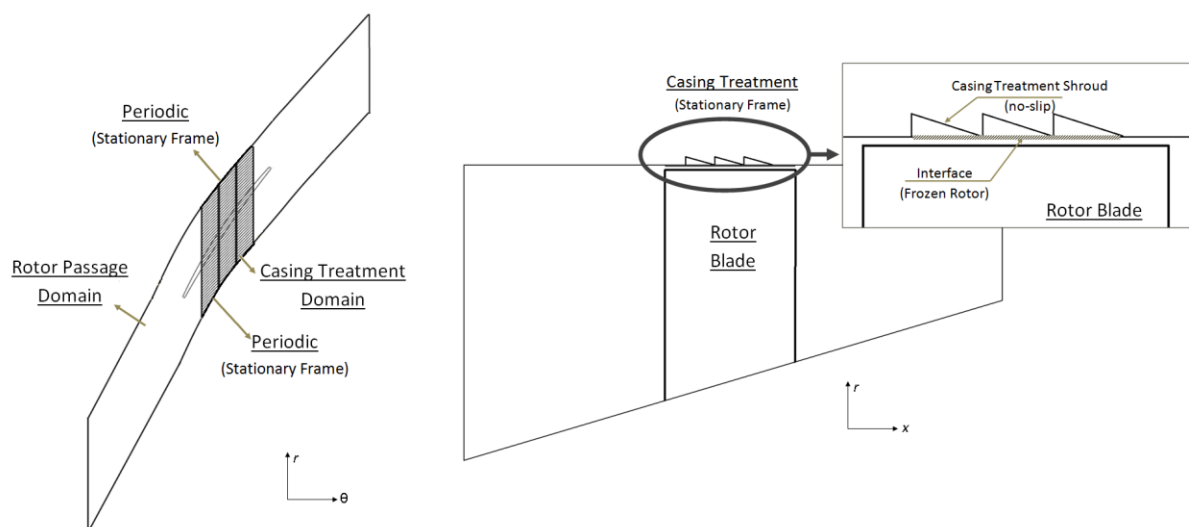
Figure 3-9: Computation domain of a rotor passage with casing treatment/indentation

With the groove domain placed on the top of the blade domain other as illustrated in Figure 3-10, the open area of the casing treatment can not be specified on the rotor shroud surface. To overcome this problem, the mixed-cell approach is employed, which is a computational method to patch interface boundaries of two different domains. The method allows the solver to consider the cells on the rotor shroud as a part of fluid domain when they are matched with open area of the casing treatment and as a wall if there is no match. The mixed-cell approach is a method tested and verified in studies such as that of Yang et al. (2003) who solved casing treatment-rotor interaction problems.
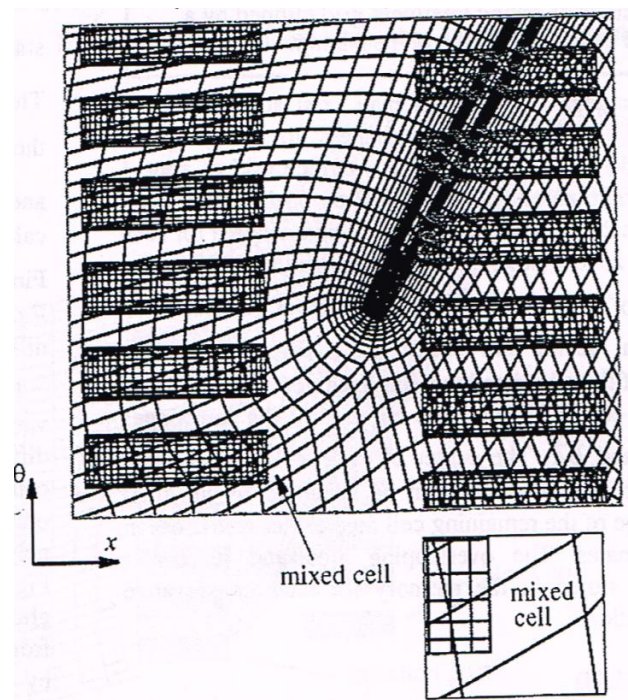
Figure 3-10: Schematic of zonal interface between casing treatment and blade passage
(Yang, et al. 2003)

For an axial stage simulation, the rotor and stator domains are solved in steady-state mode with a mixing plane (stage) interface, which transfers circumferentially-averaged flow properties between the rotational and stationary domains. While transient rotor-stator interactions such as wakes are not captured, this method is appropriate for use when the circumferential variation of

the flow is of the order of the component pitch (ANSYS 2010) and for compressor performance prediction at a stable operating point close to peak efficiency as is the case in this study.

3.3.3 Computational Mesh

The mesh generation is handled for the rotor flow domain and the casing indentation geometries separately. ANSYS TurboGrid is employed in order to generate the rotor domain mesh and GAMBIT is used for the casing treatment/indentation domains.

ANSYS Turbogrid is a meshing software integrated into CFX, specialized for generating structured mesh for turbomachinery. The required mesh convergence study for the BASE rotor flow domain had been conducted by Erler (2012) as shown in Appendix D. Since the same basic rotor geometry and mesh is used for the current study, the same mesh settings for the blade domain are used. The mesh is formed with high mesh density at the vicinity of leading and trailing edges. By assessing Reynolds Number in the range of 5×10^5 to 7×10^5 the starting length (y^+) is set around 1, as required for the no-slip boundary condition. The number of nodes in the blade boundary layers is 15 surpassing the minimum of 10 nodes recommended by ANSYS (2006) for accurate results with SST turbulence model. The grid stretching ratio is below the recommended maximum value of 1.2. The spanwise mesh distribution in the tip clearance is set at 20 for the nominal tip clearance size (0.005 in. or 0.47% of tip chord) which is a above the minimum recommended number by Van Zante et al. (2000) for adequate capture of flow physics in the tip region (at least 12 cells for 1.3% tip chord). The tip clearance gap is meshed non-uniformly in the spanwise direction by expanding from y^+ ~ 1 at the shroud to the higher values towards the blade tip region. While the y^+ value may be higher than 1, the SST turbulence model automatically switches between no-slip condition and wall function according to the y^+ value (ANSYS 2006). For the case of the contoured gas path, the mesh is adjusted for the larger axial extent of the domain, adding 50,000-100,000 nodes to the standard rotor domain. As for the mixed flow rotor and centrifugal impeller whose geometries are provided by Pratt & Whitney Canada (P&WC), the corresponding meshes also provided by P&WC are used without modification.

GAMBIT version 2.4.6 is used to generate the mesh of the casing treatment (indentation) domain. Since the casing indentation domain is an extension of rotor flow domain, the mesh settings and the density is kept exactly the same as the rotor domain mesh, particularly in the spanwise direction. In streamwise and pitchwise direction mesh density is increased in order to reflect the effect of the casing treatment shapes more accurately. A convergence study is made on the baseline casing indentation mesh with BASE rotor for both total-to-total pressure and total-to-total efficiency. Based on the results of this study, as presented in Figure 3-12:   and Figure 3-13, the mesh used for the nominal indentation geometry presented in Figure 3-5 (b) has 30 nodes in streamwise, 40 nodes in spanwise, and 80 nodes in pitchwise direction. The use of a structured mesh requires the indentation profile to be modified to remove the sharp edge of the triangular cross section, as schematically illustrated in Figure 3-14. The mesh density is kept the same for all design configurations generated for the indentation parametric study described in section 3.2.
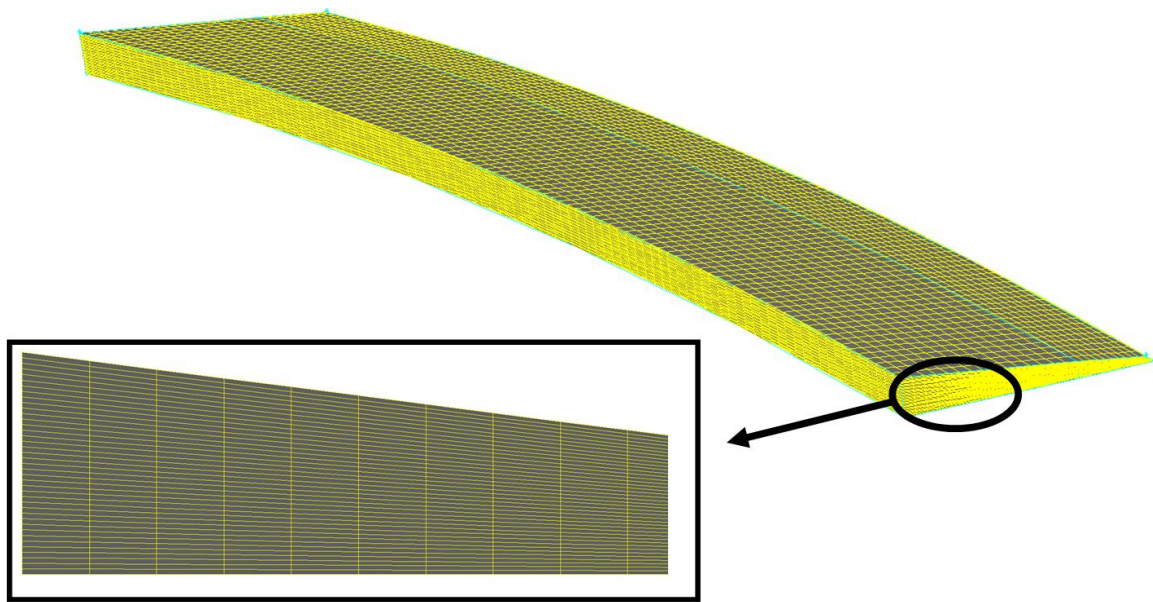
Figure 3-11: Mesh of a casing indentation groove
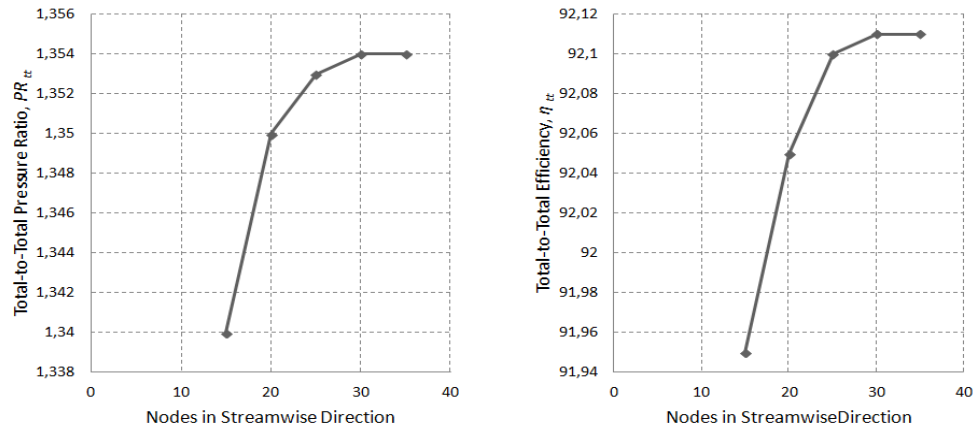
Figure 3-12: Casing indentation streamwise mesh convergence of performance parameters
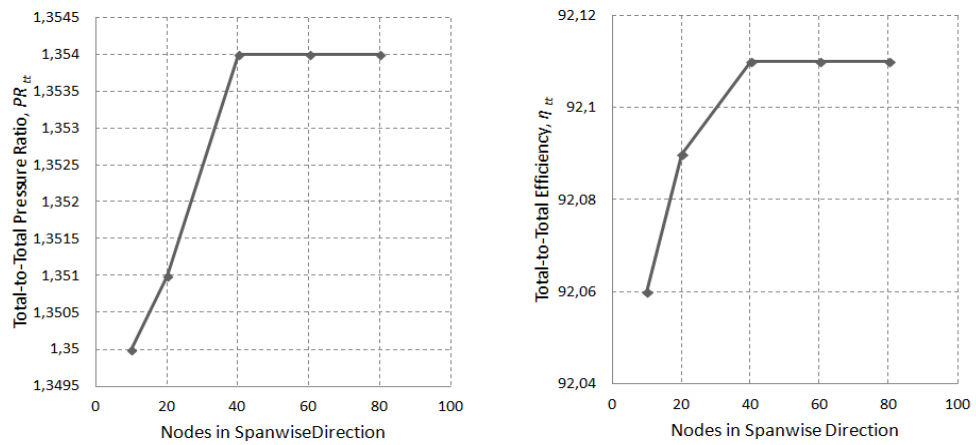
Figure 3-13: Casing indentation spanwise mesh convergence of performance parameters
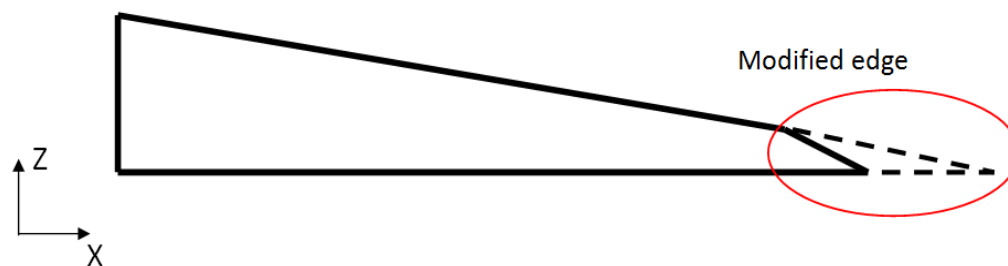
Figure 3-14: Schematic representation of the modification of casing indentation cross section

CHAPTER 4   RESULTS

This chapter presents the results of this research in the order laid out by the roadmap presented in section 3.1. First, an assessment and comparison of the two proposed gas path designs for desensitization, namely gas path contouring and shallow circumferential indentation casing treatment, is carried out to select the most promising strategy. Second, the results and analysis of the parametric study of the selected strategy are presented, leading to an improved design for the reference rotor configuration whose effectiveness is evaluated. Third, the sensitivity results from the combination of the improved gas path design configuration with a rotor design with reduced tip sensitivity are presented and evaluated in terms of the addition of desensitizing design features. The last part shows the results of a preliminary sensitivity analysis of the selected gas path design strategy applied to an axial stage and non-axial compressor rotors.   All the simulations involving axial compressors throughout this chapter are taken at the maximum efficiency corrected mass flow of the BASE rotor at minimum (0.005 in.) tip clearnce which corresponds to 3.04 kg/s.

4.1 Evaluation of Gas Path Design Strategies for Desensitization

4.1.1 Contoured Gas Path

The concave gas path designs generated in order to test the validity of contoured gas path design strategy are presented in Figure 4-1. As mentioned in section 3.1.1, the BASE blade geometry was adjusted to take into account change of incidence and endwall boundary layer behaviour to preserve as closely as possible the loading distribution of the BASE rotor, as shown in Figure 4-2 , while avoiding blade boundary layer separation at the design corrected mass flow of 3.04 kg/s. The definition of the loading distribution is given at Appendix B.

An evaluation of the two desensitizing flow features proposed by Erler (2012) is presented in Figure 4-3. The left plot indicates that the concave gas path increases the meridional velocity near the tip region by about 10% relative to straight gas path of the BASE design, as intended. The double leakage mass flow data on the right plot of Figure 4-3 shows that the concave gas path

design exhibits lower nominal double leakage value (expressed as proportion of tip leakage mass flow). The reduced nominal double leakage is accompanied by its lower sensitivity to tip clearance, a behaviour associated with increased incoming tip meridional momentum, as observed and explained by Erler (2012). The drop in double leakage with the concave gas path is evidenced by looking at the flow field. Figure 4-4 is a top view of the blade passage showing the tip clearance flow streamlines with colour according to entropy level. The high (entropy) streamlines entering the tip clearance gap are double leakage fluid that emanated from the adjacent tip clearance (explaining the high loss – high entropy) while the low entropy (blue) streamlines represents 'standard` tip clearance fluid coming from the pressure side core flow. One can observe that the amount of double leakage is noticeably reduced in the concave gas path design.
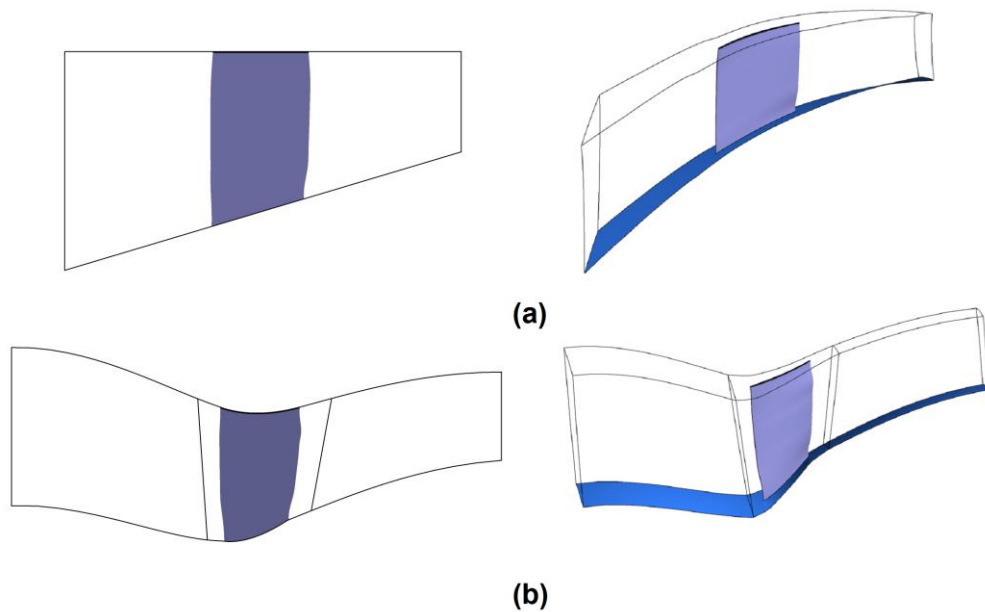
Figure 4-1: Geometries of (a) the BASE rotor and (b) the concave gas path design

The sensitivity analysis from CFD simulations at 3.04 kg/s corrected mass flow is presented in Figure 4-5 with tip clearance expressed as a percentage of rotor tip chord. The results show that the concave gas path design exhibits a slightly reduced tip clearance sensitivity of pressure ratio, efficiency and stall margin (as indirectly measured by the sensitivity of the incoming/tip clearance flow interface position as a fraction of tip axial chord x_{int}/c_x). However, the sensitivity reduction is barely noticeable and occurs only between nominal (0.005 in.) and medium (0.010

in.) tip clearance sizes. These modest results may perhaps be attributed to the limited increase in incoming meridional momentum associated with the limited gas path curvature imposed by end wall boundary layer separation considerations.

In addition, the concave gas path design brings about a large penalty in nominal performance (pressure ratio and efficiency). The source of this penalty is associated with an increase in the loss and blockage of the tip clearance region as evidenced in Figure 4-6 by the change in the high entropy region near the shroud between the inlet and exit plane, which is much more significant for the concave gas path design. Even though the concave gas path design exhibits less double leakage, Figure 4-4 indicates that its tip clearance flow have higher entropy (more red streamlines) which may perhaps be the results of increased shear loss from interaction with higher core flow velocity in the tip region. In addition, the larger tip blockage may be associated with the larger pressure gradient experienced by the tip clearance flow of the concave gas path as it turns from the mid-chord towards the trailing edge plane at higher radius. This hypothesis is based on the blockage development mechanism proposed by (Khalid, et al. 1999) as described in Figure 2-3.
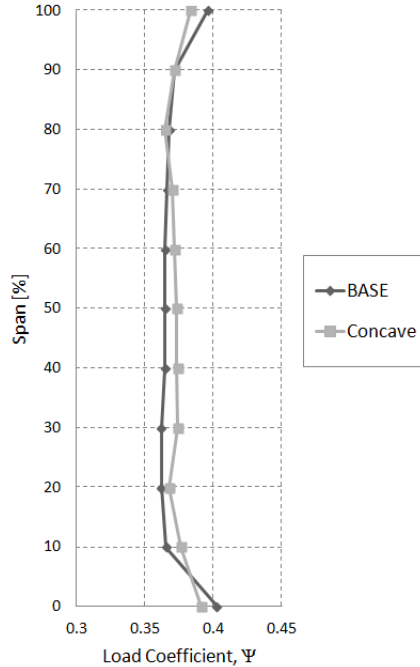
Figure 4-2: Spanwise loading of the BASE and concave gas path design at nominal tip clearance and design corrected mass flow rate (3.04 kg/s)
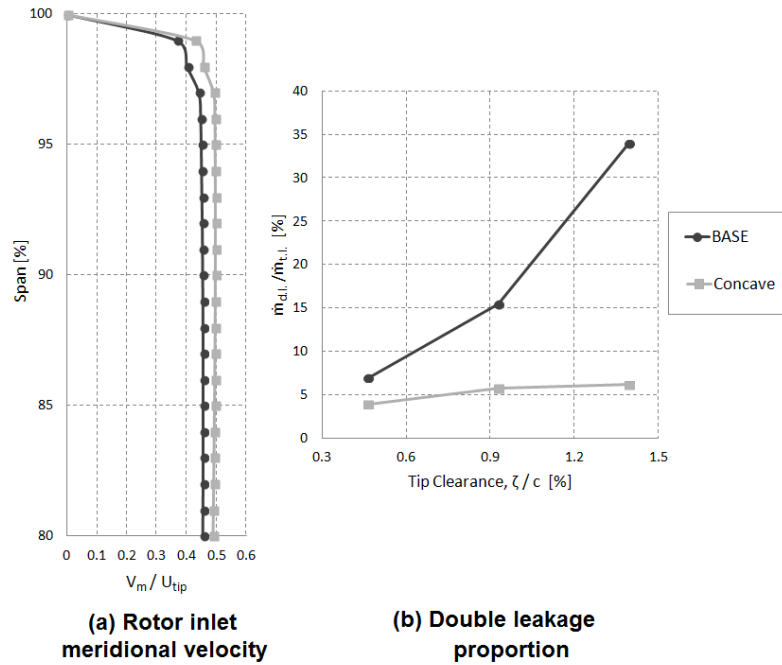
Figure 4-3: Evaluation of desensitizing flow features for concave gas path design
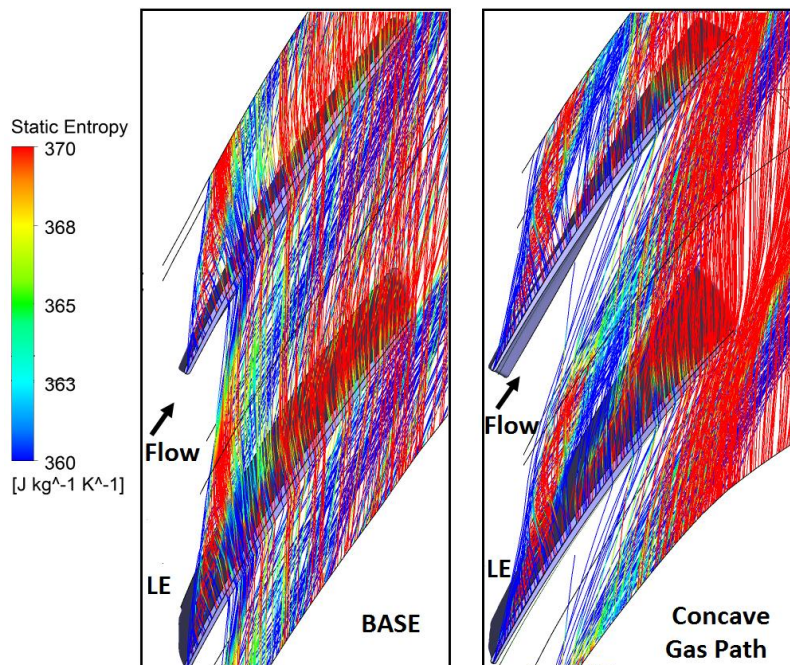
Figure 4-4: Tip leakage flow streamlines released from the suction surface side of the tip gap at

nominal t.c. size in relative frame, for the BASE and concave gas path designs
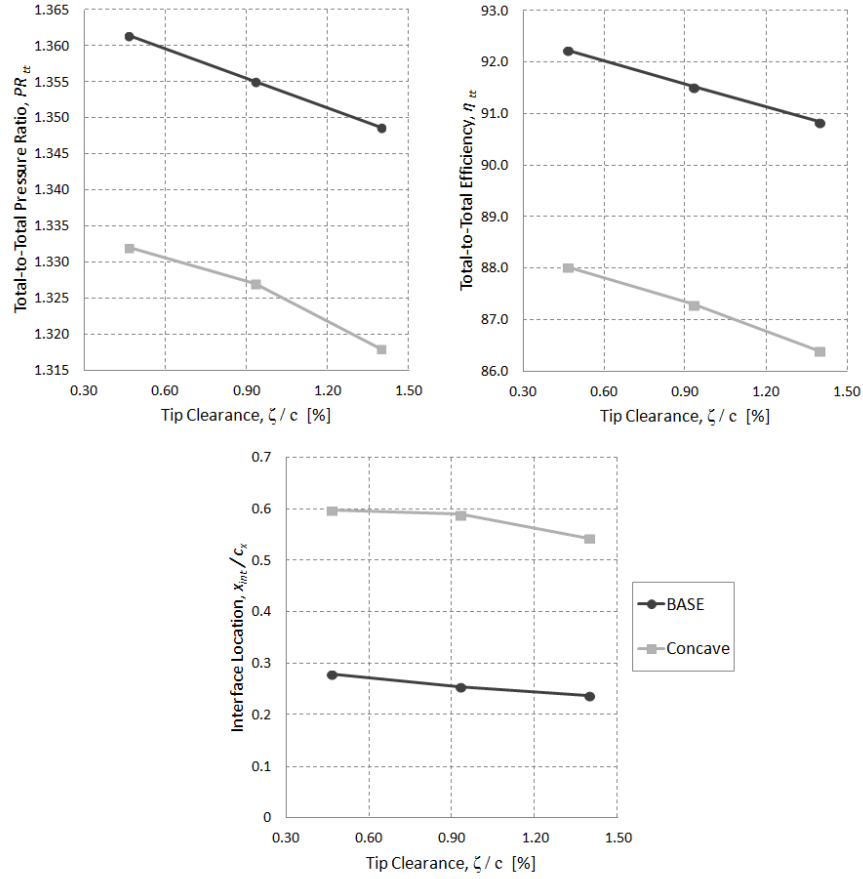
Figure 4-5: Sensitivity analysis for concave gas path design versus BASE rotor

In summary, the concave gas path strategy did accomplish the intended effect of increasing incoming meridional velocity in the tip region. However, this increase and the reduction in sensitivity is very small, in spite of the significant effort brought about to avoid endwall boundary layer separation by limiting the gas path curvature and blade redesign. In addition given geometrical constraints in length and gas path curvature in a real multi-stage compressor, it is highly unlikely that this design strategy would be effective in practice.
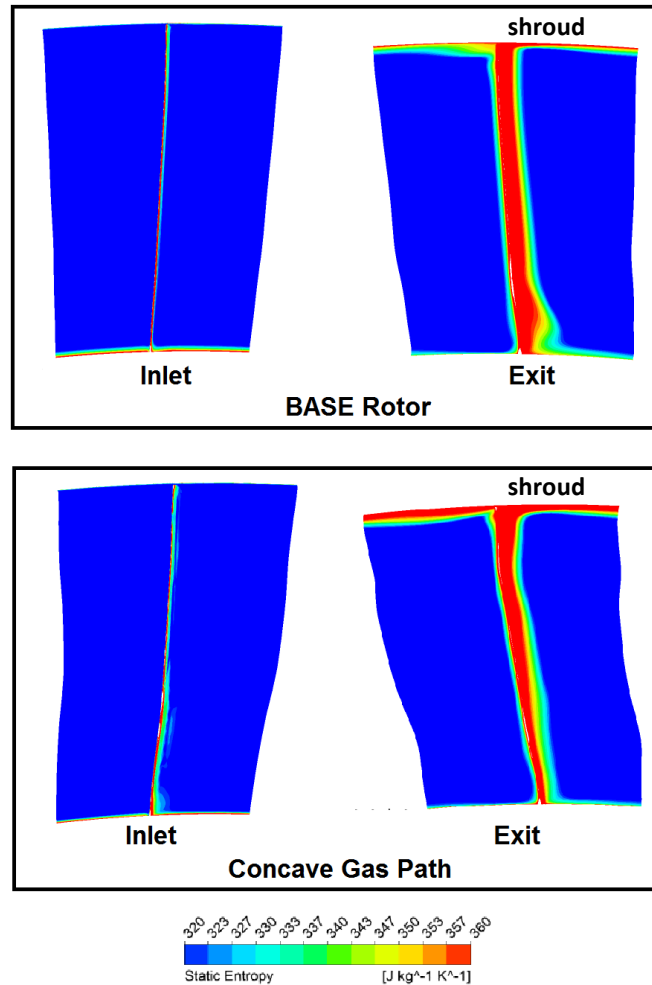
Figure 4-6: Entropy contours at rotor inlet and exit planes for BASE and concave gas path designs.

4.1.2 Casing Indentation

The casing treatment for tip desensitization with reduced performance penalty proposed and described in Figure 3-5(b) and Table 3-2 in the latter half of section 3.1.1 is shown formally to scale in Figure 4-7 with the BASE rotor. This configuration, henceforth referred to as the nominal negative sawtooth casing indentation, consists of three adjacent 0.015 inch deep triangular shape grooves (with the vertical wall or ridge on the upstream side of the indentation) covering the middle 50% of the axial extent of the blade passage.
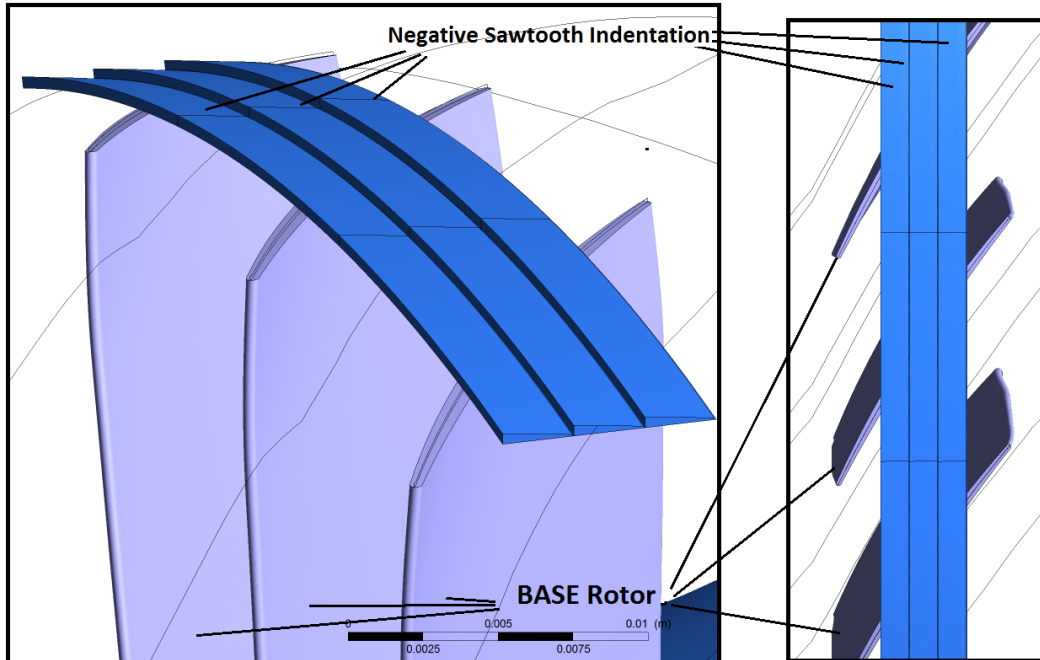
Figure 4-7: Nominal negative sawtooth casing indentation with BASE rotor

The results from CFD simulations of this nominal casing treatment were carried out at the three tip clearance sizes and 3.04 kg/s corrected mass flow and compared with the BASE rotor with smooth casing (no casing treatment). Figure 4-8 indicates that the application of the casing indentation did not reduce (but even slightly increase) the tip loading of the BASE rotor, as intended. Moreover, Figure 4-9(b) shows that the casing indentation decreases the double leakage by as much as 85% at the nominal (minimum) tip clearance gap while, as expected, having no influence on the incoming meridional velocity profile (Figure 4-9(a)). The reduction in nominal double leakage proportion can also be seen in the entropy coloured streamlines in Figure 4-10. Thus, the negative sawtooth casing indentation successfully isolated the second desensitizing flow feature proposed by Erler (2012).

Moreover, Figure 4-9(b) also indicates a reduction in the sensitivity of double leakage to tip clearance size. This is also evident by looking at the change in entropy contours at the tip clearance entrance at low and high tip clearance gaps for the BASE rotor with smooth casing (Figure 4-11) and with negative sawtooth casing indentation (Figure 4-12). The region with high

entropy at the vicinity of the shroud is double leakage fluid coming from the adjacent tip clearance gap while the rest of the gap region is filled with the fluid suctioned from the core flow ('standard' tip clearance fluid). One can observe that for the smooth casing case, the double leakage occupies a significant proportion of the tip clearance gap at 0.005 inch tip clearance and that this proportion is even larger at 0.015 inch tip clearance. With the casing indentation, the double leakage area proportion is small at minimum tip clearance and increases only modestly with tip clearance size, mostly in the grooves rather than in the tip clearance gap region.
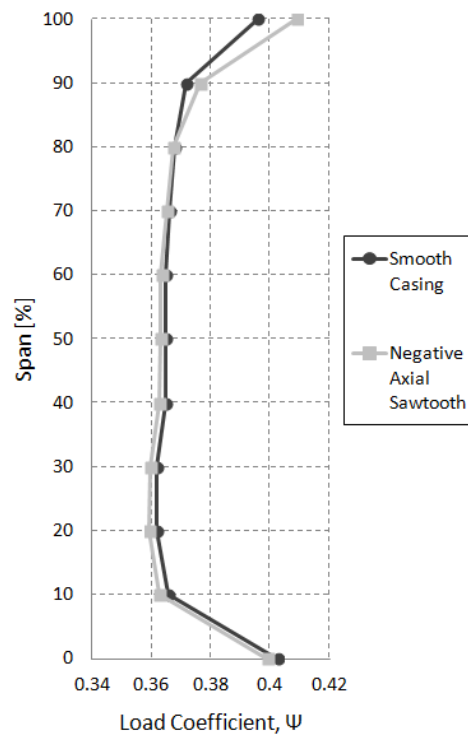
Figure 4-8: Spanwise loading of the BASE rotor with smooth casing and negative sawtooth casing indentation at nominal tip clearance and design corrected mass flow rate (3.04 kg/s)
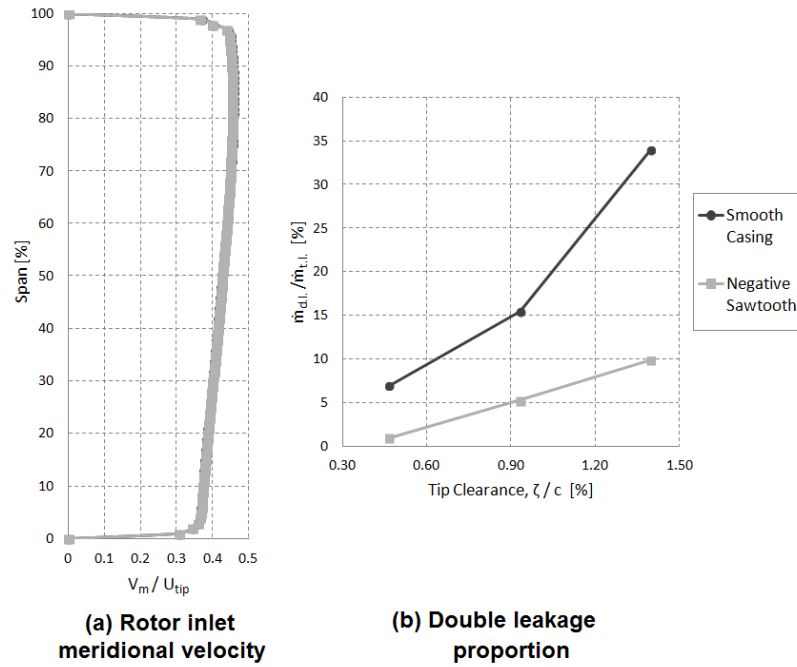
Figure 4-9: Evaluation of desensitizing flow features for nominal negative sawtooth casing indentation
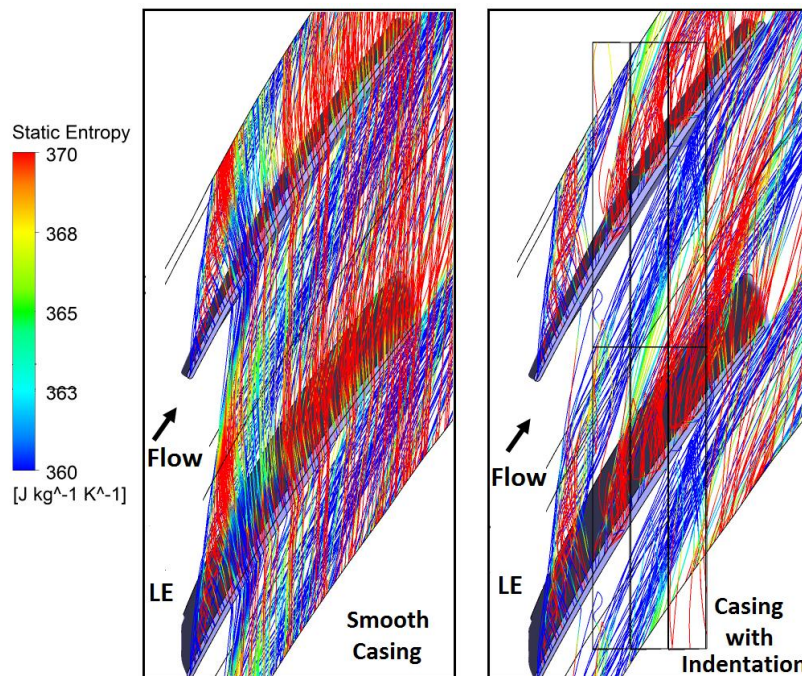
Figure 4-10: Tip leakage flow streamlines released from the suction surface side of the tip gap at nominal t.c. size in relative frame for smooth and negative sawtooth indentation casings
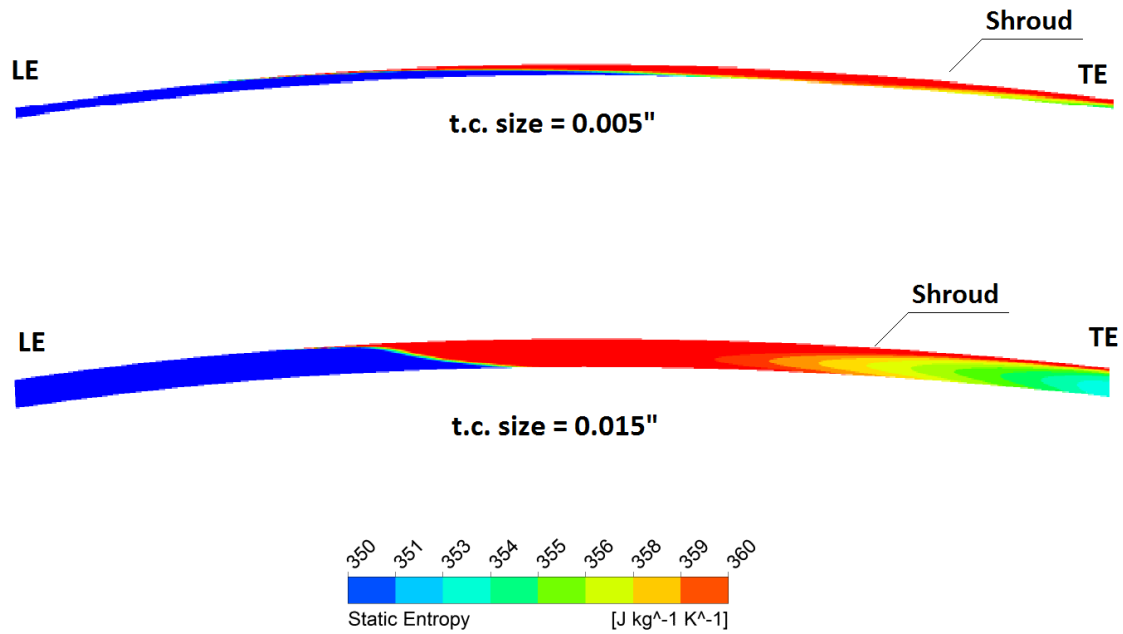
Figure 4-11: Comparison of static entropy distributions at pressure side of the tip gap of BASE
rotor with smooth casing, at nominal and maximum t.c. size
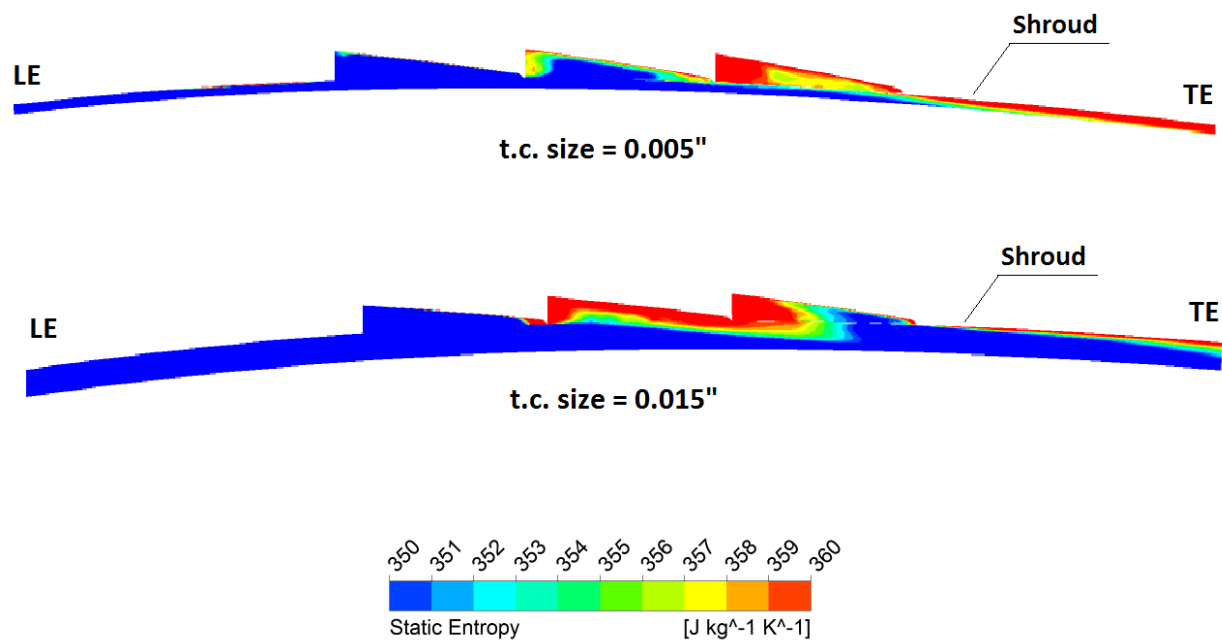
Figure 4-12: Comparison of static entropy distributions at pressure side of the tip gap of BASE
rotor with negative casing indentation, at nominal and maximum t.c. size

The sensitivity analysis results are presented in Figure 4-13 for the BASE rotor with smooth casing and with the nominal negative sawtooth casing indentation as well as the concave gas path design of section 4.1.1 for comparison. The data shows that the addition of the negative sawtooth casing indentation brings about a significant reduction the tip clearance sensitivity of pressure ratio, efficiency and stall margin (as measured by the incoming/tip clearance flow interface position), surpassing by far the desensitization effect of the concave gas path design. In addition, the nominal performance (pressure ratio and efficiency) penalty is also much lower than the concave gas path design. The only drawback is a slight penalty in nominal stall margin associated with the indentation that disappears at larger tip clearances. Based on the sensitivity and nominal loss results and given the fact that the shallow casing indentation is extremely easy to implement, even retroactively, in a real compressor, it represents a new and most promising gas path desensitization strategy which will be studied and improved in the rest of this chapter.
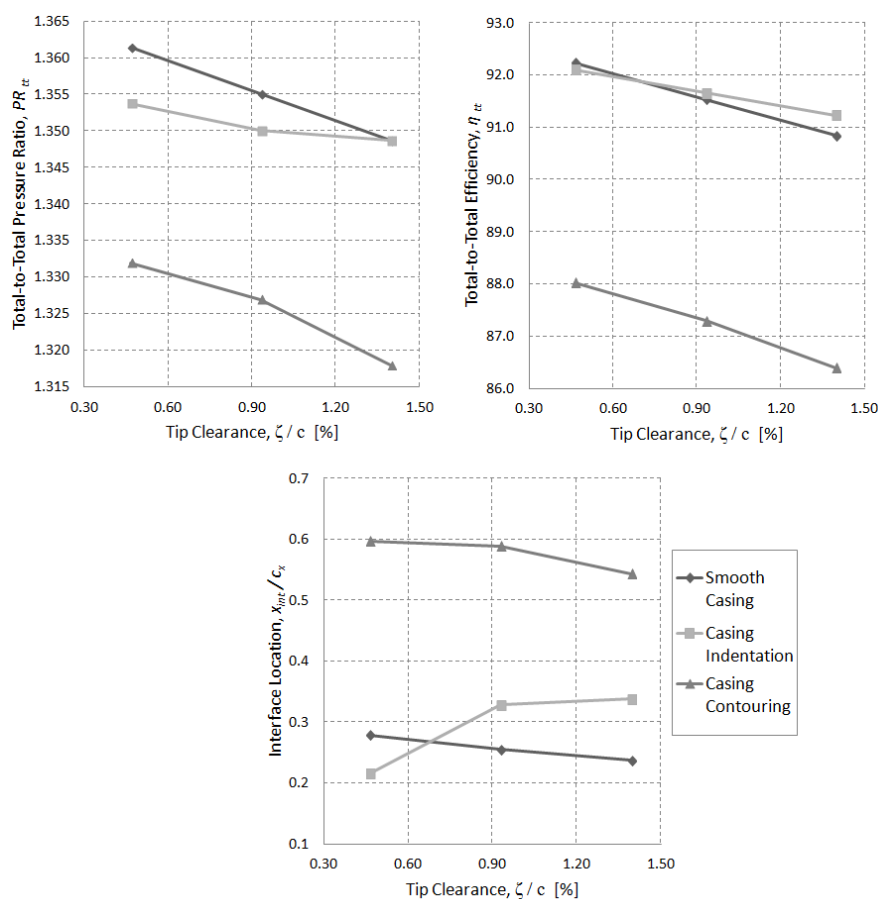
Figure 4-13: Sensitivity comparison of the BASE rotor with smooth casing and with negative sawtooth indentation casing in comparison with the concave gas path design

An exploration of the flow field was carried out to elucidate the flow mechanism by which the nominal negative sawtooth casing indentation reduces double leakage for tip desensitization and to explain the loss in nominal performance. In the standard configuration with a smooth casing, the double leakage flow starts by nature next to the shroud where the tip clearance fluid is entrained circumferentially by the shroud toward the adjacent tip clearance gap and is somewhat shielded from being entrained by the core flow in the streamwise direction by the lower layers of tip clearance flow. In the presence of the casing treatment, Figure 4-12 showed that the (high entropy) double leakage fluid goes into the circumferential indentation. The radial velocity contours taken at the shroud (Figure 4-14) indicates that pressure difference across the blade results in the fluid next to the shroud, including double leakage fluid, being suctioned (positive - red- radial velocity) into the groove on the blade pressure side and re-injected radially inward (negative –blue- radial velocity) on the blade suction side starting even inside the tip clearance gap region. This phenomenon is also shown more clearly by the radial velocity contours of Figure 4-15 for the axial plane shown by the dotted line in Figure 4-14(a), at around 60% chord. This radial injection forces the high-entropy double leakage fluid to interact with the lower low-entropy 'standard' tip clearance flow layers with higher streamwise momentum. This interaction through mixing deflects the high-entropy fluid toward the streamwise direction instead of letting it flow toward the adjacent tip clearance gap and continuing the double leakage, as initially depicted in Figure 3-4. The evidence of this mixing can be found in Figure 4-16 which plots the turbulent kinetic energy (TKE) contours for the same axial plane as Figure 4-15 for both the smooth casing and the casing indentation cases. One can observe a much larger region of high TKE near the suction side for the indentation case compared to the smooth casing case. While this interaction reduces double leakage, it brings about additional losses that can explain the observed nominal performance penalty.
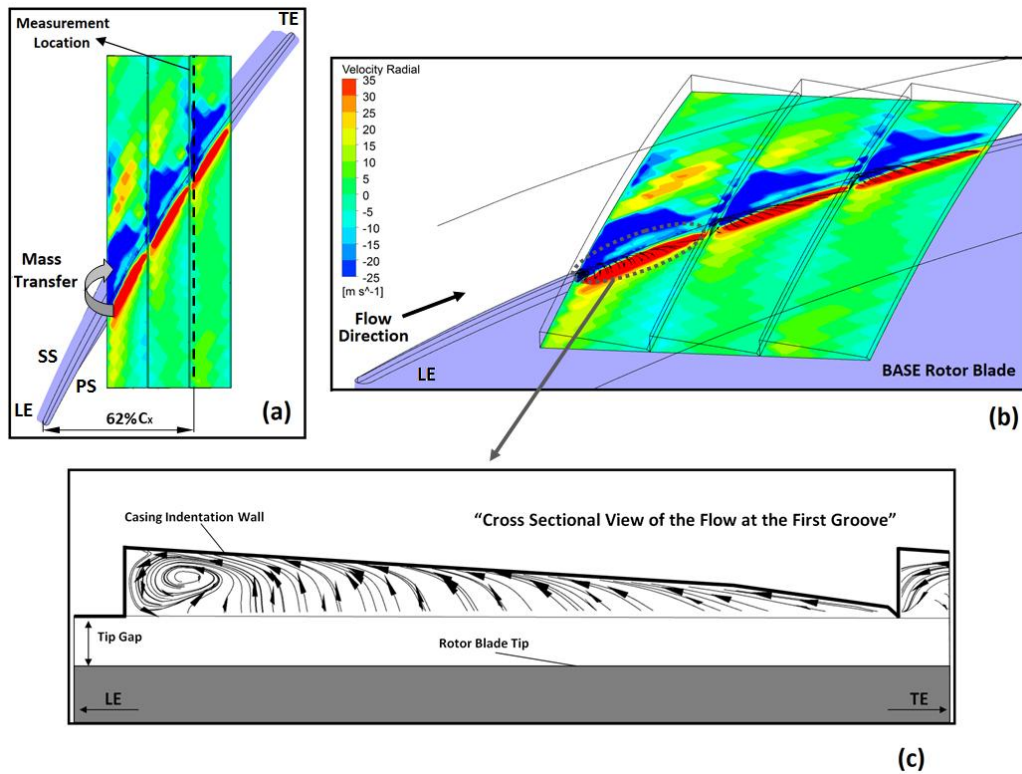
Figure 4-14:   Radial velocity contours at shroud plane for nominal casing indentation at nominal tip clearance seen in (a) top view (b) angle view and through (c) streamlines at tip near blade pressure surface, at nominal tip clearance size (0.4% chord)
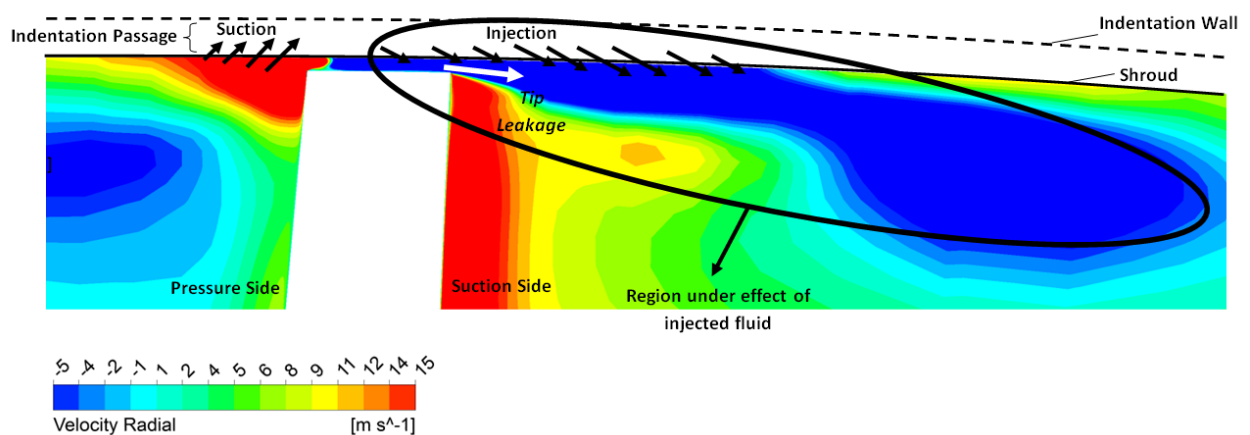
Figure 4-15: Radial velocity contours near the shroud at the axial plane shown by the dotted line in Figure 4-14(a)
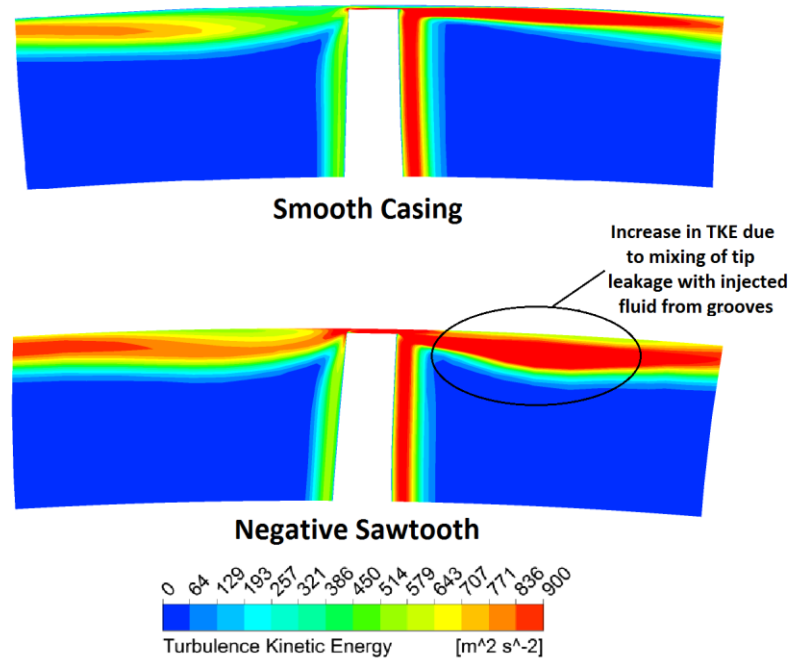
Figure 4-16: Contours of turbulent kinetic energy for outer 20% span at the axial plane shown by the dotted line in Figure 4-14(a)

In terms of sensitivity, as mentioned in chapter 2, Erler (2012) had shown that a reduction of nominal double leakage proportion also reduces the rate of increase of double leakage with tip clearance and thus performance and stall margin sensitivity. However, an interesting fact to note from Figure 4-12 is that, as the tip clearance increases, there is plenty of volume left in the grooves to collect the increase in double leakage fluid, which results in an increase in injected mass flow rate from the grooves with tip clearance increase as shown in Figure 4-17. The accompanying additional mixing of high-entropy flow from the grooves with the low-entropy flow layers beneath the shroud should further help control the double leakage increase with tip clearance and hence further reducing the tip clearance sensitivity of performance and stall margin.
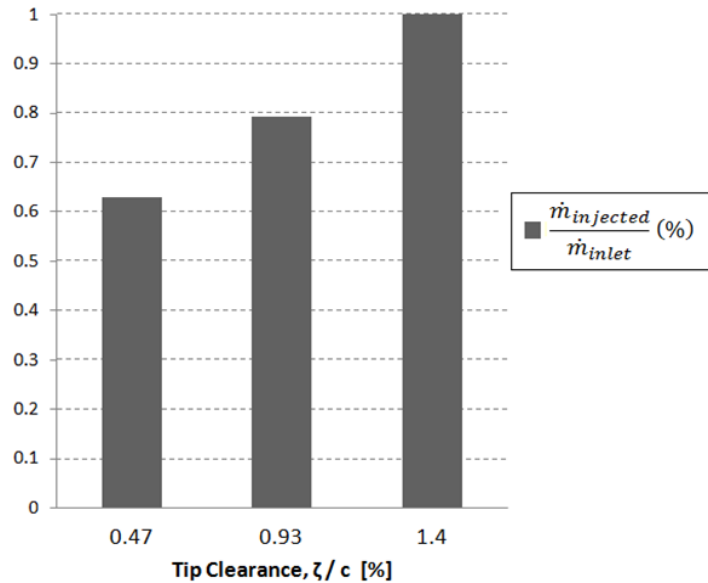
Figure 4-17: Variation of the injected mass flow rate from indentation grooves with tip clearance size

Another phenomenon is occurring in parallel that alleviates nominal loss and helps desensitization for the negative sawtooth casing indention. Figure 4-18 shows the entropy contours for the same axial plane as Figure 4-15 for both the smooth casing and the casing indentation configurations along with a zoom of the tip clearance gap region. At this axial position (around 60% chord) at nominal (minimum) tip clearance, it can be seen from both Figure 4-11 and Figure 4-18 that the (high-entropy) double leakage flow takes almost the entire height of the tip clearance gap entrance for the smooth casing configuration even at minimum tip clearance. The high double leakage proportion means not only high performance and stall margin sensitivity to tip clearance flow but also high nominal performance and stall margin penalty from low streamwise and high normal velocity components of the flow exiting the tip clearance according to the arguments laid out in Figure 2-13. However, in the casing indentation configuration, the suction of this double leakage fluid into the indentation grooves leaves room for high entropy core flow fluid with high streamwise and low/zero normal velocity components to enter the tip clearance as evidenced in Figure 4-12 and Figure 4-18. This effect results in tip clearance flow with high streamwise and low normal velocity components. This phenomenon can be clearly observed in Figure 4-19 which shows discrete increases in the streamwise velocity and discrete drops in normal velocity of the flow exiting the tip clearance gap at the chord positions

corresponding to the three indentations (item I in Figure 4-19). The velocity components are non-dimensionalized by the blade tip circumferential velocity (U_{tip}). The increased streamwise and reduced normal velocity components of the tip clearance flow first help to prevent double leakage in the adjacent tip clearance to reduce sensitivity. Secondly, they decrease shear mixing loss with the core flow and thus helps nominal performance. Finally, they weaken the tip clearance flow with respect to the incoming flow to bring the interface between these flows further downstream and thus improve nominal stall margin. In fact, it is with this 'improved' tip clearance fluid that the high-entropy flow radially injected from the indentation will first mix. This mixing that starts within the tip clearance may explain the small regions of increased streamwise and reduced normal velocity components along the chord (item II in Figure 4-19).
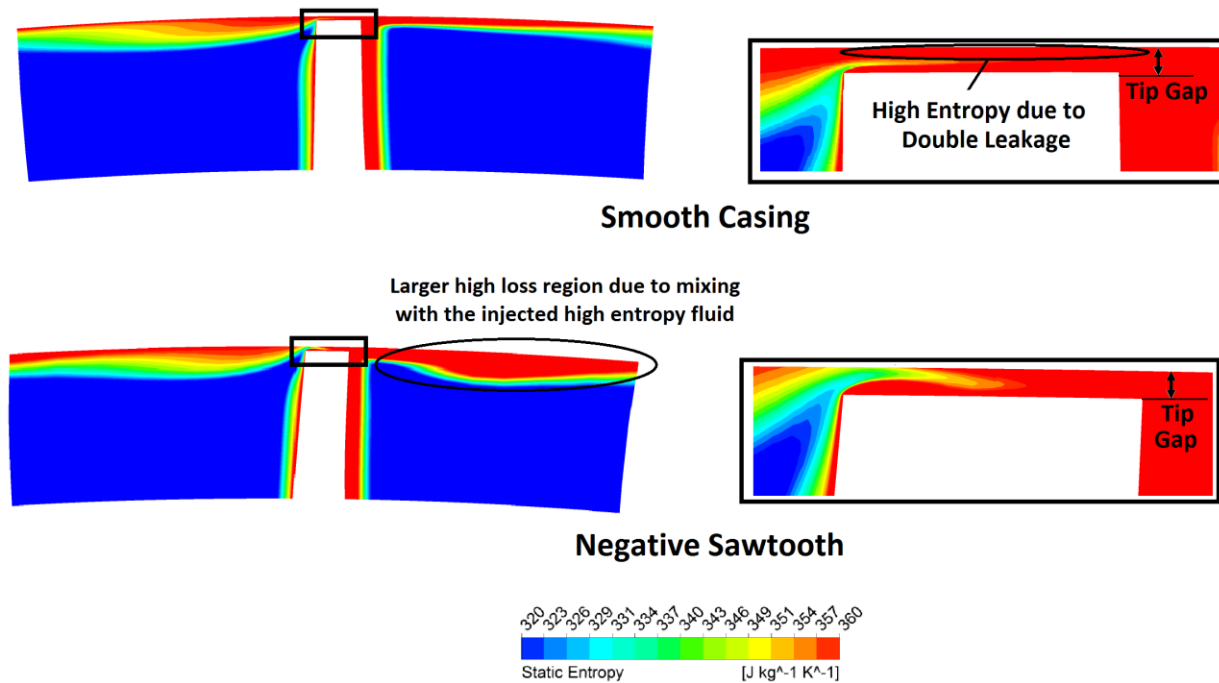
Figure 4-18: Contours of entropy for outer 20% span at the axial plane shown by the dotted line in Figure 4-14(a)
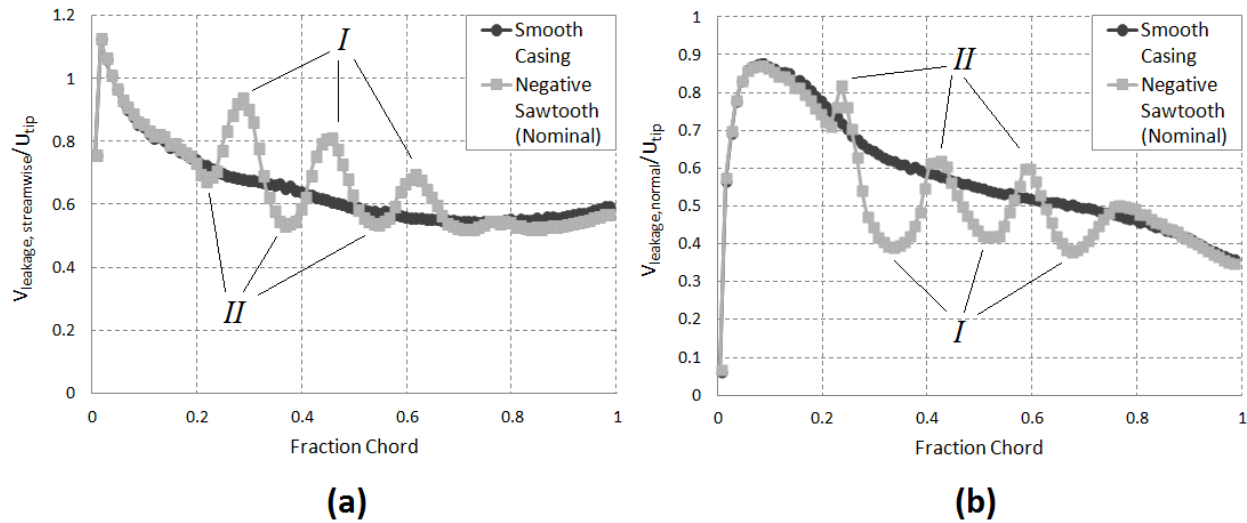
Figure 4-19: Chordwise distribution of non-dimensional (a) streamwise and (b) chordwise components of tip clearance flow velocity at tip gap exit and mass-averaged over the tip clearance gap height, for the smooth casing and the casing indentation at nominal t.c. size

Based on the above analysis of the flow field, the flow mechanism associated with casing indentation can be summarized with Figure 4-20 and Figure 4-21, which includes some itemized letters and numbers that will be referred to in the explanation and later in the chapter. Figure 4-20 shows that for a smooth casing, the high-entropy double leakage fluid lying right next to the shroud proceeds circumferentially with little or no interaction with the core flow toward the next tip clearance gap to continue the double leakage as shown by the dashed red line in Figure 4-21. The lower layers of 'standard' tip clearance flow with low entropy (having come from the core flow on the pressure side) interacts through shear/mixing with the core flow on the suction side below the blade tip to form a large loss region (item A) and the associated tip blockage/tip vortex. In the presence of an indentation in the shroud, the pressure difference across the blade drives the high-entropy double leakage flow into the groove (item B) and injects it (item 1) straight into the 'standard' tip leakage flow. The resulting mixing creates a small mixing loss region (item C) but turns the double leakage flow in the streamwise direction so that it will not double-leak into the next tip clearance gap (blue dashed line in Figure 4-21). In parallel, the suction of the high-entropy fluid into the groove makes room for more low-entropy fluid from the pressure side core flow to enter the tip clearance gap resulting in tip clearance flow at the exit of the gap with higher

streamwise velocity (item 2) and lower normal velocity components (item 3), thus reducing the angle (item 4) between the tip clearance flow and the core flow. This imparts more momentum to the injected double leakage flow from the groove that mixes with the tip clearance flow to further reduce double leakage and improve desensitization. It also reduces the traditional mixing loss region between the tip clearance and core flow (item D) and the reduction will compensate and can perhaps cancel the increase in loss from groove injection (item C). The grooves essentially allows through radial flow injection and mixing for more effective streamwise momentum transfer from the core flow to the high-entropy double leakage flow next to the shroud and preventing this fluid from double leaking into the adjacent blade's tip clearance.

When the tip clearance increases, most of the additional high-entropy double leakage fluid goes into the grooves and are re-injected. At the same time, an equally increased amount of low-entropy fluid enters the larger tip clearance gap from the pressure side core flow and mixes with the increased amount of re-injected double leakage fluid. Thus, a balance between the two streams is kept and helps control any increase in double leakage with increased tip clearance size and further reduces the tip sensitivity.

From the described mechanism, the main flow parameters that affect the performance of the casing indentation are listed below according to the item numbers shown in Figure 4-20 and Figure 4-21 and shown in the same order on the bar chart of Figure 4-22 for the smooth casing and nominal negative sawtooth indentation cases.

Item 1: Injected mass flow rate from the groove to the blade domain (item 1 in Figure 4-20) non-dimensionalized by the inlet mass rotor flow ($\dot{m}_{injected}/\dot{m}_{inlet}$). An increase in this parameter should decrease double leakage and by extension performance and stall margin sensitivity to tip clearance but increase mixing loss and thus nominal performance penalty.

Item 2: Mass-averaged tip clearance flow streamwise velocity at tip gap exit plane, non-dimensionalized by rotor tip velocity ($V_{leakage,streamwise}/U_{tip}$). An increase in this parameter should decrease double leakage and by extension performance and stall margin sensitivity and also decrease mixing loss and move the incoming/tip clearance flow interface furher downstream, thus decreasing nominal performance/stall margin penalty.

Item 3: Mass-averaged tip clearance flow normal velocity at tip gap exit plane, non-dimensionalized by rotor tip velocity ($V_{leakage,normal}/U_{tip}$). An increase in this parameter should increase double leakage and by extension performance and stall margin sensitivity and also increase mixing loss and move the incoming/tip clearance flow interface further upstream, thus increasing nominal performance/stall margin penalty.

Item 4: Ratio of item 3 over item 2 ($V_{leakage,normal}/ V_{leakage,streamwise}$), which is the tangent of the tip clearance flow angle, i.e. the angle between the tip clearance flow at the tip gap exit and the core flow. An increase in this parameter should increase double leakage and by extension performance and stall margin sensitivity and also increase mixing loss and move the incoming/tip clearance flow interface further upstream, thus increasing nominal performance/stall margin penalty.

In summary, an increase in item 1 is beneficial for sensitivity reduction but detrimental to nominal performance, while an increase in item 2 is beneficial for both sensitivity reduction and nominal performance/stall margin. On the other hand, an increase in either the item 3 or 4 is detrimental on all counts. These four flow parameters will be used to explain the trends observed during the parametric study of the casing indentation strategy in Section 4.2.
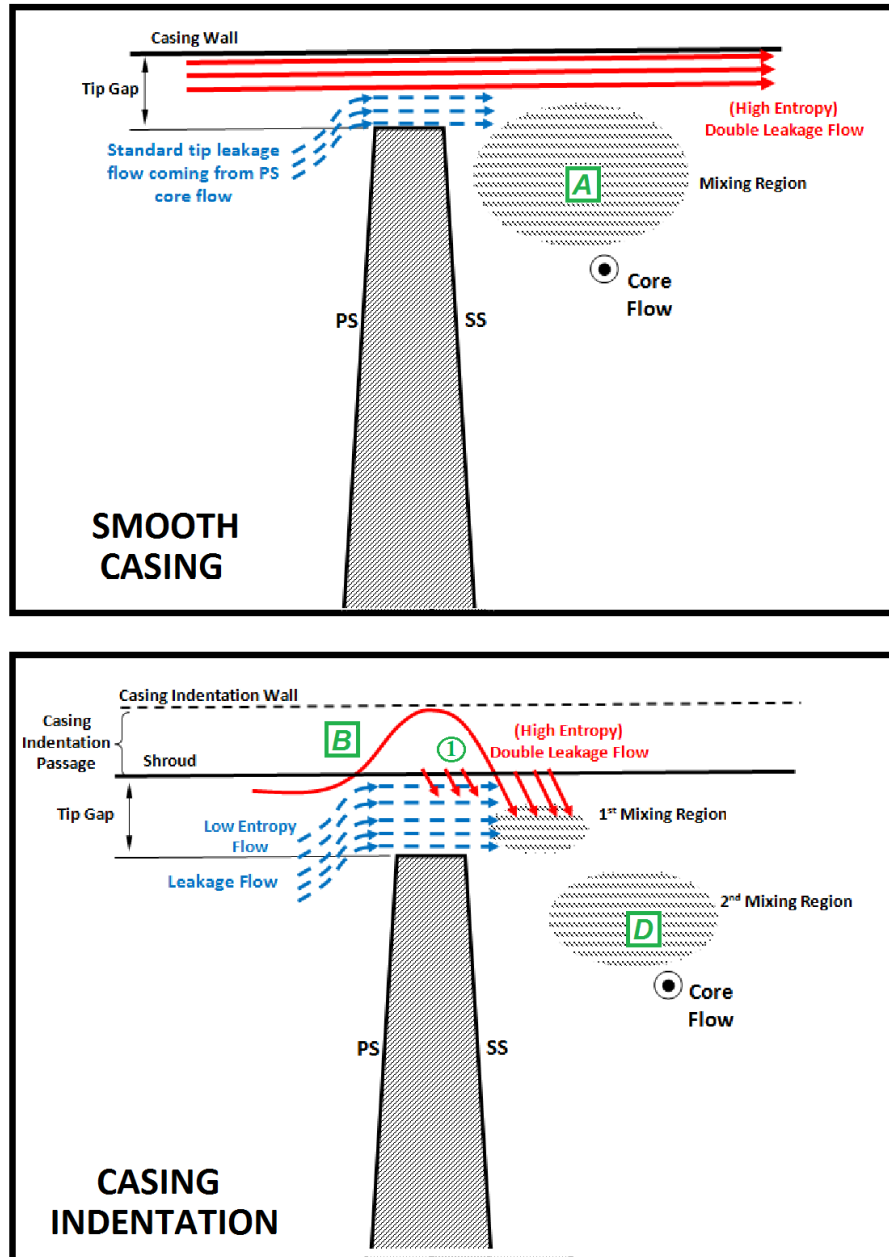
Figure 4-20: Schematic of the effect of casing indentation on the tip region flow field through an axial view of the rotor blade passage
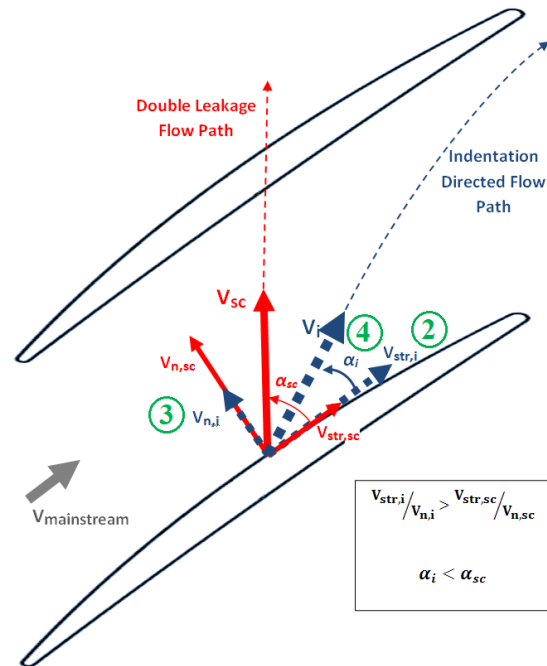
Figure 4-21: Schematic of the effect of casing indentation on the tip region flow field through a top view of the rotor blade passage
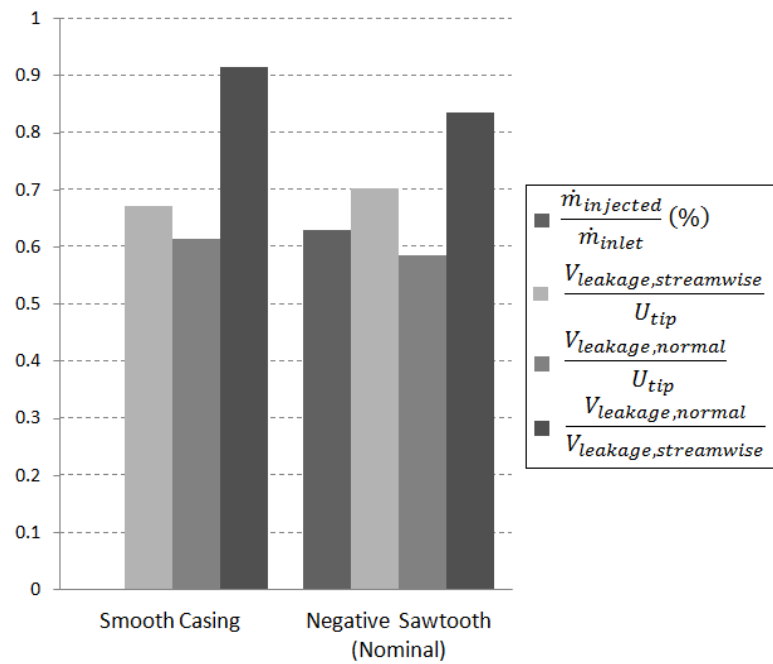
Figure 4-22: Comparison of the four flow parameters for casing indentation effectiveness as applied to the smooth casing and the nominal casing indentation at nominal t.c. size

4.2 Parametric Study and Optimization

With shallow casing indentation chosen as the most promising gas path design strategy for tip desensitization, a parametric study was performed from the nominal negative sawtooth indentation configuration of section 4.1.2 to obtain preliminary design rules and an improved design that maximizes reduction in sensitivity and nominal performance loss. The geometric design parameters of the casing treatment are as described in section 3.1.2 and illustrated in Table 3-3, namely indention shape, depth, width, number of grooves and axial location. One parameter is varied at a time and CFD simulations are carried out for each configuration at the three tip clearance sizes with the BASE rotor at its design corrected mass flow of 3.04 kg/s. Table 4-1 summarizes the parameters changed during the parametric study.

Table 4-1: Summary of parameter changes in parametric study

Parameter	Alternative 1	Alternative 2	Alternative 3	Alternative 4
Shape	Negative Sawtooth	Positive Sawtooth	Constant Width Rectangular	Constant Depth Rectangular
Depth	15×10^{-3} inch	10×10^{-3} inch	7.5×10^{-3} inch	-
Indentation Width	½ Axial Chord	1 Axial Chord	-	-
Groove Number	3 Groove	2 Groove	1 Groove	-
Location	Mid-Located	Upstream Located	Downstream Located	-

The results for each configuration are compared with the nominal negative sawtooth casing treatment according to the change (*with respect to the smooth casing configuration*) in the sensitivity to tip clearance (d/dζ) of total pressure ratio (PR), total-to-total efficiency (η) and incoming/tip clearance flow interface location (x_{int}) and in the change in their nominal (minimum tip clearance) values. The corresponding plots of PR, η and x_{int}/c_x versus tip clearance for each parameter change can be found in Appendix E. For conciseness, these parameters are quantified and placed in a table, such as in Table 4-2. The sensitivity is taken as the average slope between the minimum and maximum tip clearance sizes. The percentage change in sensitivity is

calculated from equation (4.1) with f being PR, η or x_{int}. A negative value means a reduction in sensitivity and a value that is below -100% indicates a reversed tip sensitivity which means the value of f increases with tip clearance size. The change in nominal performance or stall margin (Δf) is obtained by equation (4.2) with f being PR or while Δη is simply calculated as the difference in percentage point (pcp) efficiency between the smooth casing and an indentation configuration at nominal (minimum) tip clearance. The change in nominal efficiency (Δη) in expressed in percentile points (pcp). A positive value of Δf means an improvement and negative value a penalty in nominal performance or stall margin. When the incoming/tip clearance flow interface can not be located, usually a sign that the stall margin is very large, 'N/A' is placed in the table columns involving x_{int}.

$$\Delta\left(\frac{df}{d\zeta}\right) = \left[\frac{\left(\frac{df}{d\zeta}\right)_{indentation} - \left(\frac{df}{d\zeta}\right)_{smooth\ casing}}{\left(\frac{df}{d\zeta}\right)_{smooth\ casing}}\right] \times 100 \qquad (4.1)$$

$$\Delta f = f_{nominal\ t.c.,indentation} - f_{nominal\ t.c.,smooth\ casing} \qquad (4.2)$$

Bar charts similar to Figure 4-22 comparing the four flow parameters outlined at the end of section 4.1.2 will be shown for the different indentation configurations and a plot of double tip leakage versus tip clearance will be used to explain the trends observed in the parametric study. Additional plots may be added to better illustrate the explanation.

For each parameter in the parametric study, the configurations are placed in the table and bar chart in decreasing order of desensitization effect, roughly taken as the sum of the percentage change in sensitivity of PR, η or x_{int}.

4.2.1 Shape

Four different indentation shapes are generated and analyzed to evaluate the effect casing indentation shape on the indentation effectiveness. The cross sectional views of these indentation alternatives are illustrated in Figure 4-23. All designs have the same cross sectional area. This implies that the two rectangular indentation configurations have different depth and width dimensions to preserve the same area. The first rectangular indentation is referred to as constant width rectangular design (Figure 4-23(c)) as it has the same groove width as the nominal design but a small depth. The other rectangular indentation is referred to as constant depth design (Figure 4-23(d)) with the same depth as the nominal negative sawtooth design, but a lower width.
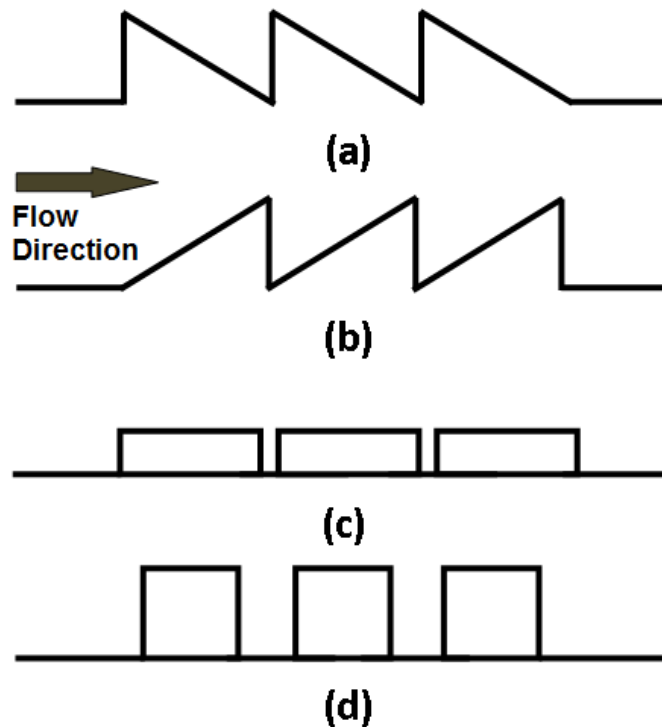
Figure 4-23: Cross sectional view of the casing indentation shapes (a) Negative sawtooth indentation, (b) Positive sawtooth indentation (c) Constant width rectangular indentation, (d) Constant depth rectangular indentation

Table 4-2 summarizes the change in sensitivity and nominal performance while Figure 4-24 compares the four flow parameters between the indentation shapes. The results show that the (nominal) negative sawtooth indentation outperforms the other shapes for the overall sensitivity (including x_{int}) and has among the lowest performance penalties. The data in Figure 4-24 does indeed show that the negative sawtooth shape has the highest injection mass flow rate, highest streamwise tip clearance velocity, lowest normal tip clearance velocity and lowest tip clearance flow angle. All these factors are beneficial to sensitivity and nominal loss reduction, except for the high injection rate which may be the factor preventing the nominal indentation configuration from achieving the lowest nominal penalty. The effectiveness in sensitivity reduction of the negative sawtooth configuration is also apparent in Figure 4-25, which shows that it has the second lowest sensitivity of double leakage, surpassed only by the constant width rectangular indentation which has a small depth and which indeed exhibit slightly better performance sensitivity.

Table 4-2: Change in tip sensitivity and nominal value of performance/aerodynamic stability for the different indentation shapes relative to the smooth casing

Configuration	Δ(dPR/dζ) [%]	Δ(dη/dζ) [%]	Δ(dXint/dζ) [%]	ΔPR	Δη [pcp]	Δ(X_{int}/c_X)
Negative Sawtooth (Nominal)	-60	-37	-392	-0.008	-0.129	-0.062
Rectangular Cnst. Width	-64	-36	-319	-0.010	-0.238	-0.062
Positive Sawtooth	-43	-32	-343	-0.010	-0.303	-0.092
Rectangular Cnst. Depth	-29	-28	-319	-0.006	-0.054	-0.062
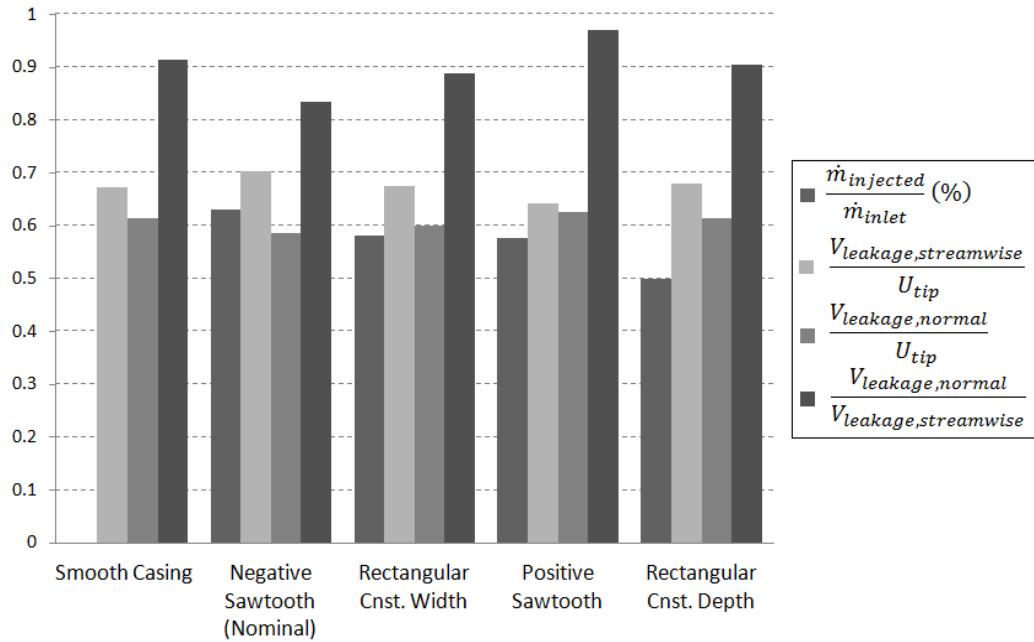
Figure 4-24: Comparison of the four flow parameters for casing indentation effectiveness for different indentation shapes
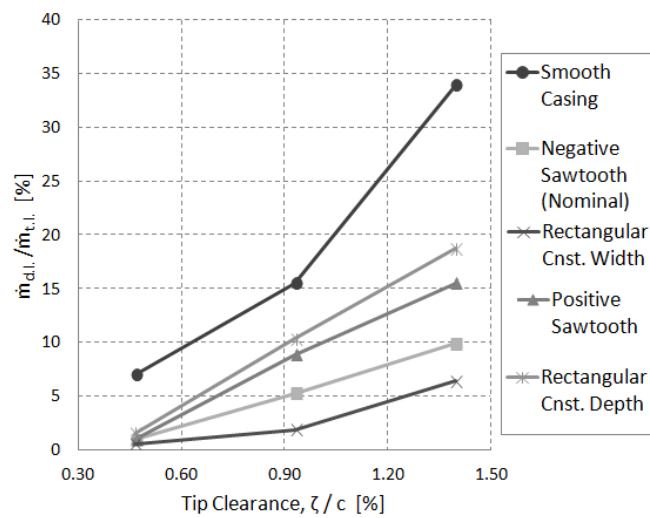
Figure 4-25:   Comparison of double leakage sensitivity for different casing indentation shapes

4.2.2 Depth

In order to assess the effect of groove depth on the effectiveness of the proposed casing treatment, the nominal indentation design is simulated at three different depths of 0.015 (nominal value), 0.010 and 0.0075 inch. As shown in Figure 4-26, the depth is changed while keeping all other parameters constant.

The change in sensitivity and nominal performance/stall margin with depth are summarized in Table 4-3 while the four flow parameters are compared in Figure 4-27. The results show that the indentation depth does not have a significant effect on sensitivity reduction (no effect at all for stall margin), with the 0.010 inch depth configuration achieving slightly better performance sensitivity despite the fact the values of its four flow parameters lies between those of the other two depths. The low effect of depth on sensitivity is consistent with its low effect of the sensitivity of double leakage to tip clearance increase in Figure 4-28. However the change in depth affects the mass injection level significantly as shown in Figure 4-27, and accordingly on the nominal efficiency. Indeed, according to Table 4-3, the nominal efficiency for the 0.0075 and 0.010 inch deep configurations are even above that of the smooth casing. This may be explained by the fact that the tip clearance streamwise velocity for these two cases are higher than that of the smooth casing which results in a shear/mixing loss reduction (item D in Figure 4-20) that is more important than the small increase in mixing loss (item C in Figure 4-20) from the small amount of injected mass flow. The results also indicate that, for a particular rotor geometry there may be an optimum value for injected mass flow rate from the groove for sensitivity reduction, beyond which only more loss is generated.
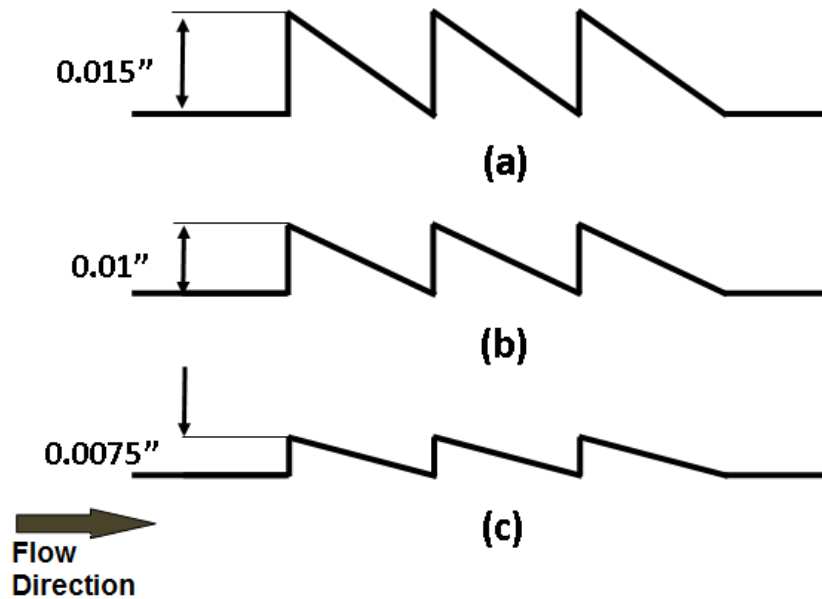
Figure 4-26: Cross sectional view of the negative sawtooth (nominal) casing indentation with three different depths, (a) 0.015 inch, (b) 0.010 inch and (c) 0.0075 inch

Table 4-3: Change in tip sensitivity and nominal value of performance/aerodynamic stability for negative sawtooth indentation with different depths relative to the smooth casing

Configuration	$\Delta(dPR/d\zeta)$ [%]	$\Delta(d\eta/d\zeta)$ [%]	$\Delta(dXint/d\zeta)$ [%]	ΔPR	$\Delta\eta$ [pcp]	$\Delta(X_{int}/c_x)$
Depth=0.01"	-67	-37	-392	-0.005	0.121	-0.062
Depth=0.015" (Nominal)	-60	-37	-392	-0.008	-0.129	-0.062
Depth=0.0075"	-61	-33	-392	-0.004	0.259	-0.062
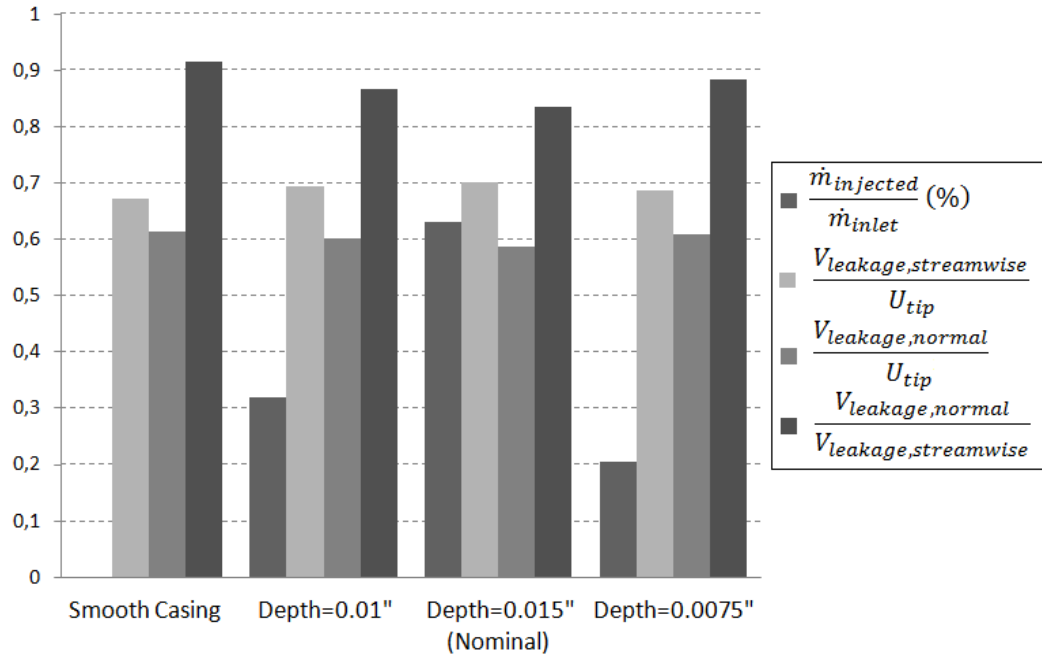
Figure 4-27: Comparison of the four flow parameters for casing indentation effectiveness for the smooth casing and negative sawtooth indentations of different depths, at nominal t.c. size
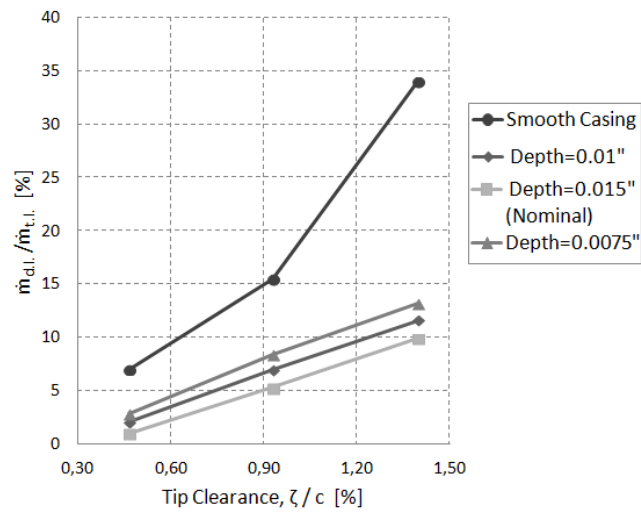
Figure 4-28: Comparison of double leakage sensitivity for the various indentation depths

4.2.3 Indentation Width

Two sizes of indentation width (or axial extent) were simulated in order to evaluate the effect of this parameter. The first configuration is the nominal design which has the half axial chord length axial extent as shown in Figure 4-29(a). The second configuration covers the full axial chord length from the leading to the trailing edge as shown in Figure 4-29(b). All other parameters were kept the same.
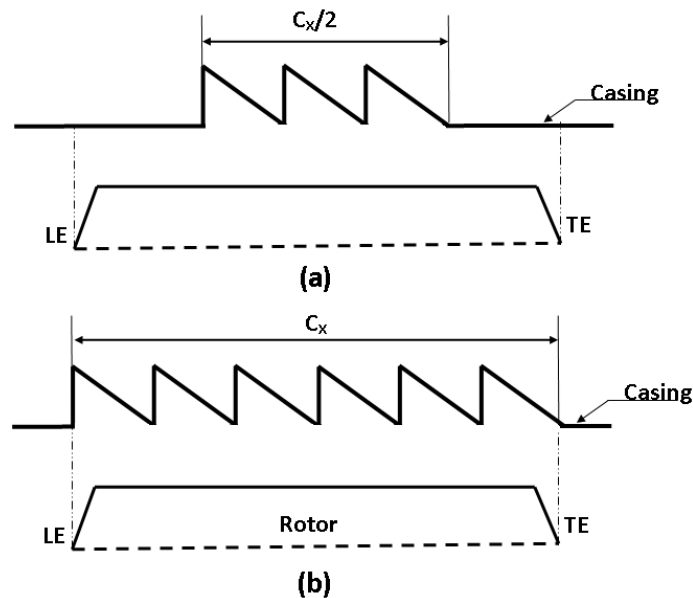
Figure 4-29: Cross sectional view of the negative sawtooth casing indentation with two different axial extents, (a) half axial chord (nominal) and (b) one axial chord

The change in sensitivity and nominal performance/stall margin is summarized in Table 4-4 while the four flow parameters are compared in Figure 4-30 according to the change in indentation width. The results show that the axial extent has a large effect on tip desensitization but also on nominal performance. Increased axial extent greatly decreases sensitivity of performance and stability but also significantly reduces nominal efficiency. This can be explained with the flow parameters in Figure 4-30 which show that the full-axial extent configuration has the highest mass flow injection, streamwise tip clearance flow velocity combined with the lowest tip clearance flow normal velocity and angle, all of which work in favour of lower sensitivity as

corroborated by Figure 4-31 which shows that this configuration completely desensitizes double leakage. However, the excessive mass flow injection rate from the grooves should explain the large nominal efficiency penalty presented in Table 4-4.

Table 4-4: Change in tip sensitivity and nominal value of performance/aerodynamic stability for negative sawtooth indentation of different widths (axial extent) relative to the smooth casing

Configuration	$\Delta(dPR/d\zeta)$ [%]	$\Delta(d\eta/d\zeta)$ [%]	$\Delta(dXint/d\zeta)$ [%]	ΔPR	$\Delta\eta$ [pcp]	$\Delta(X_{int}/c_X)$
1 Axial Chord Width	-129	-78	N/A	-0.015	-1.153	N/A
½ Axial Chord Width (Nominal)	-60	-37	-392	-0.008	-0.129	-0.062
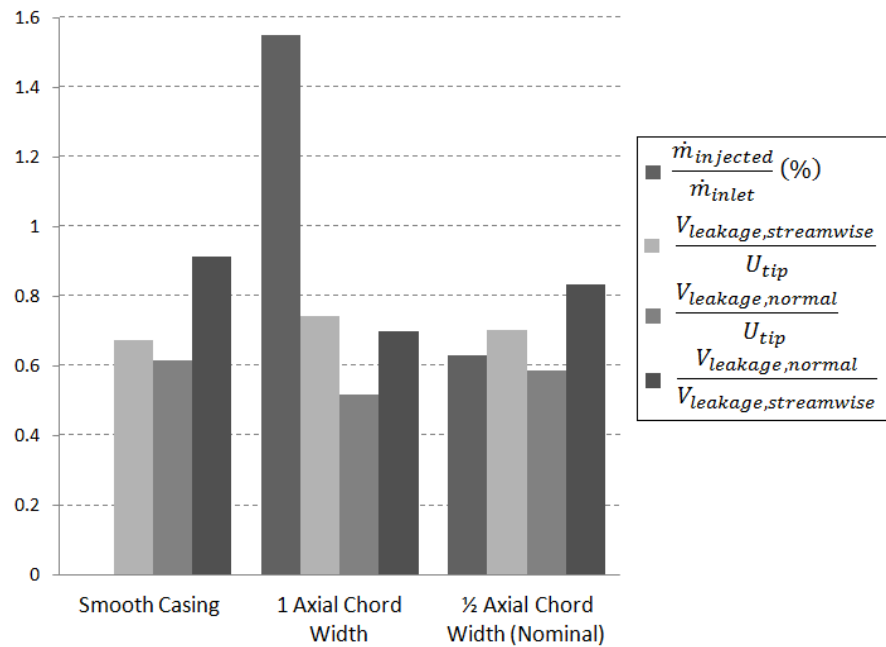
Figure 4-30: Comparison of the four flow parameters for casing indentation effectiveness for the smooth casing and negative sawtooth with different widths (axial extents) at nominal t.c. size
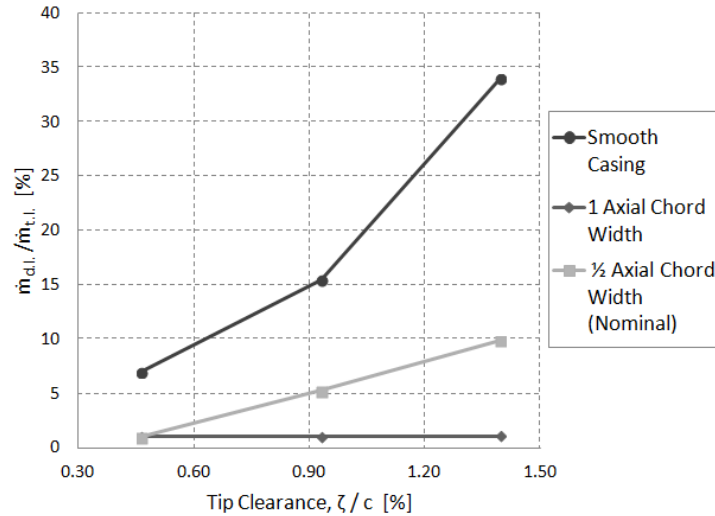
Figure 4-31: Comparison of double leakage sensitivity for the different width (axial extents)

4.2.4 Groove Number

The effect of groove number is investigated by changing the number of grooves from three to one for the same axial extent as the nominal configuration, as shown in Figure 4-32. Table 4-5 shows that similar to groove depth, this parameter has only a small impact on sensitivity reduction, but a more significant, if still moderate, impact on nominal efficiency. Reducing the number of grooves through increased groove width is slightly detrimental to sensitivity reduction as well as nominal performance as it reduces tip clearance streamwise velocity while increasing its angle of mass flow injection (Figure 4-33). These factors work against each other for sensitivity reduction, but the largest impact of the number of grooves on the flow parameters is on injected mass flow, which explains the large effect on efficiency loss. These results are corroborated by the double leakage data in Figure 4-34 which shows that all three configurations have a similar increase in double leakage with tip clearance, which is consistent with the similar sensitivity reduction. This figure also shows that the increased mass flow injection associated with less grooves does not translate in reduced double leakage likely because any beneficial effect in double leakage from increased injection is being cancelled/reversed by the trends in other flow parameters.
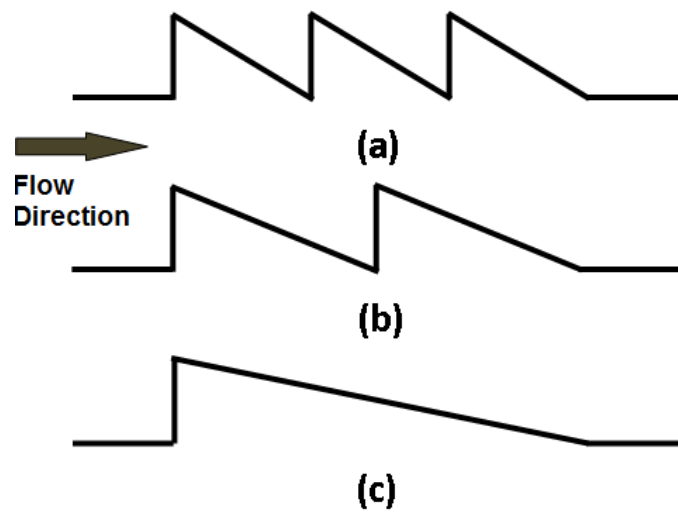
Figure 4-32: Cross sectional view of the negative sawtooth (nominal) casing indentation with different number of grooves (a) 3 grooved design (nominal), (b) 2 grooved design, (c) 1 grooved design

Table 4-5: Change in tip sensitivity and nominal value of performance/aerodynamic stability for negative sawtooth indentation with different number of grooves relative to the smooth casing

| Configuration	$\Delta(dPR/d\zeta)$ [%]	$\Delta(d\eta/d\zeta)$ [%]	$\Delta(dXint/d\zeta)$ [%]	ΔPR	$\Delta\eta$ [pcp]	$\Delta(X_{int}/c_X)$
3 Grooves (Nominal)	-60	-37	-392	-0.008	-0.129	-0.062
2 Grooves	-62	-35	-348	-0.009	-0.178	-0.062
1 Groove	-56	-32	-396	-0.011	-0.378	-0.092
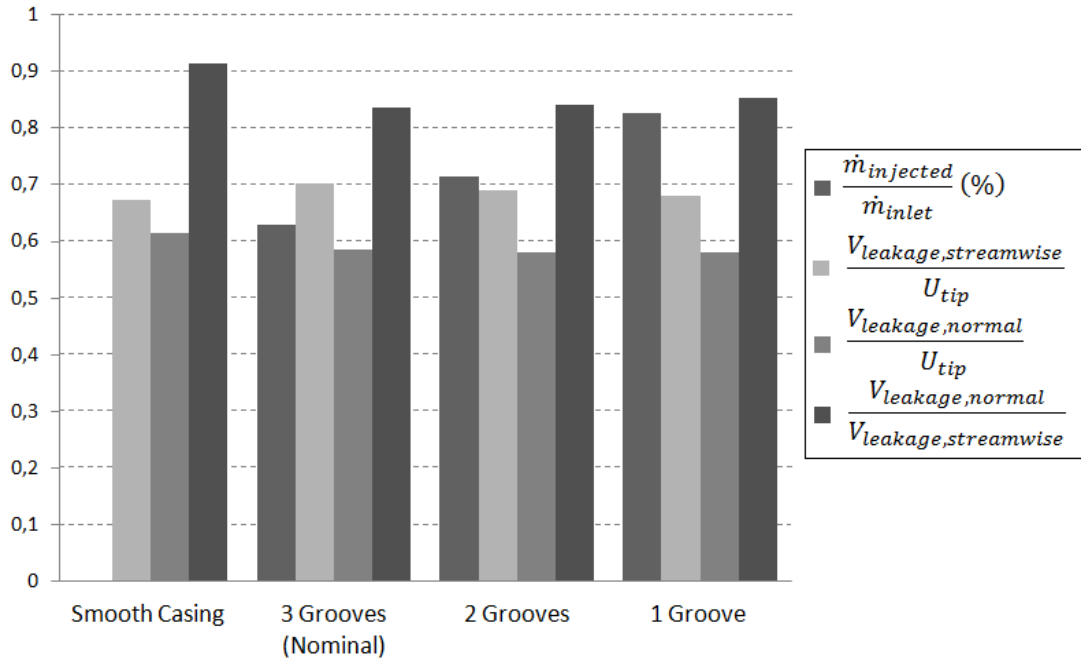
Figure 4-33: Comparison of the four flow parameters for casing indentation effectiveness for the smooth casing and negative sawtooth indentation with different groove numbers, at nominal t.c. size
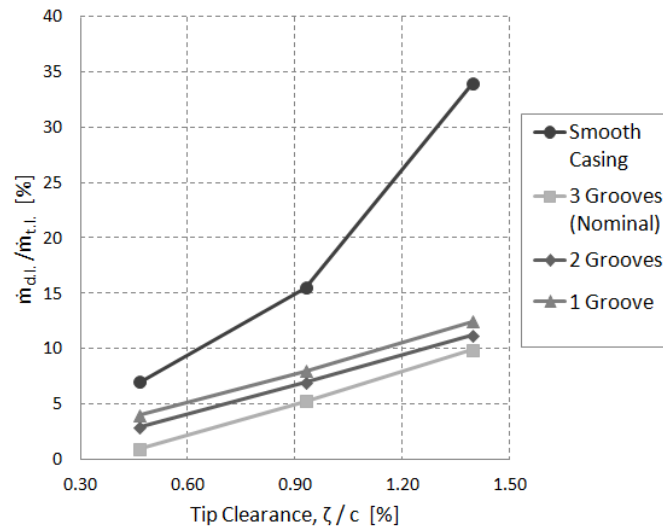
Figure 4-34: Comparison of double leakage sensitivity for the varying numbers of groove

4.2.5 Location

The effect of indentation location was investigated with three configurations in which the negative axial sawtooth indentations are placed more upstream near the leading edge, in the middle passage (nominal configuration), and downstream near the trailing edge, as illustrated in Figure 4-35. The sensitivity and performance/stall margin change data is summarized in Table 4-6, which shows that like the axial extent (indentation width), the location has a large impact on sensitivity as well as nominal performance. Moving the grooves toward the rotor leading edge greatly improves desensitization by increasing mass flow injection, tip clearance streamwise velocity and decreasing normal velocity and flow angle according to the data in Figure 4-36. Indeed, this configuration achieves a full desensitization of double leakage (Figure 4-37) and greatly reduces sensitivity of performance and stall margin according to Table 4-6. However, this is accompanied by a significant drop in nominal efficiency likely due to the large increase in mass flow injection from the grooves, which is driven by the larger tip loading in the front of the blade as can be inferred from the chordwise distribution of tip clearance flow normal velocity component in Figure 4-38(b). Indeed, Figure 4-38 shows that the upstream located configuration has a far higher influence on the momentum distribution then the two other configurations, where the grooves are located in region with lower blade loading.
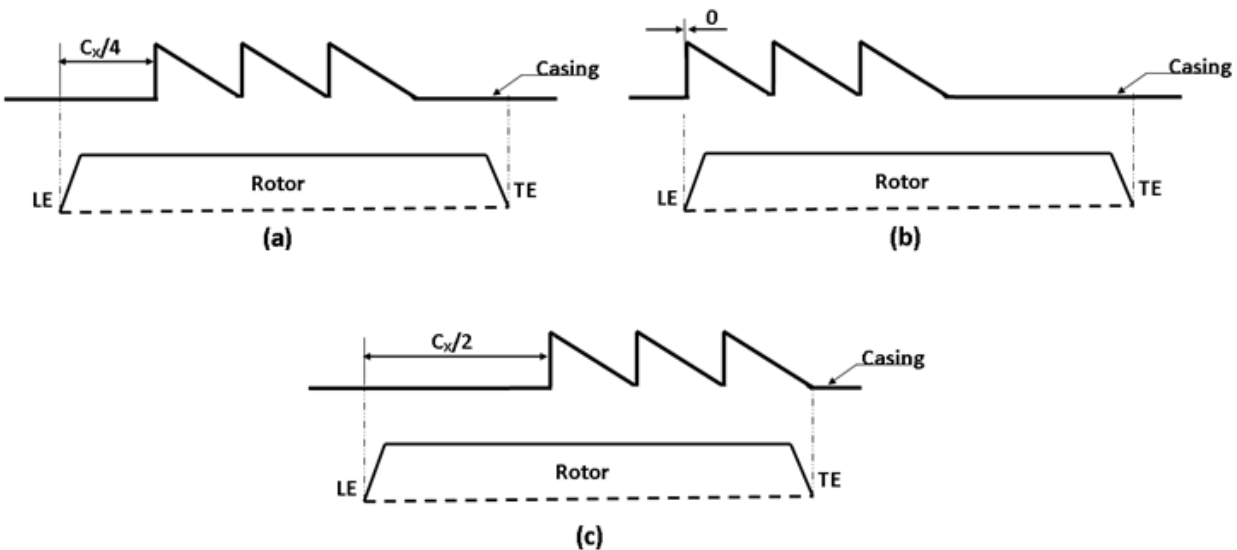
Figure 4-35: Cross sectional view of the negative sawtooth (nominal) casing indentation at different locations (a) mid-located, (b) upstream located, (c) downstream located

Table 4-6: Change in tip sensitivity and nominal value of performance/aerodynamic stability for negative sawtooth indentation with different locations relative to the smooth casing

Configuration	Δ(dPR/dζ) [%]	Δ(dη/dζ) [%]	Δ(dXint/dζ) [%]	ΔPR	Δη [pcp]	Δ(X$_{int}$/c$_X$)
Upstream Located	-97	-67	N/A	-0.009	-0.727	N/A
Mid-Located (Nominal)	-60	-37	-392	-0.008	-0.129	-0.062
Downstream Located	-12	-21	-100	-0.008	0.071	0.009
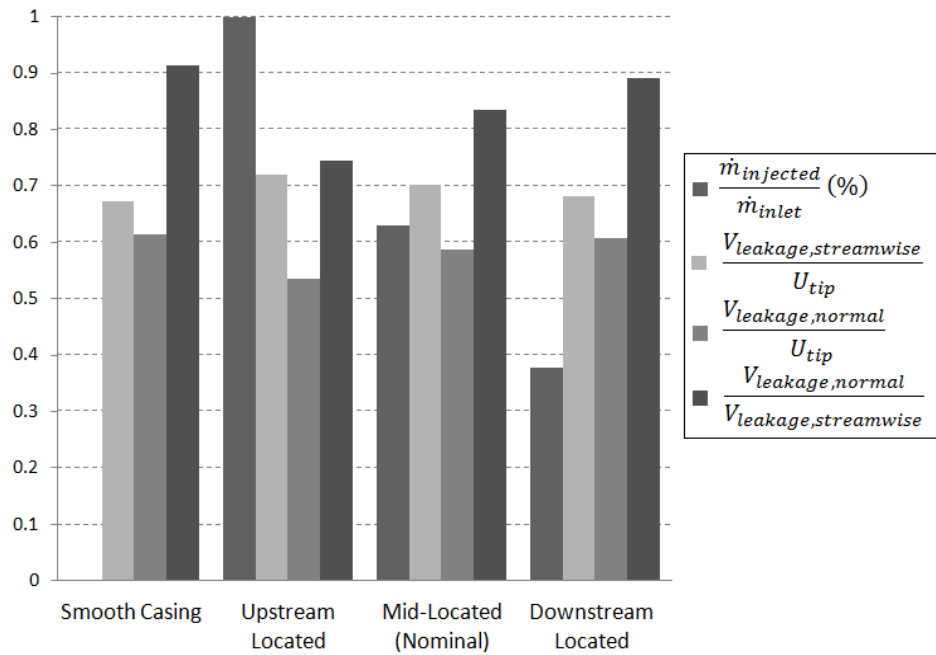
Figure 4-36: Comparison of the four flow parameters for casing indentation effectiveness for the smooth casing and negative sawtooh casing with different locations at nominal t.c. size
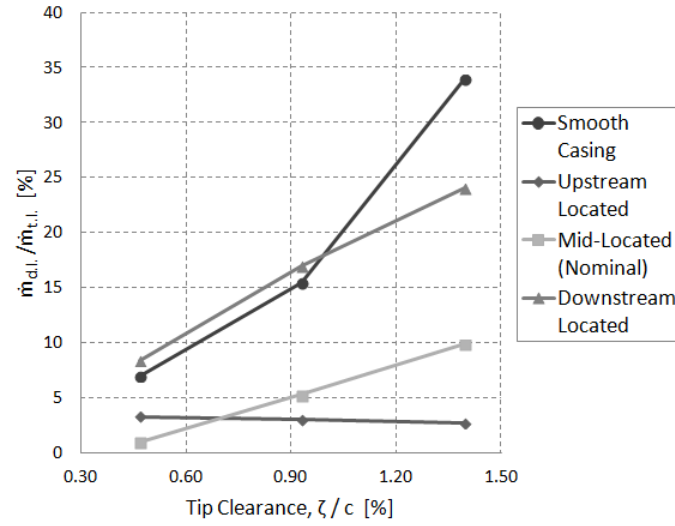
Figure 4-37: Comparison of double leakage sensitivity with indentation location variations
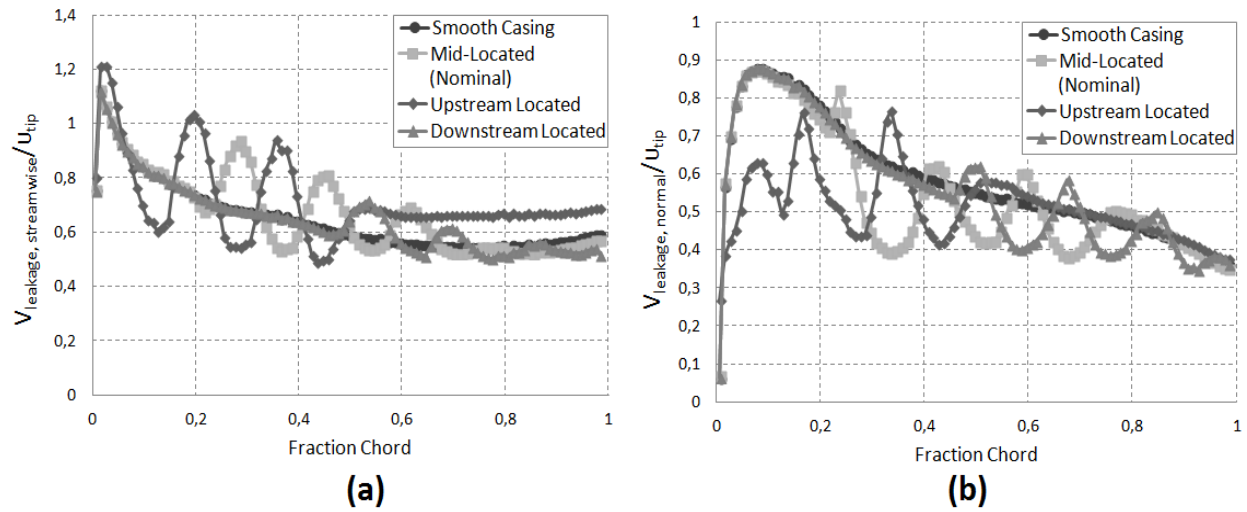
Figure 4-38: Effect of the indentation location on chordwise distribution of tip leakage flow (a) streamwise velocity and (b) normal velocity at tip gap exit and at nominal t.c. size

4.2.6 Final Casing Indentation Design

Following the parametric study, a final casing indentation design is generated to improve the tip desensitization while reducing the performance penalty relative to the nominal indentation design. Based on the results of the parametric study, the negative sawtooth indentation shape is kept, but with a lower depth and higher groove number to reduce nominal performance loss. The axial extent (indentation width) is slightly increased and a slightly more upstream location is chosen to improve sensitivity reduction, with a limit on these two parameters to avoid nominal efficiency penalties. The design features of the resulting casing treatment are summarized at Table 4-7 and illustrated in Figure 4-39 and Figure 4-40.

The comparison of tip desensitization and nominal performance/stall margin change is summarized in Table 4-8, which shows that final casing treatment design achieves its goals of significantly reducing the BASE rotor performance sensitivity (stall margin was already desensitized) while reducing the performance/stall margin penalty. In fact, the final design desensitizes the pressure ratio completely and significantly decreases the efficiency sensitivity, while even producing a gain in nominal efficiency and stall margin. Although the desensitization effect on aerodynamic stability seems to be reduced, the stall margin already had reversed sensitivity with the nominal casing treatment which is still the case with the final design.

In terms of the four flow parameters, Figure 4-41 shows that, compared to the nominal negative sawtooth casing indentation design, the final design has higher streamwise velocity and lower angle for tip clearance flow, which all contribute to better sensitivity reduction and lower loss. The fact that the final design also has lower injection but achieves better sensitivity reduction while having less nominal performance loss indicates that it achieves a level of injection that is closer to the optimum value, beyond which loss would have been generated without additional sensitivity benefits. The double leakage data in Figure 4-42 also supports this conclusion with lower double leakage sensitivity for the new design. In addition, the fact that its nominal double leakage level is higher and yet double leakage sensitivity is lower than the nominal design (as was also the case for the upstream located indentation configuration in Figure 4-37) lends support to the additional desensitization mechanism for the indentation (beyond the reduced nominal double leakage) described at the end of section 4.1.2.

Table 4-7: Design features of the final casing indentation design

Parameter	Nominal Design
Shape	Negative Sawtooth
Depth	1×10^{-3} inch
Indentation Width	0.6 Axial Chord
Groove Number	4 Groove
Location	0.15 Axial Chord from Leading Edge
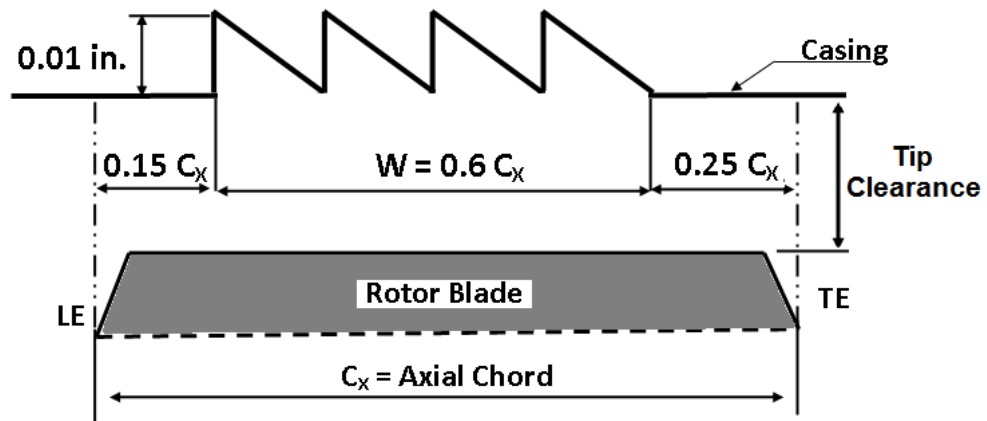
Figure 4-39: Cross sectional view and the dimensions of the final casing indentation design
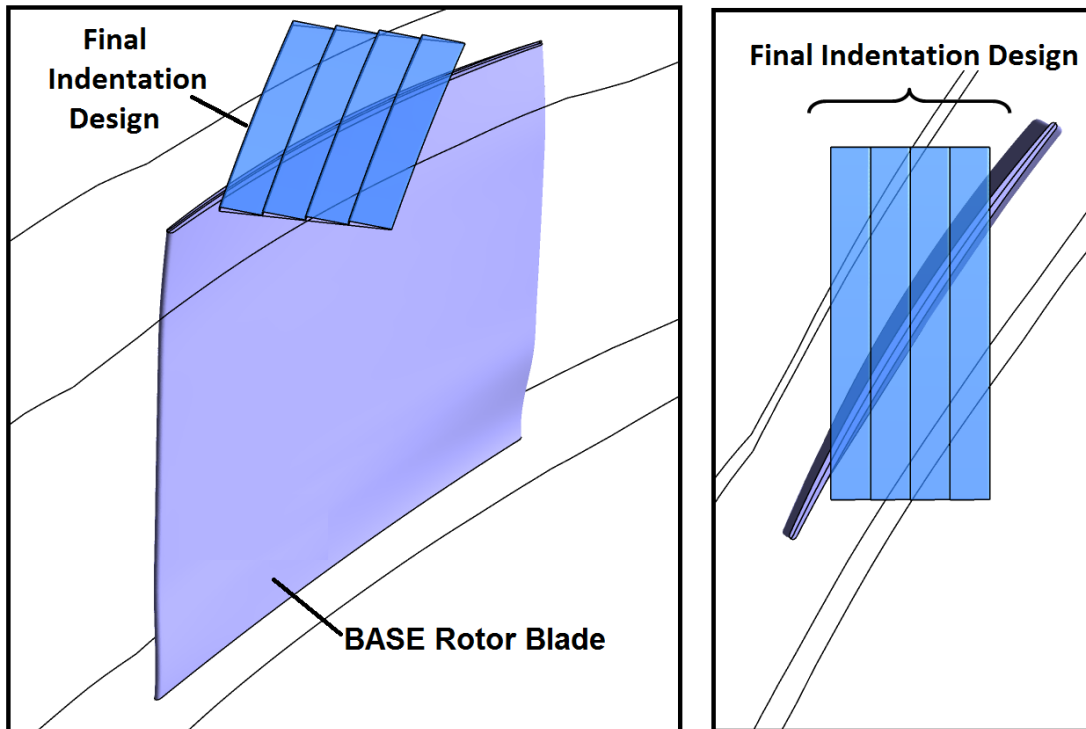
Figure 4-40: Placement of the final casing indentation on the BASE rotor passage

Table 4-8: Change of tip sensitivity and level of performance and aerodynamic stability of the BASE rotor with nominal and final casing indentation relative to the smooth casing

Configuration	$\Delta(dPR/d\zeta)$ [%]	$\Delta(d\eta/d\zeta)$ [%]	$\Delta(dXint/d\zeta)$ [%]	ΔPR	$\Delta\eta$ [pcp]	$\Delta(X_{int}/c_X)$
Final Design	-100	-49	-367	-0.005	0.004	0.263
Nominal Design	-60	-37	-392	-0.008	-0.129	-0.062
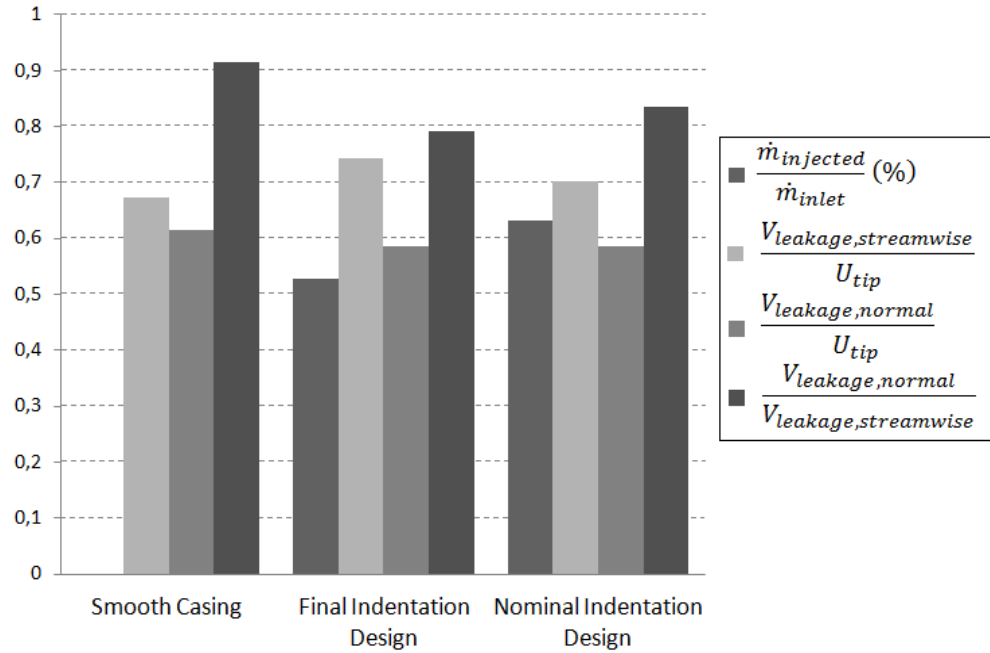
Figure 4-41: Comparison of the four flow parameters for casing indentation effectiveness for the smooth casing, nominal indentation and final indentation designs at nominal t.c. size
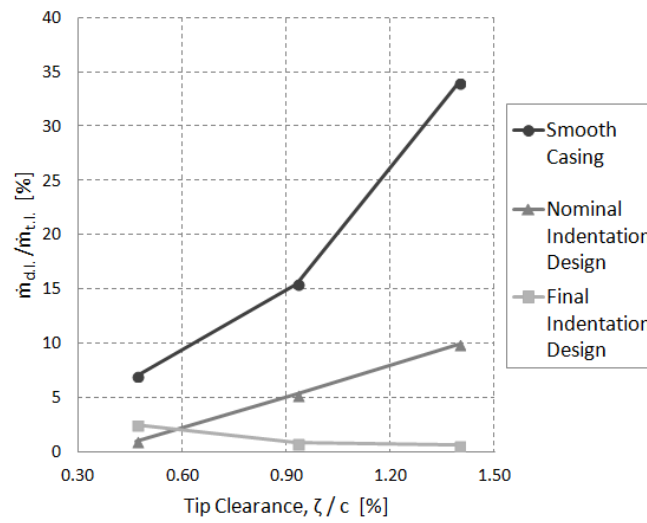
Figure 4-42: Comparison of double leakage sensitivity for the final casing indentation design

4.3 Integration with Blade Design Strategies

To evaluate the possibility of combining desensitizing design features for gas path and blade geometries to add desensitization effects, the final casing treatment design from section 4.2.6 is applied to the FFCS rotor geometry, the most desensitized geometry generated by Erler (2012) that is equivalent to the BASE rotor in term of spanwise loading distribution, design mass flow and pressure ratio with a better nominal efficiency. The resulting configuration is shown in Figure 4-43. The sensitivity of performance and aerodynamic stability, presented in Figure 4-44, show that the integrated design outperforms both of the FFCS rotor with smooth casing and the BASE rotor with casing indentation in terms of tip desensitization and the sensitivities of either configuration seem to add up to give the final combined sensitivity. Moreover, the effect on nominal performance seems to also add up, even if not linearly in the case of efficiency, but enough to show a significant improvement in nominal efficiency. The double leakage sensitivity data in Figure 4-45 shows that the double leakage is almost completely eliminated by the application of indentation which agrees with the performance and stability study. In summary, these results indicate that gas path and blade design strategies can be combined to improve sensitivity reduction as well as nominal performance.
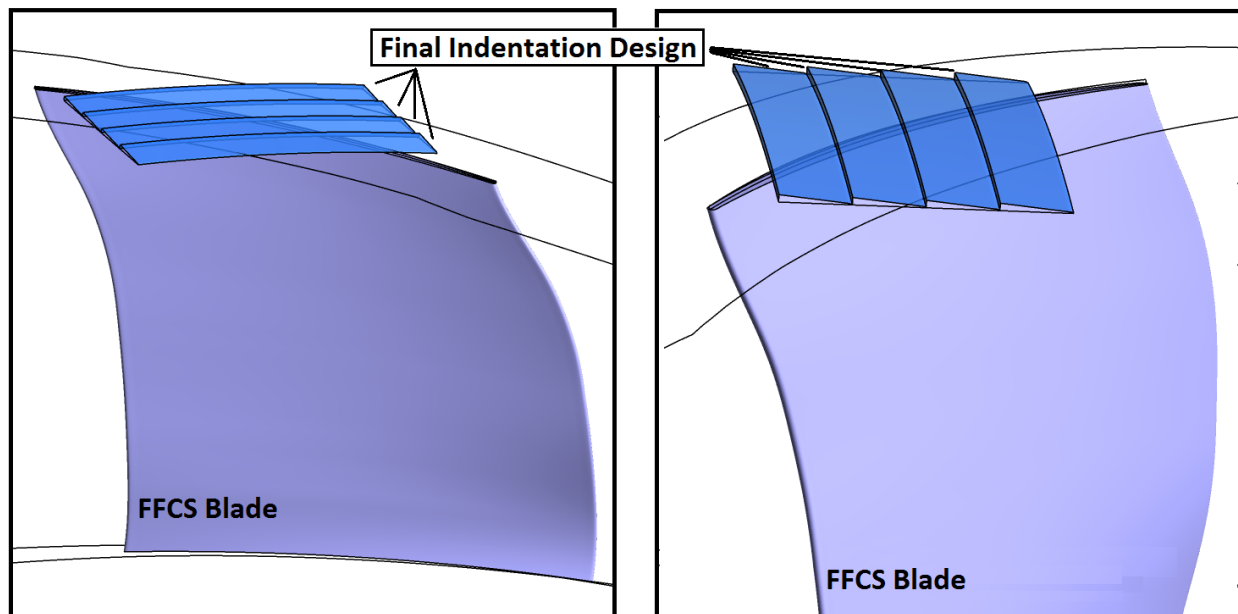
Figure 4-43: Placement of the final casing indentation on the FFCS rotor passage
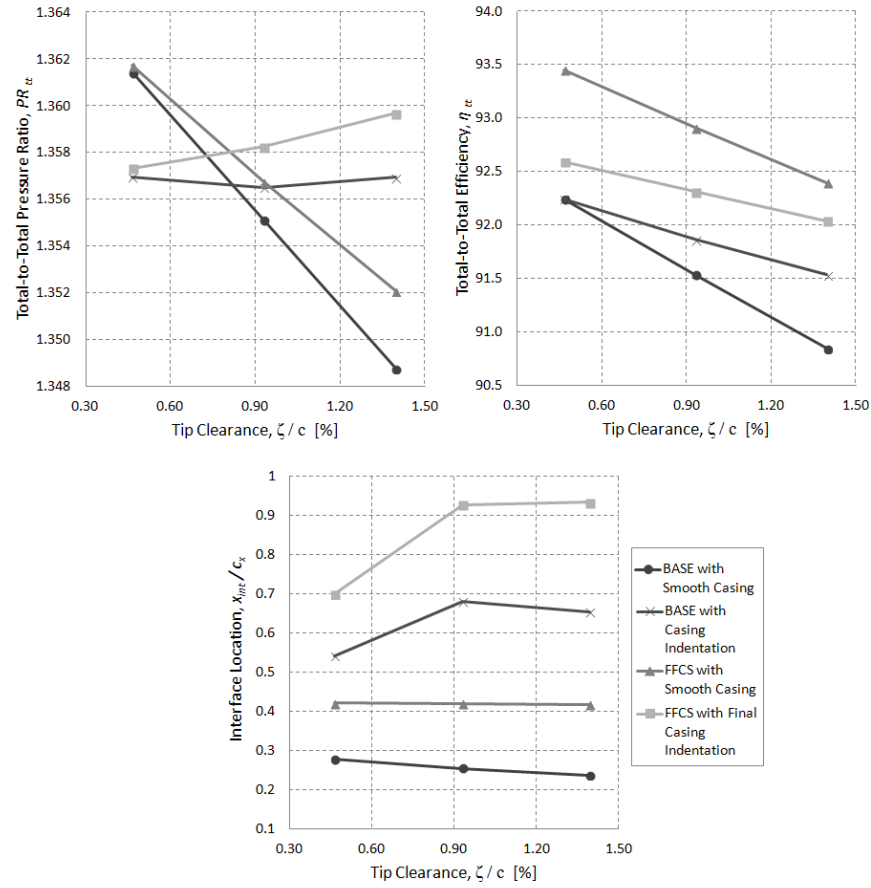
Figure 4-44: Sensitivity study of the BASE and FFCS rotors with final casing indentation design
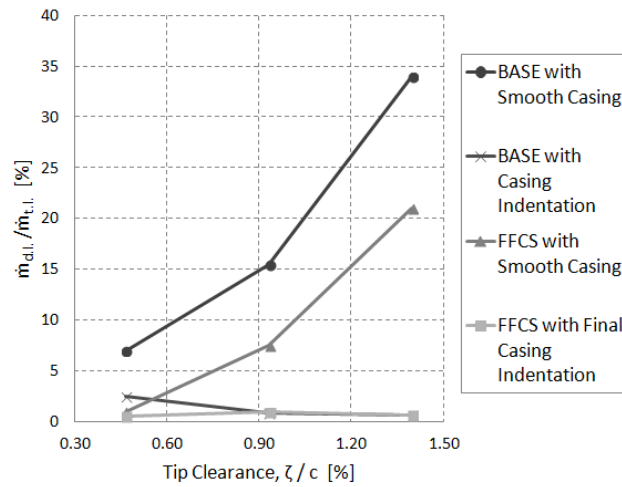
Figure 4-45: Comparison of double leakage sensitivity of BASE and FFCS rotors with final casing indentation design

4.4 Preliminary Assessment for Real Compressors

In this final part of the study, the casing indentation design strategy is evaluated on a preliminary basis for application in real compressors that involve multiple stage and non-axial compressors. This section presents the results of preliminary CFD simulations of the shallow groove casing treatment on to an axial compressor stage, a mixed flow rotor (MFR) and a centrifugal compressor impeller.

4.4.1 Axial Compressor Stage

In order to investigate the effect of the casing indentation on an axial compressor stage, a stator is designed for the BASE rotor which turns the flow back to the axial direction without having any boundary layer separation on blade surfaces at design point conditions. The stator has the same pitch size and the same axial chord length as the BASE rotor and is devoid of hub clearance gap. The final casing indentation design is applied to the BASE rotor in the axial compressor stage. The inlet boundary conditions and rotational speed of the BASE rotor are used for this case and the results are also taken at the corrected mass flow of 3.04 kg/s as in the isolated rotor case. The stage is analyzed at the same three tip clearance levels as the isolated rotor.

The stage geometry with the casing indentation is presented in Figure 4-46. The corresponding performance and aerodynamic stability results, presented in Figure 4-47, show that the pressure ratio and efficiency are desensitized in the same manner as with the isolated rotor. On the other hand, the aerodynamic stability change to the tip clearance shows a parallel behavior to the isolated rotor. While the stall margin is increased at nominal tip clearance, the tip sensitivity is positive as in the isolated rotor case. However, a nominal efficiency penalty is encountered which was not observed in the isolated rotor simulations. The reason of this penalty is attributed to the increase in tip blockage at the rotor exit that creates higher incidence at the inlet of the stator. As shown in Figure 4-48 the incidence angle at stator inlet is increased near the shroud region with the addition of the casing indentation. The resulting increased incidence induces more loss in the stator and this is a slight performance penalty on the stage. Nevertheless the results show that the casing indentation is also effective in reducing tip sensitivity of performance and stall margin in stage conditions.
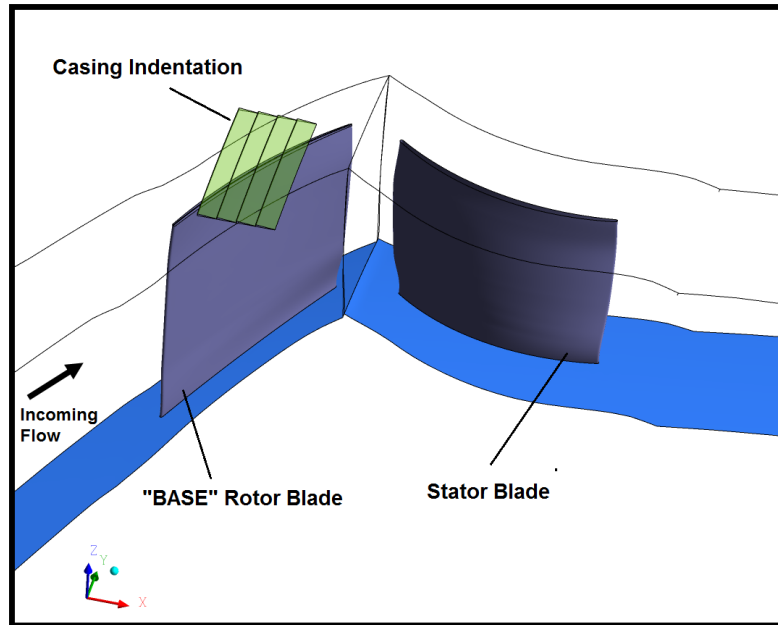
Figure 4-46: Axial compressor stage with the final casing indentation design
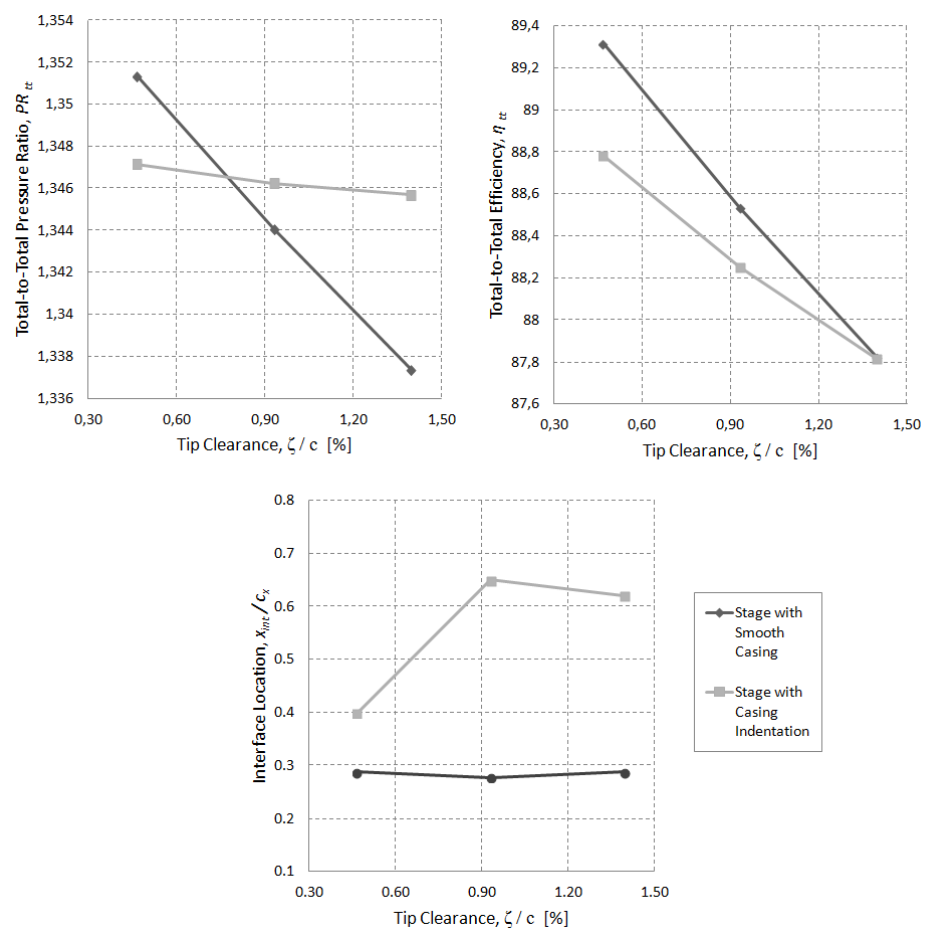
Figure 4-47: Sensitivity study for the axial compressor stage
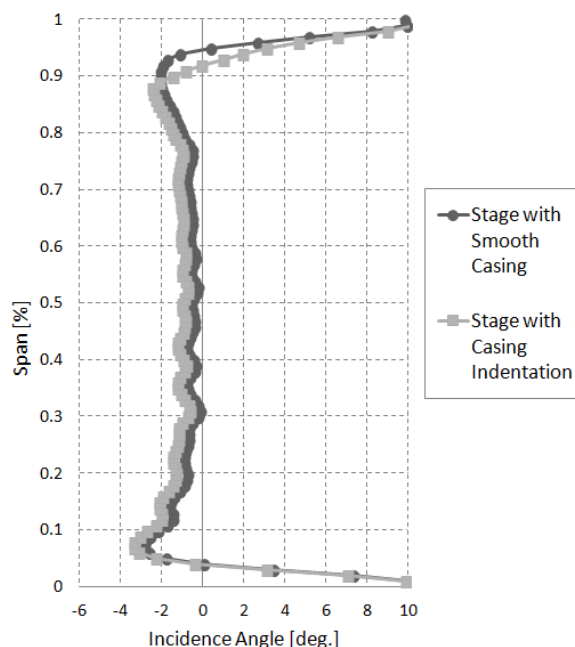
Figure 4-48: Spanwise distribution of the incidence angle at stator inlet taken from 10% axial chord distance upstream of the stator leading edge

4.4.2 Mixed Flow Rotor

A casing indentation design is generated for the Mixed Flow Rotor (MFR) with design features of the nominal indentation design presented in section 3.1.2. The only difference between the nominal indentation shape and that used on the MFR is the width which increases to account for the difference in the axial chord lengths between the BASE rotor and MFR. The indentation design applied to the MFR is shown in Figure 4-49. The operation conditions of the MFR, which are provided by P&WC, are presented at Table 4-9. The values correspond to operating conditions at 5.4 kg/s corrected mass flow. Simulations are carried out at the tip clearance sizes of 0.39% and 0.78% of chord which corresponds 0.01 in. and 0.02 in. respectively.

As shown in Figure 4-50, the double leakage is reduced by almost 50% at nominal tip clearance level but its sensitivity is not decreased by the application of indentation. The reduction in nominal double leakage flow can also be observed in the entropy coloured streamlines in

Figure 4-51. The performance sensitivity results presented in Figure 4-52 show that, the casing indentation has a tip desensitizing effect, but not as strong as it was in the BASE rotor case. The difference probably arises from the need for tailoring the casing indentation geometry according to the flow field characteristics of MFR. Nevertheless, these results demonstrate that the casing indentation can potentially be an effective design strategy for tip desensitization of performance of mixed flow rotors.

Table 4-9 "Operating conditions of the mixed flow rotor (MFR)"

Property	Value
Inlet Total Pressure	101.344 kPa
Inlet Total Temperature	288.14 K
Rotation Speed	46946 rpm
Blade Number	21
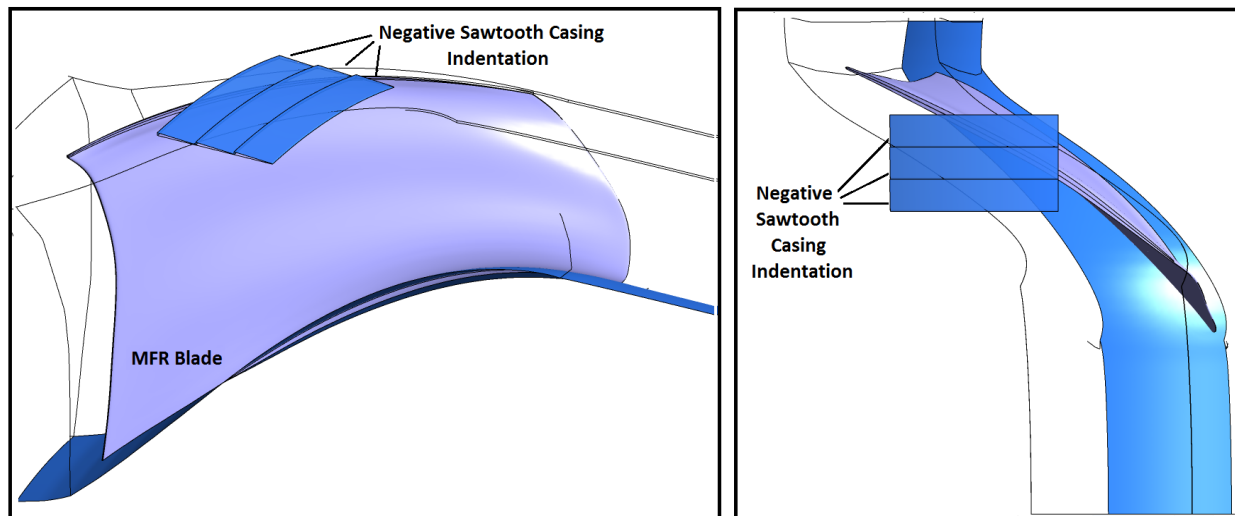
Figure 4-49: MFR blade with the negative sawtooth casing indentation

Figure 4-50: Comparison of the meridional velocity at rotor inlet and the change of double leakage for the MFR with casing indentation

Figure 4-51: Tip clearance flow streamlines of the MFR with 0.01 in. t.c. size in relative frame, for smooth casing, and casing indentation applied cases

Figure 4-52: Sensitivity study for the MFR with casing indentation

4.4.3 Centrifugal Compressor Impeller

For the impeller of a centrifugal compressor, a different type of casing indentation design is used from the previous case. Instead of directly applying the design settings of the nominal casing indentation, a new indentation geometry is tailored according to the geometric features and the flow field of the impeller. The simulations on smooth casing impeller showed that, the double leakage phenomena becomes intense at the downstream part of the impeller passage, as presented in Figure 4-56, such that the indentations are placed at this location. In addition, a rectangular shape indentation is used instead of the negative sawtooth for ease of numerical implementation in this case, and the depth is reduced to 0.010 inch for the same reason. The schematic cross sectional view of the placement of the indentation is presented in Figure 4-53, and a 3-D view is shown in Figure 4-54. The impeller is simulated at the operating conditions given in Table 4-10 and the results are taken at the corrected mass flow rate of 6.26 kg/s. Simulations are carried out at the tip clearance sizes of 0.24% and 0.47% of chord which corresponds 0.010 inches and 0.020 inches respectively.

As shown in Figure 4-55, both the double leakage tip sensitivity and level are reduced significantly. The reduction of nominal double leakage flow can also be observed in the entropy coloured streamlines in Figure 4-56. The performance sensitivity data in Figure 4-57 show that the pressure ratio is almost completely desensitized to tip clearance, while the efficiency is slightly desensitized. However the performance levels indicate that there is a trade off between

tip desensitization and nominal performance penalty similar to the BASE rotor case, which would likely require design tailoring to be reduced/eliminated. These results show that casing indentation can be an effective gas path design strategy for tip desensitization of performance in centrifugal compressors.

Table 4-10 "Operating conditions of the impeller"

Property	Value
Inlet Total Pressure	229.638 kPa
Inlet Total Temperature	378.86 K
Rotation Speed	46946 rpm
Blade Number	11
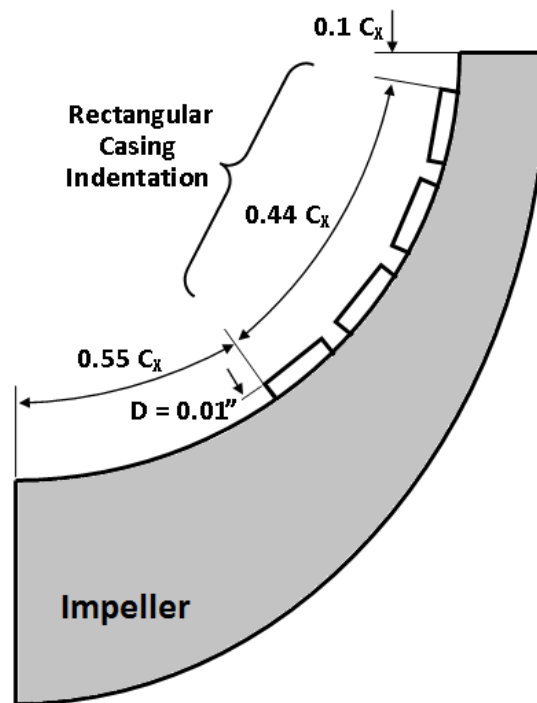
Figure 4-53: Schematical drawing of the cross sectional view and the dimensions of the rectangular shaped casing indentation design of impeller blade
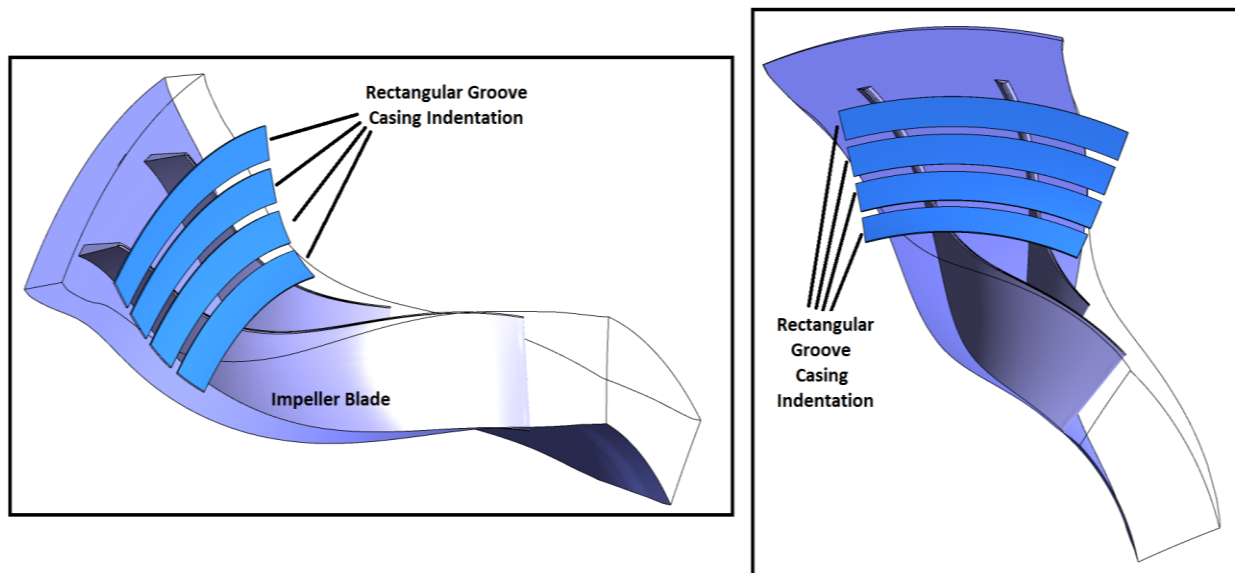
Figure 4-54: Centrifugal compressor impeller with the casing indentation
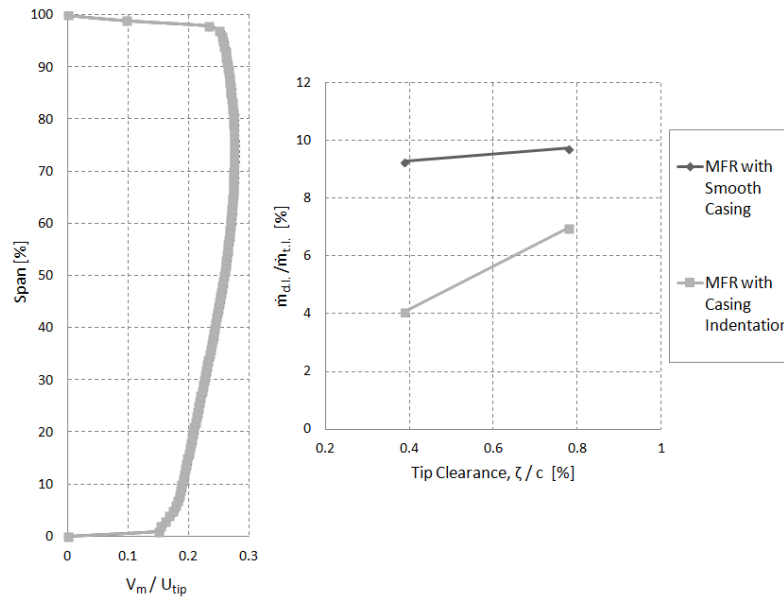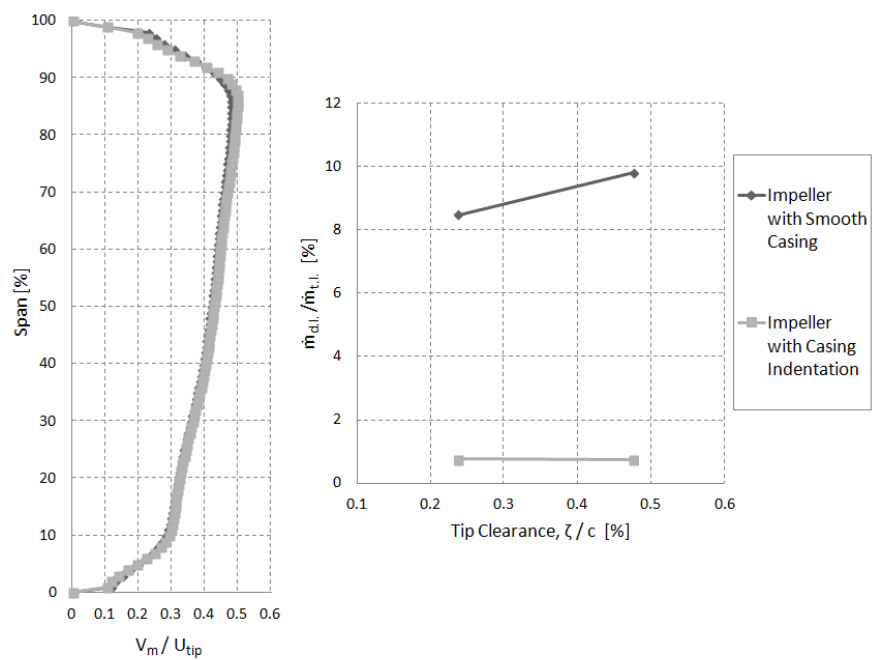

Figure 4-55: Comparison of the meridional velocity at rotor inlet and the change of double leakage for the impeller with casing indentation
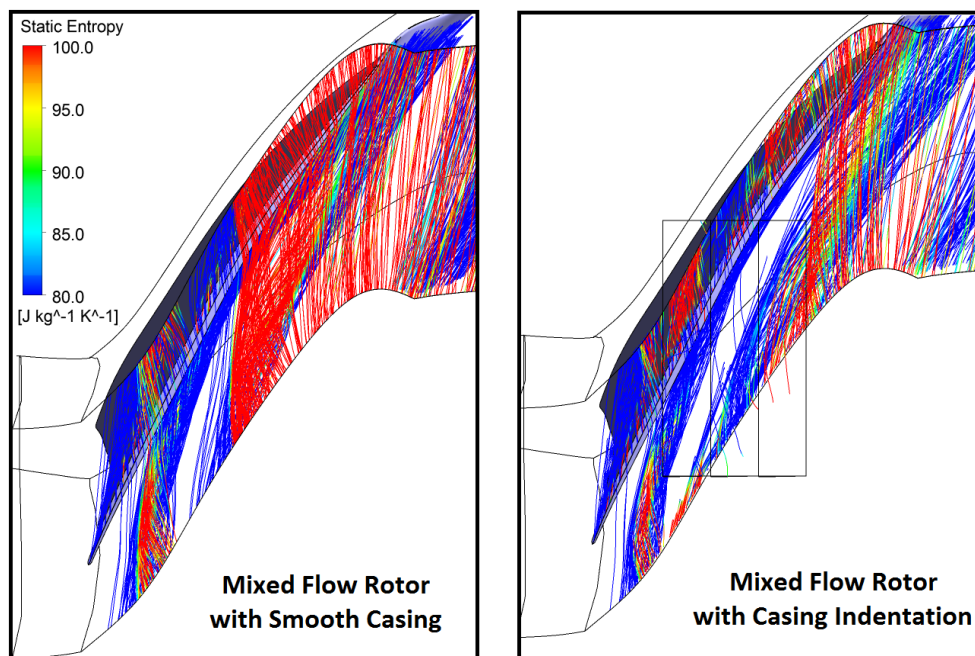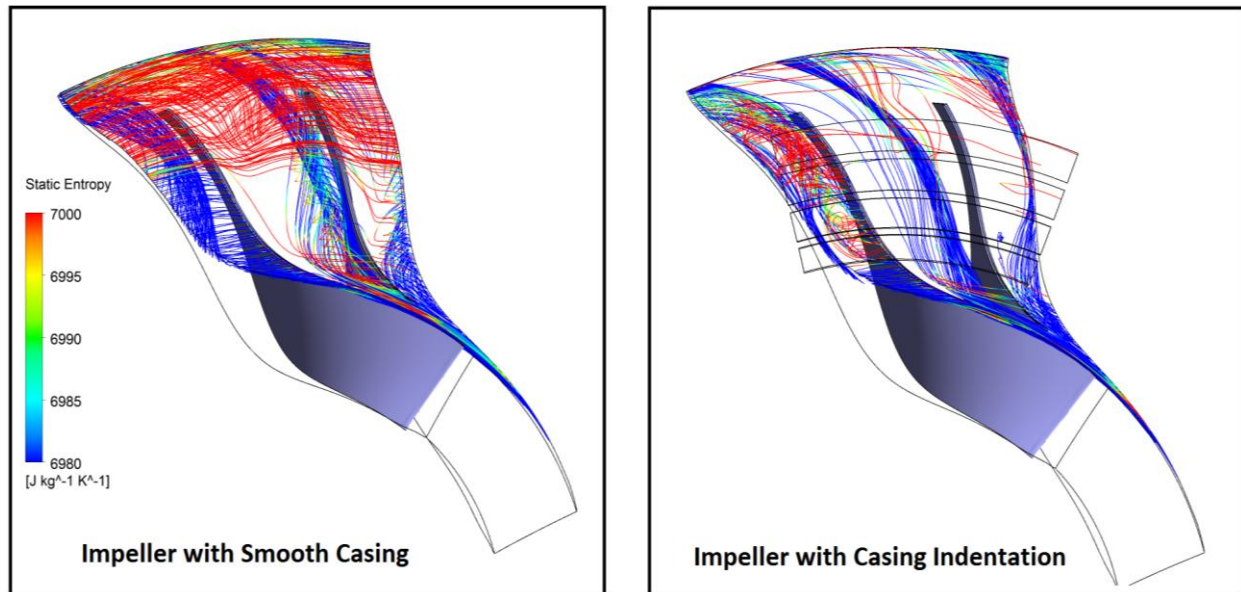
Figure 4-56: Tip clearance flow streamlines of the impeller with 0.01 in. t.c. size in relative frame, for smooth casing, and casing indentation applied cases
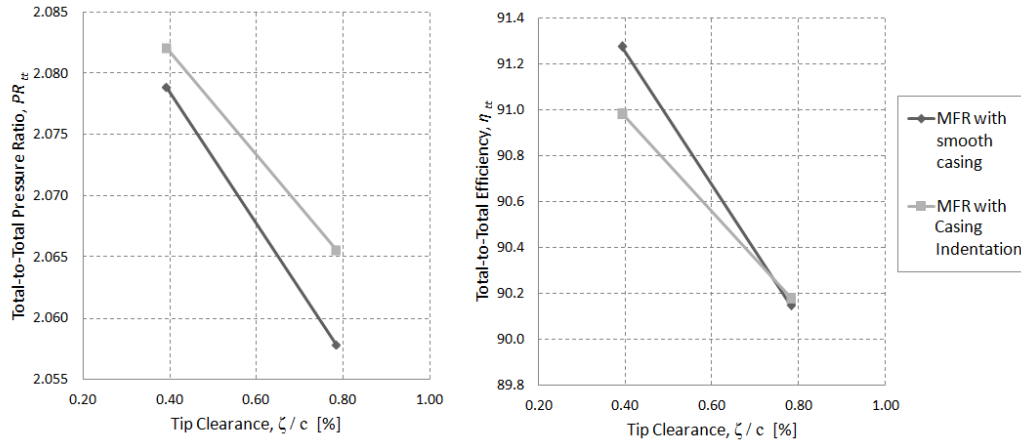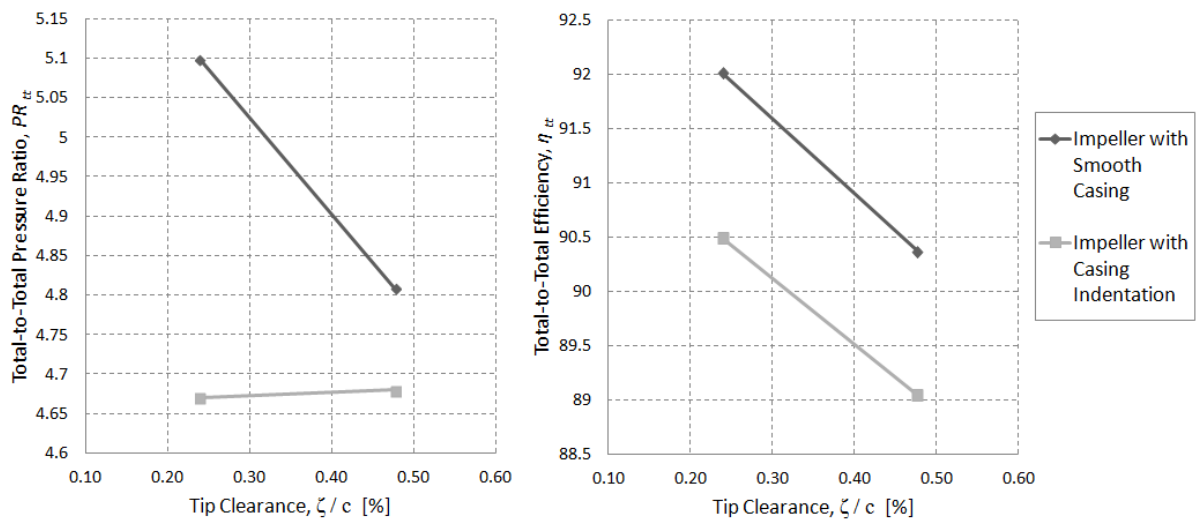

Figure 4-57: Sensitivity study for the impeller with casing indentation

CHAPTER 5   CONCLUSIONS AND FUTURE WORK

A computational study was carried out to develop and evaluate gas path design strategies that can reduce the sensitivity of compressor performance and aerodynamic stability to tip clearance. The search for gas path design strategies was based on the exploitation of the two flow desensitizing features discovered by Erler (2012) for axial compressor rotors, namely the reduction of double leakage flow and increasing incoming meridional velocity near the rotor tip. Two gas path design strategies were proposed and analyzed. The first was gas path contouring in the form of a concave gas path to increase tip meridional momentum. The second is a casing treatment in the form of sawtooth shaped circumferential indentations with a depth on the order of the tip clearance gap placed on the shroud over the rotor to reduce double leakage, which had been shown to have a detrimental effect on performance and stall margin.

An assessment of the two strategies on a double circular arc high subsonic axial compressor rotor showed that the sawtooth casing indentation provided much larger sensitivity reduction and much lower performance penalty. A detailed flow field analysis was carried out on the sawtooth indentations scheme to elucidate the flow mechanism and a parametric study was carried out to obtain preliminary design rules for minimizing performance and stall margin sensitivity to tip clearance as well as nominal performance loss. The effectiveness of the sawtooth indentation strategy was then evaluated for a reduced-sensitivity axial rotor blade design, an axial compressor stage, a mixed flow rotor and a centrifugal compressor impeller.

The main conclusions/findings are;

1. The negative axial sawtooth indentation casing treatment provides a significant reduction in double leakage and its increase with tip clearance size and hence reduces the sensitivity of performance and stall margin to tip clearance.

2. The flow mechanism relies on suction of the high-entropy double leakage fluid into the indentation grooves by the pressure difference across the blade and injecting it radially inward over and beyond the tip gap on the blade suction side. In its place, low-entropy flow from the pressure side core flow enters the tip clearance gap producing tip clearance

flow with high streamwise and low normal velocity components. This 'improved' tip clearance flow mixes with the injected high-entropy flow from the grooves to redirect its path streamwise and prevent it from contributing to double leakage in the next tip gap. An increase in tip gap size results in the increase in both high-entropy injected flow by the groves and low-entropy flow in the tip clearance thus controlling the rise in double leakage and by extension the drop in performance and stall margin with tip clearance, associated with tip sensitivity. The indentations essentially provides a mechanism for improved streamwise momentum transfer between the high entropy flow next to the shroud associated with double leakage and the low-entropy core flow.

3. The geometric design parameters affect the effectiveness of the casing treatment through their influence on four flow parameters, namely injected mass flow from the grooves, streamwise and normal velocity components and flow angle of tip clearance flow. Increased axial extent and forward location of the indentations provide the largest reduction in sensitivity but with large performance penalty. The impacts of groove depth and groove width are small for sensitivity but large for nominal performance penalty, the latter decreasing with reduced depth and increased number of grooves. The groove shape has a moderate impact on sensitivity and nominal performance loss. An improved design can be obtained that reduces both performance/stall margin sensitivity and nominal performance penalty.

4. The desensitization effect of the indentation casing treatment can be combined with those blade design strategies to further reduce sensitivity and reduce/eliminate/reverse nominal performance penalty.

5. The indentation casing treatment also works in a compressor stage environment and in non-axial compressor rotors and is thus a highly technology to develop for real multi-stage compressors.

The main contributions of this research are;

1. Development of a new casing treatment concept consisting of shallow grooves that can significantly reduce the sensitivity of compressor performance and aerodynamic stability to tip clearance increase with minimal nominal performance penalty, and can work for axial as well as all non-axial compressors.

2. Elucidation of the associated flow mechanism (which could perhaps be generally applicable to all circumferential grooves casing treatment) and development of preliminary design rules for minimizing tip sensitivity and nominal performance loss for an axial compressor rotor.

From the results of the current research, the recommendations for future work are:

1. Verify the validity of the two desensitizing flow features for mixed flow and centrifugal compressors

2. Verify the flow mechanism and preliminary design rules for shallow grooves casing treatment on mixed flow and centrifugal compressors

3. Investigate the effects of flow unsteadiness in a multi-stage compressor on the effectiveness of the shallow grooves casing treatment

4. Investigate the possible effects of flow unsteadiness introduced by the shallow grooves casing treatment such as in terms of acoustic excitations.

5. Experimentally assess the effectiveness of shallow grooves casing treatment on a compressor cascade and/or test rig

BIBLIOGRAPHY

ANSYS. *ANSYS CFX-Solver Modeling Guide.* ANSYS Inc., 2010.

ANSYS. *Innovative Turbulence Modeling: SST model in ANSYS CFX.* Technical Report, ANSYS Inc., 2006.

Benini, E., and R. Biollo. "Aerodynamics of Swept and Leaned Transonic Compressor Rotors." *Applied Energy* 84 (2007): 1012-1027.

Camp, T. R., and I. J. Day. "A Study of Spike and Modal Stall Phenomena in a Low-Speed Axial Compressor." *Journal of Turbomachinery* 120 (1998): 393-401.

Chima, R. V. "Calculation of Tip Clearance Effects in aTransonic Compressor Rotor." *Journal of Turbomachinery* 120 (1998): 131-140.

Cumpsty, N. A. *Compressor Aerodynamics.* _: Longman Scientific&Technical, 1989.

Danner, F., H. P. Kau, M. M. Muller, H. P. Schiffer, and A. B. Giovanni. "Experimental and Numerical Analysis of Axial Skewed Slot Casing Treatments for a Transonic Compressor Stage." *Proceedings of ASME Turbo Expo: Power for Land, Sea and Air.* Orlando, USA, 2009.

Day, I. J. "Stall Inception in Axial Flow Compressors." *Journal of Turbomachinery* 115 (1993): 1-9.

Denton, J. D. "Loss Mechanisms in Turbomachines." *Journal of Turbomachinery* 115 (1993): 621-656.

Denton, J., and L. Xu. "The Exploitation of Three-Dimensional Flow in Turbomachinery Design." *Proceedings of the Institution of Mechanical Engineers, Part C: Journal of Mechanical Engineering Science* 213 (1998): 125-137.

Deppe, A., H. Saathoff, and U. Stark. "Spike-Type Stall Inception in Axial-Flow Compressors." *Proceedings of 6th European Conference on Turbomachinery-Fluid Dynamics and Thermodynamics.* Lille, France, 2005.

Erler, Engin. *Axial Compressor Blade Design for Desensitization of Aerodynamic Performance and Stability to Tip Clearance.* Montreal: PhD Thesis, École Polytechnique de Montréal, 2012.

Freeman, C. *Effect of Tip Clearance Flow on Compressor Stability and Engine Performance.* Rhode-St-Genèse, Belgium: Von Karman Institute for Fluid Dynamics Lecture Series, 1985.

Fujita, H., and H. Takata. "A Study on Configurations of Casing Treatment for Axial Compressors." *Bulletin of JSME* 27 (1984): 1675-1681.

Gallimore, S. J., J. J. Bolger, N. A. Cumpsty, M. Taylor, P. I. Wright, and J. M. Place. "The Use of Sweep and Dihedral inMultistage Axial Flow Compressor Blading Part I:University Research and Methods Development." *Journal of Turbomachinery* 124 (2002): 521-532.

Goller, M., V. Gummer, C. Clemen, and M. Swoboda. "Enhancement of Highly-Loaded Axial Compressor Stage Performance Using Rotor Blade Tip Tailoring Part-I Numerical Design Studies." *Proceedings of the 6th European Conference on Turbomachinery Fluid Dynamics and Thermodynamics.* Lille, France, 2005. 88-99.

Greitzer, E. M. "Surge and Rotating Stall in Axial Compressors, Part I and II." *Journal of Engineering for Power* 98 (1976): 190-217.

Hah, C., J. Bergner, and H. Schiffer. "Short Length-Scale Rotating Stall Inception in a Transonic Axial Compressor: Criteria for Mechanisms." *Proceedings of ASME Turbo Expo: Power for Land, Sea and Air.* Barcelona, Spain, 2006.

Iandoli, C. L., and E. Sciubba. "3-D Numerical Calculation of the Local Entropy Generation Rates in a Radial Compressor Stage." *International Journal of Applied Thermodynamics* 8 (2005): 83-94.

Inoue, M., and M. Kuroumaru. "Structure of Tip Clearance Flow in an Isolated Axial Compressor Rotor." *Journal of Turbomachinery* 111 (1989): 250-256.

Inoue, M., M. Kuroumaru, and M. Fukuhara. "Behavior of Tip Leakage Flow Behind an Axial Compressor Rotor." *Journal of Engineering for Gas Turbines and Power* 108 (1986): 7-14.

Khalid, S. A., et al. "Endwall Blockage in Axial Compressors." *Journal of Turbomachinery* 121 (1999): 499-509.

Kroger, G., C. Cornelius, and E. Nicke. "Rotor Casing Contouring in High Pressure Stages of Heavy Duty Gas Turbine Compressors with Large Tip Clearance Heights." *Proceedings of ASME Turbo Expo: Power for Land, Sea and Air.* Orlando, Florida, USA, 2009.

Lakshminarayana, B. *Turbomachinery Fluid Dynamics and Heat Transfer.* _: Johnson Wiley & Sons, Inc., 1996.

Lee, K., K. Kim, and A. Samad. "Design Optimization of low-speed Axial Flow Fan Blade with Three-Dimensional RANS Analysis." *Journal of Mechanical Science and Technology* 22 (2008): 1864-1869.

Legras, G., N. Gourdain, and I. Trebinjac. "Numerical Analysis of the Tip Leakage Flow Field in a Transonic Axial Compressor with Circumferential Casing Treatment." *Journal of Thermal Science* 19 (2010): 198-205.

Liu, Y., X. Yu, and B. Liu. "Turbulence models assessment for large-scale tip vortices in axial compressor rotor." *Journal of Propulsion and Power* 24 (2008).

Lu, X., W. Chu, J. Zhu, and Y. Wu. "Mechanism of the Interaction Between Casing Treatment and Tip Leakage Flow in a Subsonic Axial Compressor." *Proceedings of ASME Turbo Expo 2006: Power for Land, Sea and Air.* Barcelona, Spain, 2006.

Ma, H., and B. Li. "Effects of Axial Non-uniform Tip Clearances on Aerodynamic Performance of a Transonic Axial Compressor." *Journal of Thermal Science* 17 (2008): 331-336.

McNulty, G. S., J. J. Decker, B. F. Beacher, and S. A. Khalid. "The Impact of Forward Swept Rotors on Tip Clearance Flows in Subsonic Axial Compressors." *Journal of Turbomachinery* 126 (2004): 445-453.

Mileshin, V., I. Brailko, and A. Startsev. "Application of Casing Circumferential Grooves to Counteract the Influence of Tip Clearance." *Proceedings of ASME Turbo Expo 2008: Power for Land, Sea and Air.* Berlin, Germany, 2008.

Moore, F. K., and E. M. Greitzer. "A Theory of Post-Stall Transients in Axial Compressors- Part I: Development of Equations." *Journal of Engineering for Gas Turbines and Power* 108 (1986): 68-76.

Muller, M. W., P. Schiffer, and C. Hah. "Effect of Circumferential Grooves on the Aerodynamic Performance of an Axial Single-Stage Transonic Compressor." *Proceedings of ASME Turbo Expo 2007: Power for Land, Sea and Air.* Montreal, Canada, 2007.

Passrucker, H., M. Engber, S. Kablitz, and D. K. Hennecke. "Effect of Forward Sweep in a Transonic Compressor Rotor." *Proceedings of the Institution of Mechanical Engineers: Journal of Power and Energy* 217 (2003): 357-365.

Ramakrishna, P. V., and M. Govardhan. "Study of Sweep and Inducaed Dihedral Effects in Subsonic Axial Flow Compressor Passages-Part II:Detailed Study of the Effects on Tip Leakage Phenomena." *International Journal of Rotating Machinery*, 2010.

Reid, L., and R. Moore. *Design and Overall Performance of Four Highly Loaded High Speed Inlet Stages for an Advanced High Pressure-Ratio Core Compressor.* NASA Report, NASA TP 1337, 1978.

Shabbir, Aamir, and John J. Adamczyk. "Flow Mechanism for Stall Margin Improvement due to Circumferential Casing Grooves on Axial Compressors." *Journal of Turbomachinery* 127 (2005): 708-717.

Shao, W., and L. Ji. "Basic Analysis of Tip Leakage Mixing Loss." *Proceedings of ASME Turbo Expo 2007: Power for Land, Sea and Air.* Montreal, Canada, 2007.

Smith, G. D. J., and N. A. Cumpsty. "Flow Phenomena in Compressor Casing Treatment." *Journal of Engineering for Gas Turbines and Power* 106 (1984): 532-541.

Smith, L. H., Jr. "Casing Boundary Layers in Multistage Axial-Flow Compressors." *Proceedings of Symposium on Flow Research on Blading.* Baden, Switzerland, 1970.

Storer, J. A., and N. A. Cumpsty. "An Approximate Analysis and Prediction Method for Tip Clearance Loss in Axial Compressors." *Journal of Turbomachinery* 116 (1994): 648-656.

Storer, J. A., and N. A. Cumpsty. "Tip Leakage Flow in Axial Compressors." *Journal of Turbomachinery* 113 (1991): 252-259.

Suder, K. L. "Blockage Development in a Transonic, Axial Compressor Rotor." *Journal of Turbomachinery* 120 (1998): 465-476.

Suder, K. L., and M. L. Celestina. "Experimental and Computational Investigation of the Tip Clearance Flow in a Transonic Axial Compressor Rotor." *Journal of Turbomachinery* 118 (1996): 218-229.

Takata, H., and Y. Tsukuda. "Stall Margin Improvement by Casing Treatment-Its Mecanism and Effectiveness." *Journal of Engineering for Power* 99 (1977): 121-133.

Thompson, D. W., P. I. King, and D. C. Rabe. "Experimental Investigation of Stepped Tip Gap Effects on the Performance of a Transonic Axial-Flow Compressor Rotor." *Journal of Turbomachinery* 120 (1998): 477-485.

Van Zante, D. E., A. J. Strazisar, J. R. Wood, M. D. Hathaway, and T. H. Okiishii. "Recommendations for Achieving Accurate Numerical Simulation of Tip Clearance Flows in Transonic Compressor Rotors." *Journal of Turbomachinery* 122 (2000): 733-742.

Vo, H. D. "Role of Tip Clearance Flow on Axial Compressor Stability." PhD Thesis, Massachusetts Institute of Technology, 2001.

Vo, H. D., C. S. Tan, and E. M. Greitzer. "Criteria for Spike Initiated Rotating Stall." *Journal of Turbomachinery* 130 (2008): 011023.

Wadia, A. R., C. S. Hah, and D. Rabe. "The Impact of Forward Sweep On Tip Clearance Flows in Transonic Compressors." *Proceedings of ICAS 2004, 24th International Congress of the Aeronautical Sciences.* Yokohama, Japan, 2004.

Wang, Z., X. Jia, and R. Cai. "Influence of Blade Tip Clearance Shapes on Aerodynamic Performance of an Axial Flow Compressor Stator." *Proceedings of 15th International Symposium on Air Breathing Engines.* Bangalore, India, 2002.

Wilke, I., and H. P. Kau. "A Numerical Investigation of the Flow Mechanisms in a HPC Front Stage with Axial Slots." *Proceedings of ASME Turbo Expo 2003: Power for Land, Sea and Air.* Atlanta, USA, 2003.

—. "A Numerical Investigation of the Influence of Casing Treatments on the Tip Leakage Flow in a HPC Front Stage." *Proceedings of ASME Turbo Expo 2002: Power for Land, Sea and Air.* Amsterdam, Netherlands, 2002. 1155-1165.

Wisler, D. C. "Aerodynamic Effects of Tip Clearance, Shrouds, Leakage Flow, Casing Treatment and Trenching in Compressor Design." *Lecture Series 1985-5.* Rhode-St-Genèse, Belgium: Von Karman Institute for Fluid Dynamics, 1985.

Yang, H., D. Nuernberger, E. Nicke, and A. Weber. "Numerical Investigation of Casing Treatment Mechanisms with a Conservative Mixed-Cell Approach." *Proceedings of ASME Turbo Expo 2003: Power for Land, Sea and Air.* Atlanta, USA, 2003.

Zhang, Hui, and Hongwell Ma. "Study of Sloped Trench Casing Treatment on Performance and Stability of a Transonic Axial Compressor." *Proceedings of ASME Turbo Expo 2007; Power for Land, Sea and Air.* Montreal, Canada, 2007.

Appendix A   Reference (BASE) Blade Design

Reference blade designed by Erler (2012) is used as the base rotor design during this study which is referred as "BASE" rotor. The BASE rotor was designed to ensure ease of modifications on both blade and gas path geometries.

It was designed to be tip-critical hence the effect of any design modification on the sensitivity of performance and stability to the tip clearance size would be apparent. The reference blade profile is set as double circular arc (DCA) which is recommended for high-speed/transonic speed operating conditions (Lakshminarayana 1996). The loading along the chord is distributed uniformly by using one circular arc camber. The blade was designed as radially stacked in spanwise direction in order to observe an effect of any design modification on either blade or gas path isolated from the three-dimensional blade design features, such as sweep or lean.

Inlet conditions are also simplified by setting the inlet flow as axial. The gas path is also designed plain by keeping the shroud radius constant which helped the gas path modifications to be made with less effort. The input loading distribution is also assigned uniform in spanwise direction (as shown in Figure A-1) to avoid any hub/blade boundary layer separation and to ensure that no desensitization occurs due to any reduction in tip loading.

The sensitivity of performance and stability of BASE rotor to change in tip clearance size are presented at Figure A-2. According to these results, at nominal tip clearance level, design corrected mass flow rate is determined as 3.04 kg/s, total-to-total pressure ratio as 1.361, total-to-total efficiency as 92.24% and, stall margin as 16.61% . These values and the sensitivity characteristics are taken as the benchmark in order to evaluate the improvements achieved by the gas path modifications made on the BASE rotor during this study.
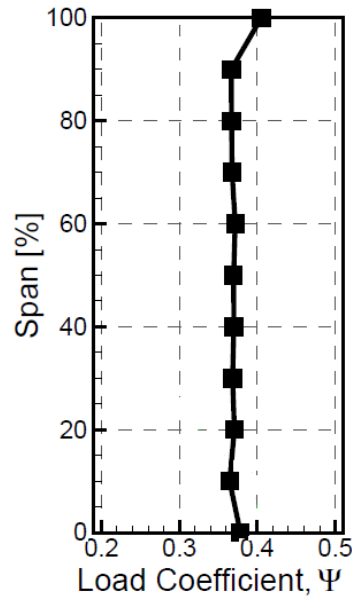
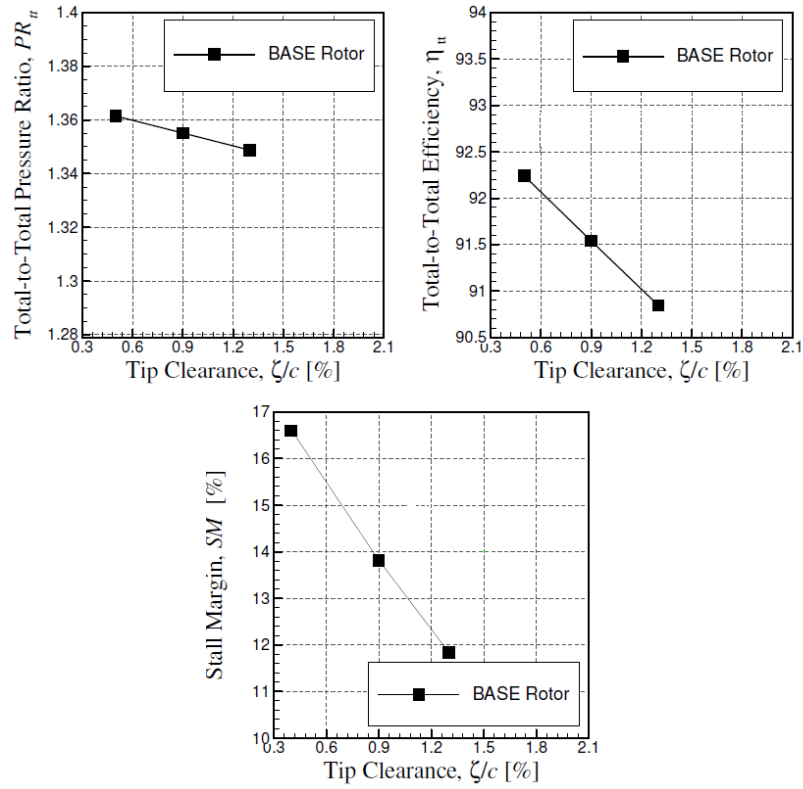Figure A-1: Spanwise loading distribution of the BASE rotor blade (Erler 2012)

Figure A-2: Performance and Stabilitiy sensitivity of the BASE rotor (Erler 2012)

Appendix B   Definitions of Important Parameters

The measurements of sensitivity parameters are held from four planes located at the computational domain inlet, at 10% chord upstream of the leading edge, at 10% chord downstream of trailing edge and, at the computational domain outlet. These measurement locations are referred respectively as, Plane 1, 2, 3 and 4.

The formulations of general performance and stability parameters are given as follows;

- Corrected mass flow rate ($\dot{m}_c$) is defined as given Equation B.3. $P_{t,2}$ and $T_{t,2}$ terms in this equation are total pressure and temperature in stationary frame.

$$\dot{m}_{corr} = \frac{\dot{m}\sqrt{T_{t,2}/T_{ref}}}{P_{t,2}/P_{ref}} \qquad \text{B.3}$$

- Total-to-total pressure ratio (PR_{tt}) is defined as given in Equation B.4, where $P_{t,3}$ and $P_{t,2}$ are total pressures in stationary frame, measured at Plane 3 and 2 respectively.

$$PR_{tt} = \frac{P_{t,3}}{P_{t,2}} \qquad \text{B.4}$$

- The total-to-total efficiency is defined as given in Equation B.5, the definition is made by assuming the air as ideal gas with constant specific heats. $T_{t,3}$ and $T_{t,2}$ are total temperatures in stationary frame measured at Plane 2 and 3.

$$\eta_{tt} = \frac{\left(P_{t,3}/P_{t,2}\right)^{\gamma/\gamma-1} - 1}{\left(T_{t,3}/T_{t,2}\right) - 1} \qquad \text{B.5}$$

- The stall margin is (SM) is defined as the difference between the corrected mass flow rate at stall point ($\dot{m}_{c,stall}$) and at design point ($\dot{m}_{c,design}$) (i.e. corrected mass flow rate at maximum efficiency), non-dimensionalized by the design point corrected mass flow. Its formulation is presented at Equation B.6.

$$SM = \frac{\dot{m}_{c,stall} - \dot{m}_{c,design}}{\dot{m}_{c,design}} \qquad \text{B.6}$$

- The incoming/tip clearance flow interface is located at the highest entropy gradient line at the rotor tip plane. The position of the interface is defined by the intersection of this highest entropy line and the pitch line that passes 85% of pitch distance away from the suction surface of the blade tip. The 85% pitch distance is selected to be as close to pressure side as possible while keeping the measurement isolated from the effects of pressure side boundary layer entropy gradient. Figure B-1 shows the interface location for an axial compressor rotor. As the figure shows, the interface position (x_{int}) is measured from the leading edge plane, since stall criterion would be satisfied when incoming/tip clearance flow interface reaches the leading edge plane. Interface positions measured in this study are non-dimensionalized with the axial chord (c_x). Since having interface position at leading edge means that the blade is stalled, the interface position can also substitute for stall margin in cases where the speedline could not be simulated the way up to the stall point.
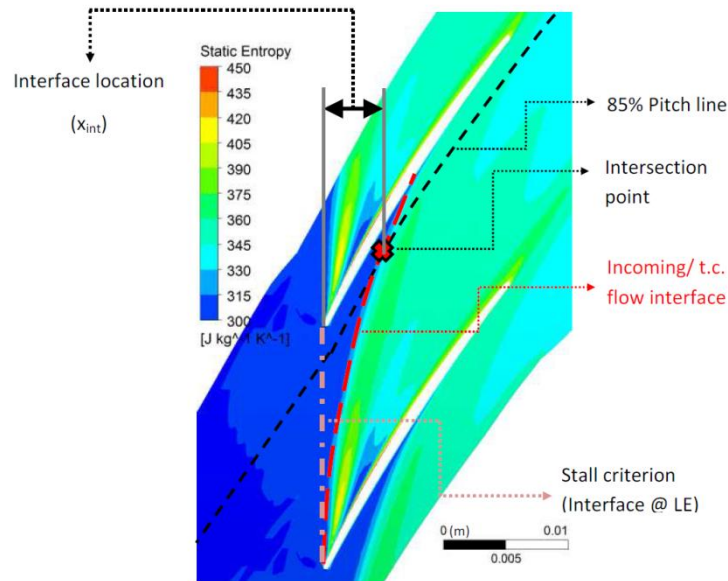
Figure B-1: Definition of interface position (Erler 2012)

Double Leakage Calculation:

Double leakage calculation is performed by a post processing procedure on the results of simulations. Double leakage is distinguishable with three features which could be summarized as;

- To have higher flow angle than the rest of tip clearance flow

- To have higher static entropy level than the rest of tip clearance flow

- To occur at the vicinity of the shroud in tip gap and passage

Depending on these features, double leakage flow region is identified by using the entropy contoured streamlines emanating from the tip clearance with high entropy and high flow angle as shown in Figure B-2. Since the streamlines are not practical to quantify the double leakage mass flow rate, entropy contours on the pressure side of the tip gap is examined. Figure B-3 shows the entropy contours on the negative sawtooth indentation applied rotor tip gap pressure side, and the marked region is determined to be under the influence of double leakage according to a comparison of these contours with streamline plots. For the quantification of double leakage the flow angle values are also used to precisely distinguish double leakage flow region.
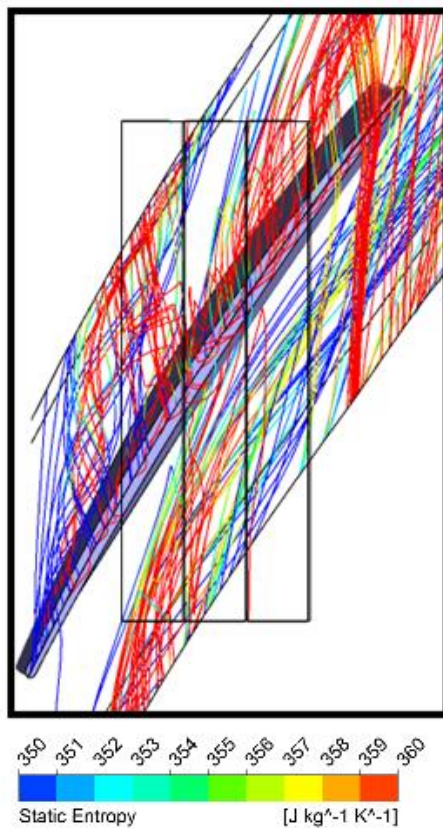
Figure B-2: Tip clearance flow streamlines of negative sawtooth indentation applied rotor, at peak efficiency mass flow (3.04 kg/s) and nominal tip clearance size
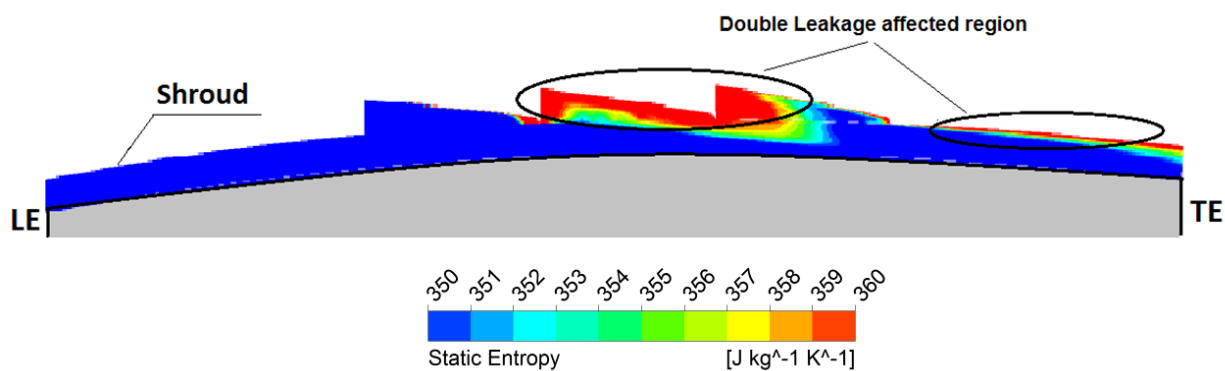

Figure B-3: Contour of static entropy at tip clearance pressure surface of negative sawtooth indentation applied rotor, at peak efficiency mass flow (3.04 kg/s) and nominal tip clearance size

Loading Calculation:

The spanwise loading is measured by using an enthalpy based loading coefficient (ψ) which is calculated according to the formulation presented at Equation B.7. In this formulation $h_{t,2}$ and $h_{t,3}$ represents total enthalpy at stationary frame which are measured 10% away from the leading and the trailing edge planes, respectively.

$$\psi = \frac{h_{t,3} - h_{t,2}}{U^2} \qquad\qquad \text{B.7}$$

Mass Flow Transfer Calculation:

The mass flow transfer driven by the grooves between the blade pressure and suction sides is obtained from the radial velocity distribution at the shroud radial plane between the rotor and indentation flow fields. As illustrated in Figure B-4, the (red) positive radial velocity region along the blade pressure side represents the suctioned flow into the groove while the (blue) negative radial velocity region along the blade suction side represents the corresponding injected flow from the groove into the blade passage. The mass flow transfer can be calculated by using the local density and local radial velocity distribution and, area within either of these regions. However, there is often injection (blue) regions slightly beyond the blade suction side that come from local passage flow recirculation within the groove (see appendix E) and not linked to mass flow transfer from the blade suction side. Thus, the mass flow transfer value is calculated from the suction (red) flow region near the blade pressure side with verification that it is similar to the value from the (blue) injection region near the blade suction side.
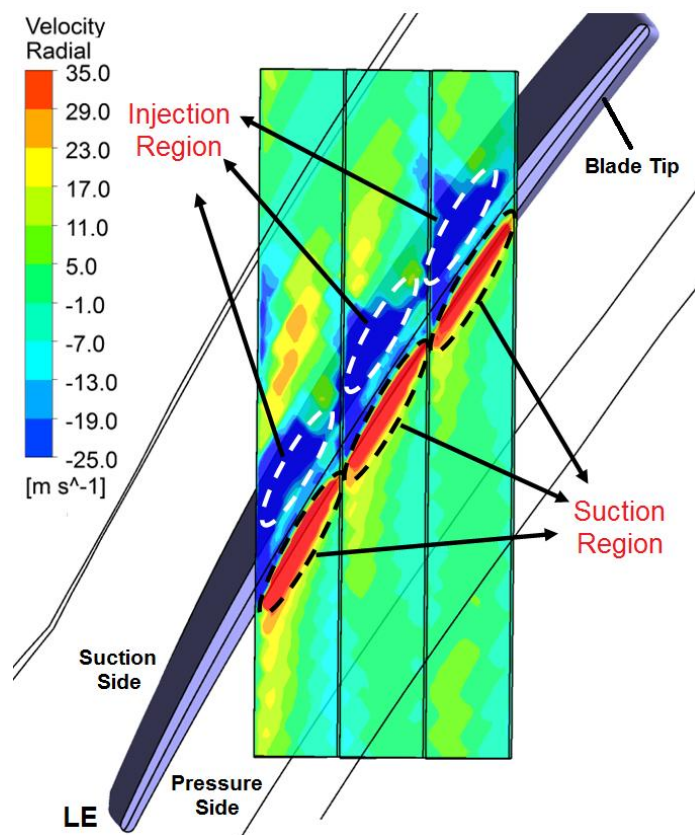
Figure B-4: Mass flow transfer regions (suction and injection) between the groove and rotor domains

Appendix C   Comparison of Turbulence Models

To assess the effect of turbulence model on tip sensitivity characteristics, simulations are also carried out for the BASE (smooth casing) configuration and nominal negative sawtooth casing indentation are simulated with the k-ε turbulence model at minimum and maximum tip clearance sizes. The boundary conditions are kept the same as in the initial simulations with the SST turbulence model. Figure C-1 presents the performance with respect to tip clearance size for the two turbulence model. The comparison shows that the main effect of changing the turbulence model is to shift the predicted performance parameters (pressure ratio and efficiency) without any significant effect on their rate of change with (i.e. sensitivity to) tip clearance size. One can thus conclude that the choice of turbulence model does not affect the main results of the study.
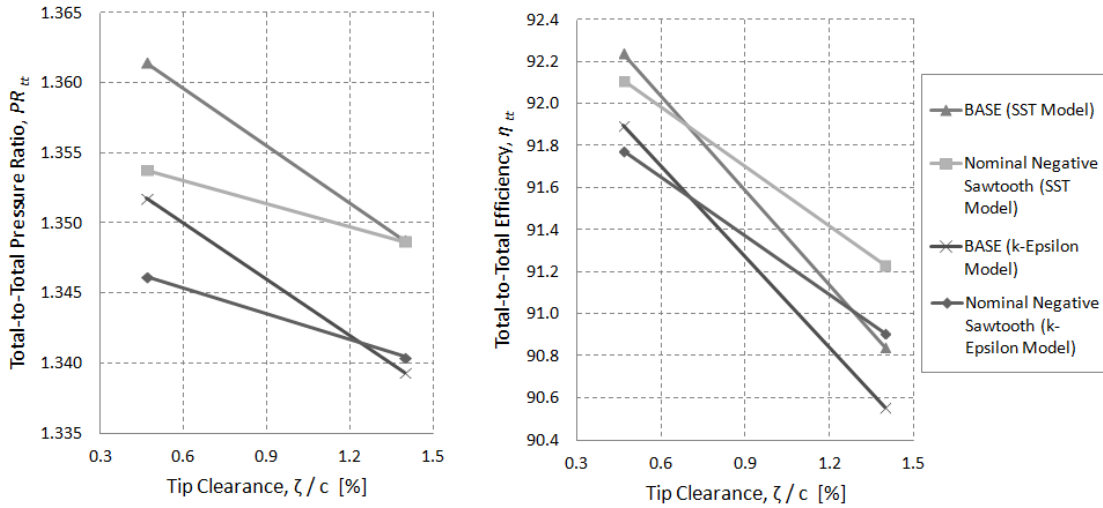

Figure C-1: Sensitivity comparison of the BASE rotor with the smooth casing and nominal negative sawtooth indentation, analyzed with SST and k- ε turbulence models

Appendix D   Mesh Convergence Study for BASE Design

Erler (2012) presented two mesh convergence studies, one for streamwise and the other for spanwise mesh density, by using NASA Rotor 37 blade profile. Convergence in both total-to-total pressure ratio and total-to-total efficiency was seek to decide on the mesh size. The simulated streamwise and spanwise mesh resolutions are given in Table D-1 and Table D-2. As shown in Figure D-1, the performance features converged at 82 nodes for streamwise mesh. For the spanwise mesh although the convergence was achieved for 50 nodes as shown in Figure D-2, 100 nodes was selected for conservatism to keep tip clearance mesh density high according to the recommendations of Van Zante et al. (2000). Based on these results, the mesh resolution was selected as 82 in streamwise, 70 in pitchwise and 100 nodes in spanwise direction, for nominal tip clearance of 0.4% chord.For higher top clearances, 110 spanwise nodes was used for 0.9% chord tip clearance and 120 spanwise nodes was used for 1.3% chord tip clearance.

Table D-1: Mesh resolutions for streamwise mesh convergence study

Direction	Number of Nodes			
Streamwise	48	66	82	98
Pitchwise	54	62	70	78
Spanwise	100	100	100	100
Total	$\sim 3 \times 10^5$	$\sim 4 \times 10^5$	$\sim 5 \times 10^5$	$\sim 7.5 \times 10^5$

Table D-2: Mesh resolutions for streamwise mesh convergence study

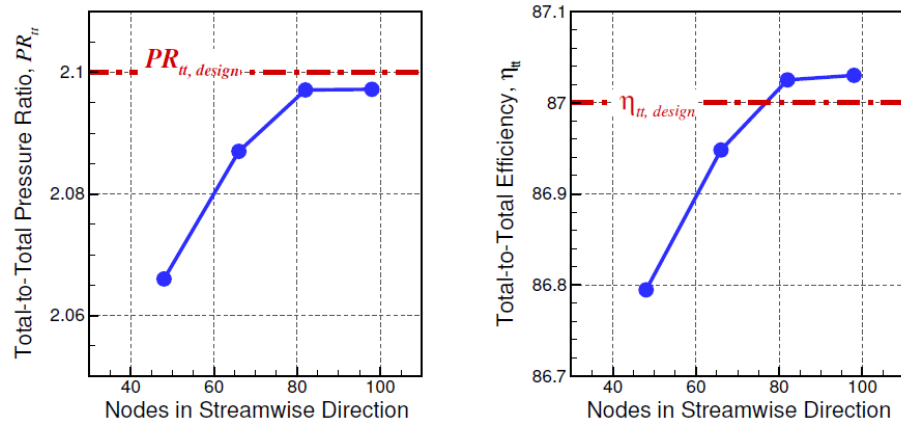| Direction	Number of Nodes			
Streamwise	82	82	82	82
Pitchwise	70	70	70	70
Spanwise	50	75	100	150
Total	$\sim 3 \times 10^5$	$\sim 4 \times 10^5$	$\sim 5 \times 10^5$	$\sim 7.5 \times 10^5$

Figure D-1: Rotor 37 streamwise mesh convergence of total-to-total pressure ratio and efficiency
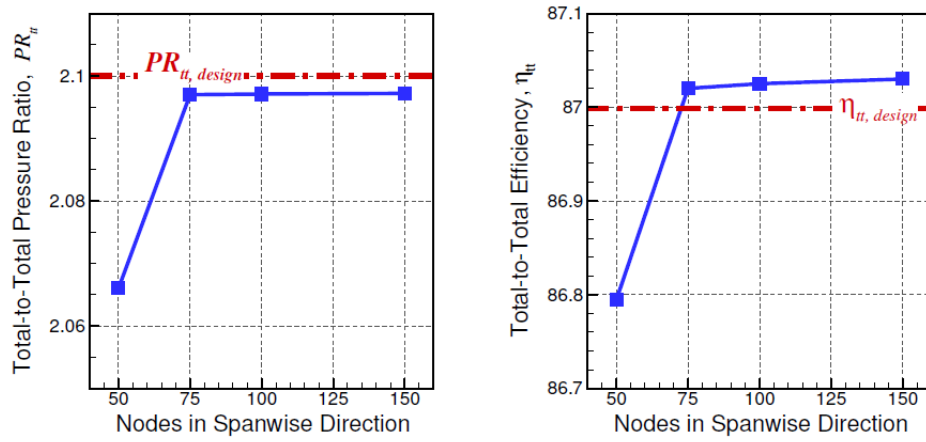

Figure D-2: Rotor 37 spanwise mesh convergence of total-to-total pressure ratio and efficiency

Appendix E   Results of the Unsteady Simulations of Nominal Casing Indentation

To evaluate the effect of unsteady simulations on the results and mechanism obtained from steady simulations, CFX simulations are carried out in transient mode for the nominal casing indentation configuration at minimum and maximum tip clearances. The boundary conditions are preserved but a sliding mesh interface is used between rotor and casing indentation domains instead of the frozen rotor interface used in steady simulations. Since the simulations are carried out at a stable operating point far from the stall point, a setting of ten time steps per blade pitch with ten sub-iterations is used. With the corresponding steady solution as initial condition for each run, convergence is achieved at about 1350 time steps with insignificant oscillation amplitudes in flow field variables (e.g. 0.002% of mean outlet pressure).

The comparison of predicted performance versus tip clearance in Figure E-1 between the steady and unsteady simulations of rotor with casing indentation and the steady simulation of smooth casing (BASE) rotor shows that the unsteady simulation predicts better nominal performance than that of the steady simulation. Although desensitization level is slightly less in unsteady simulation, it clearly presents the performance desensitization effect. A detailed look of the flow field in the tip region can explain this observation.
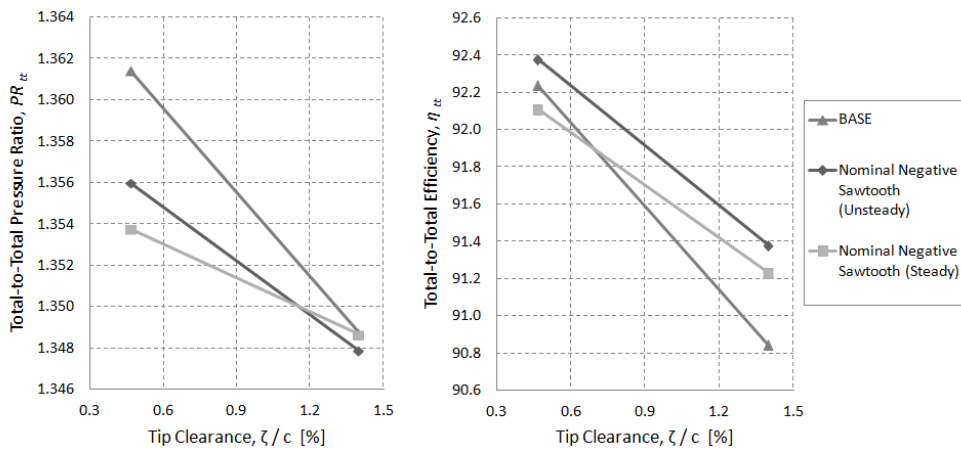

Figure E-1:   Comparison of the change of performance with tip clearance size for the smooth casing and nominal casing indentation with steady and unsteady simulations

The velocity contours at the shroud in Figure E-2 indicate that the mass flow transfer between pressure and suction side by the grooves is lower in the unsteady simulations. This is evident by the smaller suction (red - positive radial velocity) region near the blade pressure side and the smaller injection (blue - negative radial velocity) region near the blade suction side. It is noted that the large circumferential blue region in the mid passage along the first indentation as shown in the right plot of Figure E-2 for the unsteady simulations is due to local axial mass flow recirculation in the groove of mid-passage flow and not from mass transfer between the blade pressure and suction side. This is shown in Figure E-3(a), where this circumferential negative radial velocity (blue) region is immediately followed downstream by a circumferential (red) region of positive radial velocity. This is the evidence of a vortical structure flow recirculation as also shown by streamlines at different circumferential cuts in the grooves away from the blade as presented in Figure E-3(b).

However, if one looks at the flow field near the blade, as shown in Figures E-4 and E-5, the mechanism involving high entropy mass flow transfer between the pressure and suction side through the groove is present in both steady and unsteady simulations, with the latter case providing less mass flow transfer. A calculation of the amount of mass flow transfer according to the procedure, as laid out at the end of appendix B, indicates that the mass flow transfer in the unsteady simulations is about 65% lower than in the steady simulations. According to the mechanism proposed in section 4.1.2, increased mass flow transfer increases nominal loss but improves sensitivity reduction. This would explain the observed improved nominal performance and lower sensitivity reduction for the unsteady simulations versus steady simulations. Furthermore, the results from the parametric study involving groove depth in section 4.2.2 (Table 4-3 and Figure 4-27) indicate that the mass flow transfer level in the nominal groove configuration may be excessive and a shallower groove with much less mass transfer than the nominal indentation configuration achieved similar sensitivity reduction with higher nominal performance. This is perfectly consistent with the fact that the reduction in performance desensitization for the unsteady simulation for the nominal indentation configuration is rather small despite the large reduction in mass flow transfer compared to the steady simulation.

Based on the above results, one can conclude that unsteady simulations affect the absolute value of nominal performance and sensitivity reduction but not the observed trends nor the proposed mechanism behind the desensitization effect.
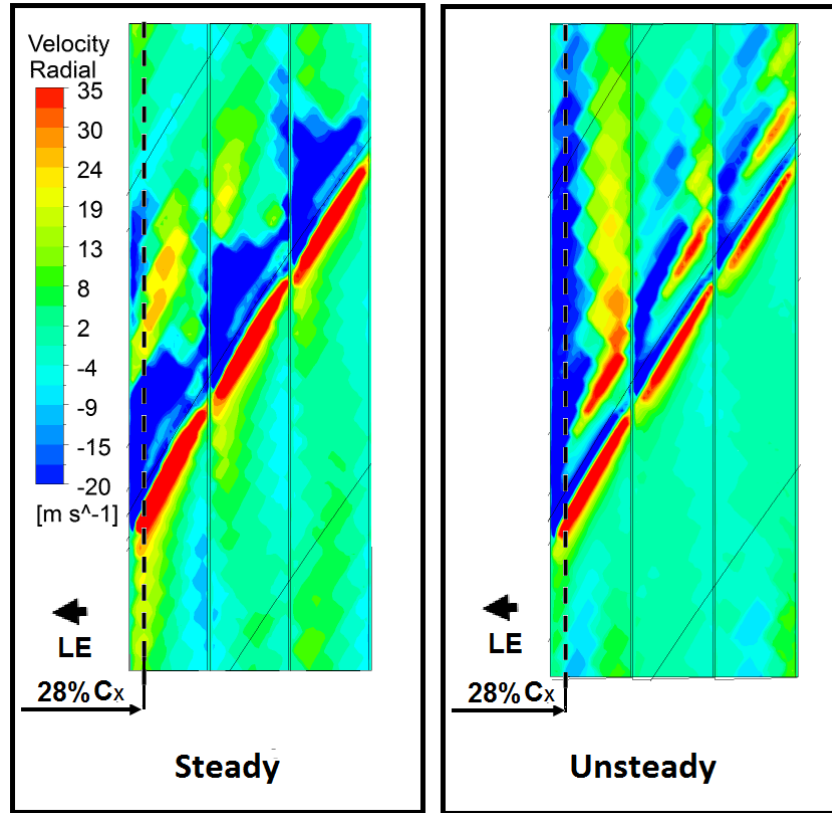
Figure E-2:   Radial velocity contours at shroud plane for nominal casing indentation at nominal tip clearance for steady and unsteady simulations
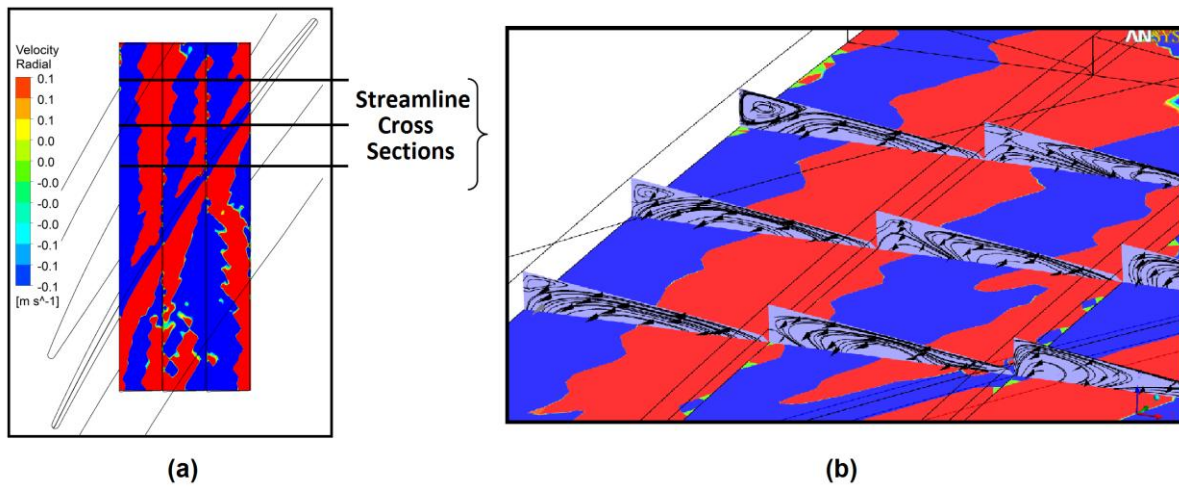

Figure E-3:   Radial velocity contours at the shroud plane of nominal casing indentation at nominal tip clearance size for unsteady simulation (a) from top view and (b) combined with streamlines
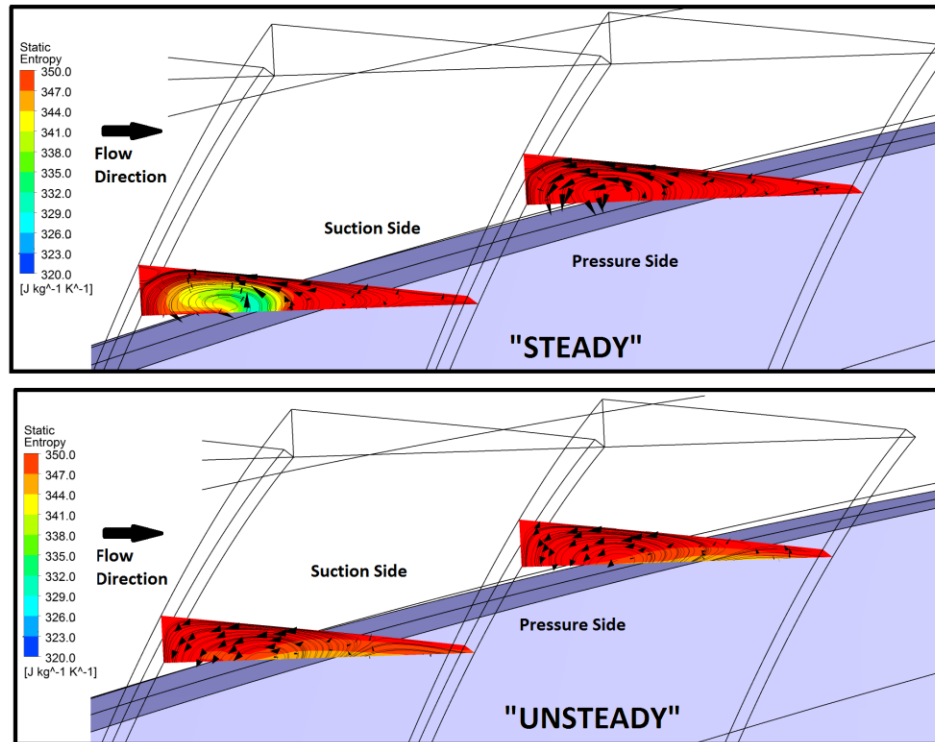
Figure E-4:   Entropy contours and streamlines showing transfer of high entropy fluid by the grooves from the pressure side to the suction side of blade tip for steady and unsteady simulations, at nominal tip clearance size
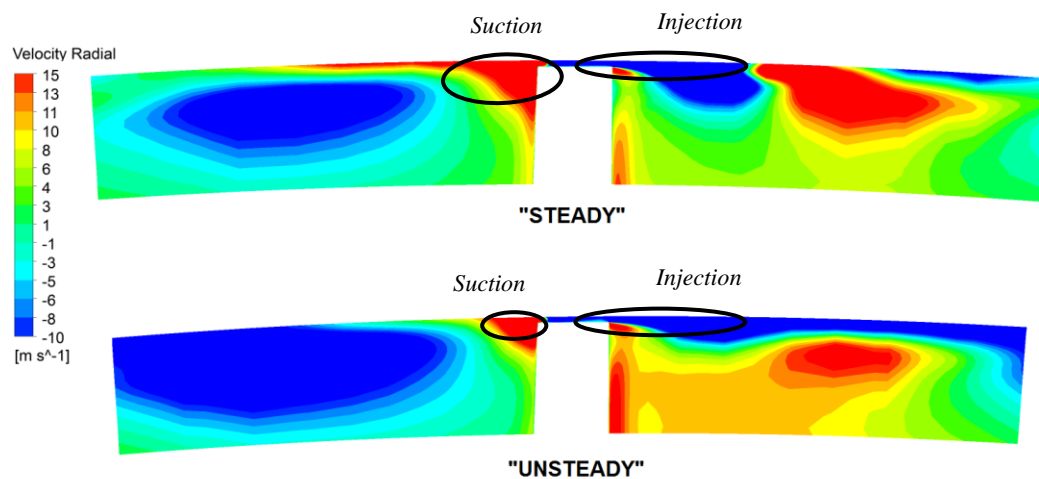
Figure E-5:   Radial velocity contours at the axial plane (28% C_x) shown by the dotted line in Figure E-2, for the steady and unsteady simulations at nominal tip clearance size

Appendix F   Performance and Stability Data of the Parametric Study

The plots of variation of performance and aerodynamic stability (i.e. interface location) with respect to tip clearance size, for the configurations simulated in parametric study, are presented from Figure F-1 to Figure F-5. The values are calculated at peak efficiency corrected mass flow rate (3.04 kg/s) of the smooth casing BASE rotor with nominal (i.e. minimum) tip clearance level (0.005 inch).
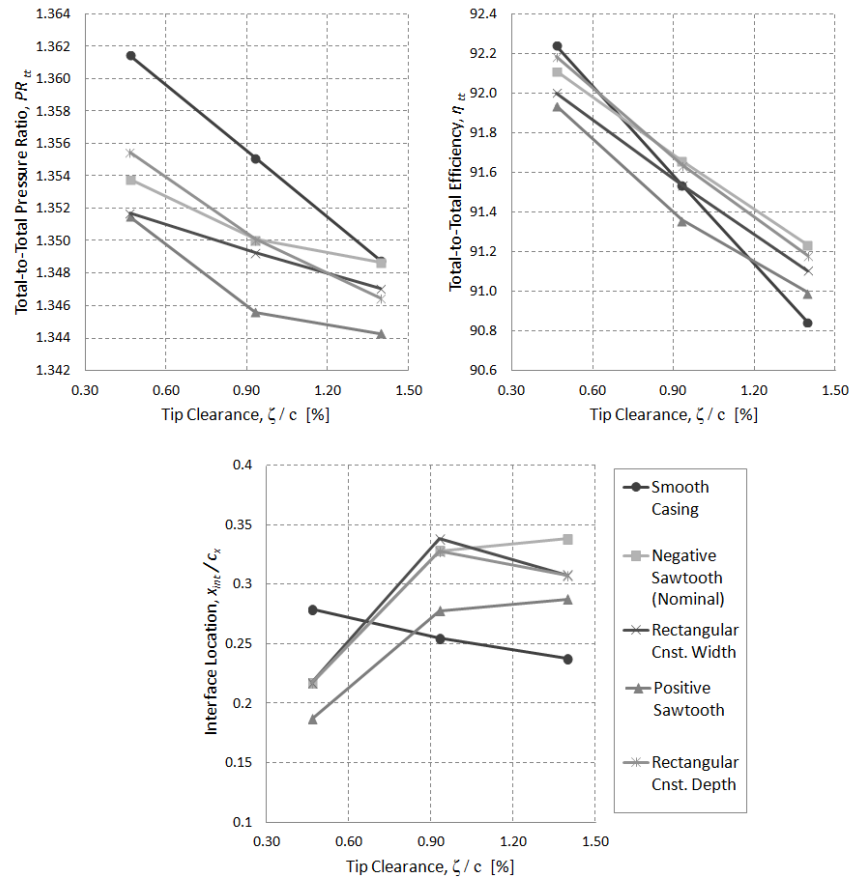

Figure F-1:   Change of performance and stability of the shape configurations with tip clearance size
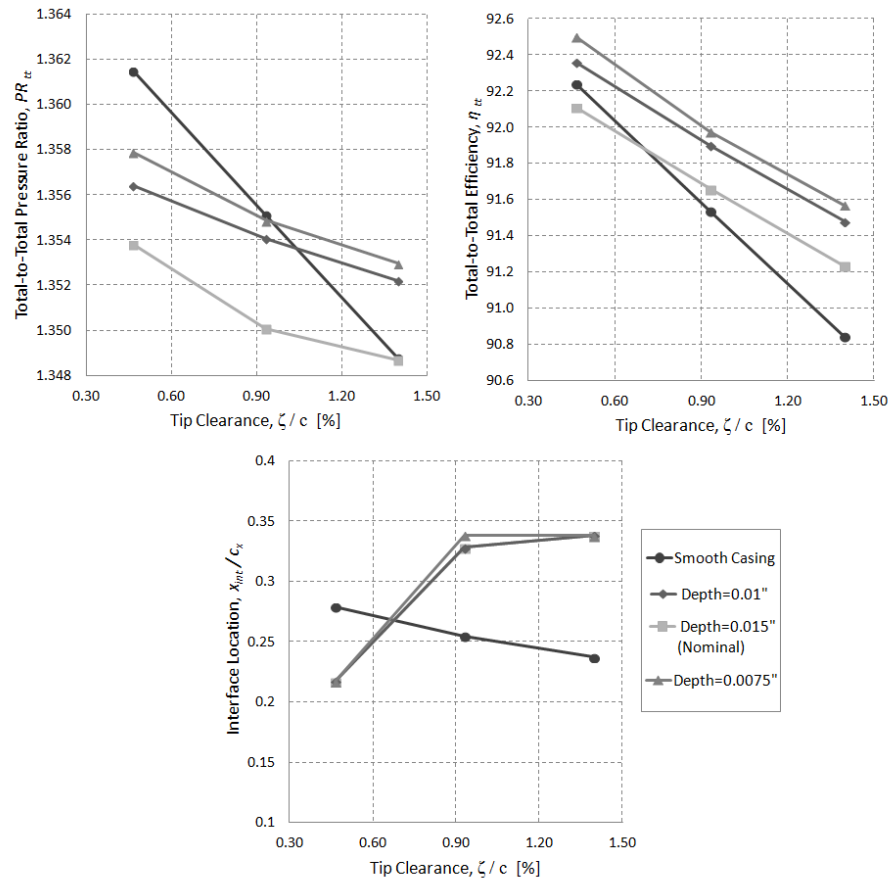
Figure F-2:   Change of performance and stability of the depth configurations with tip clearance size
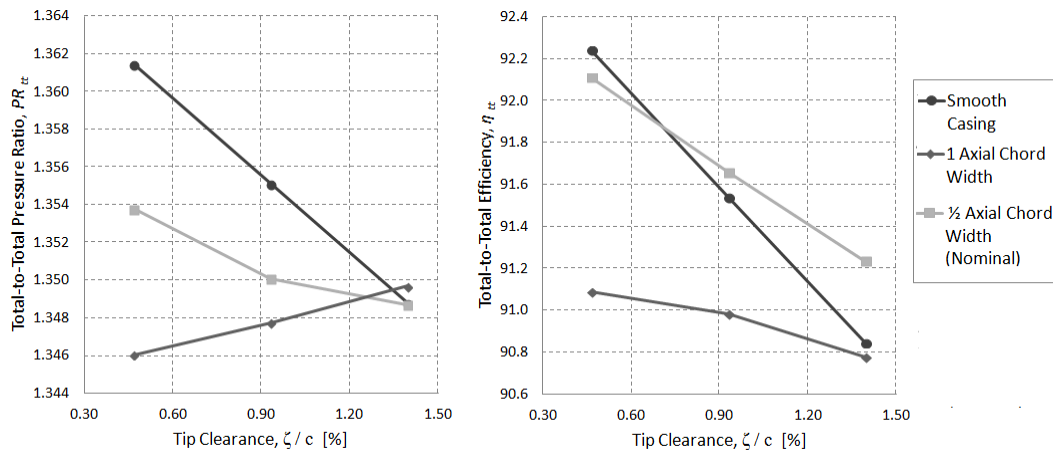

Figure F-3:   Change of performance of the indentation width configurations with tip clearance size
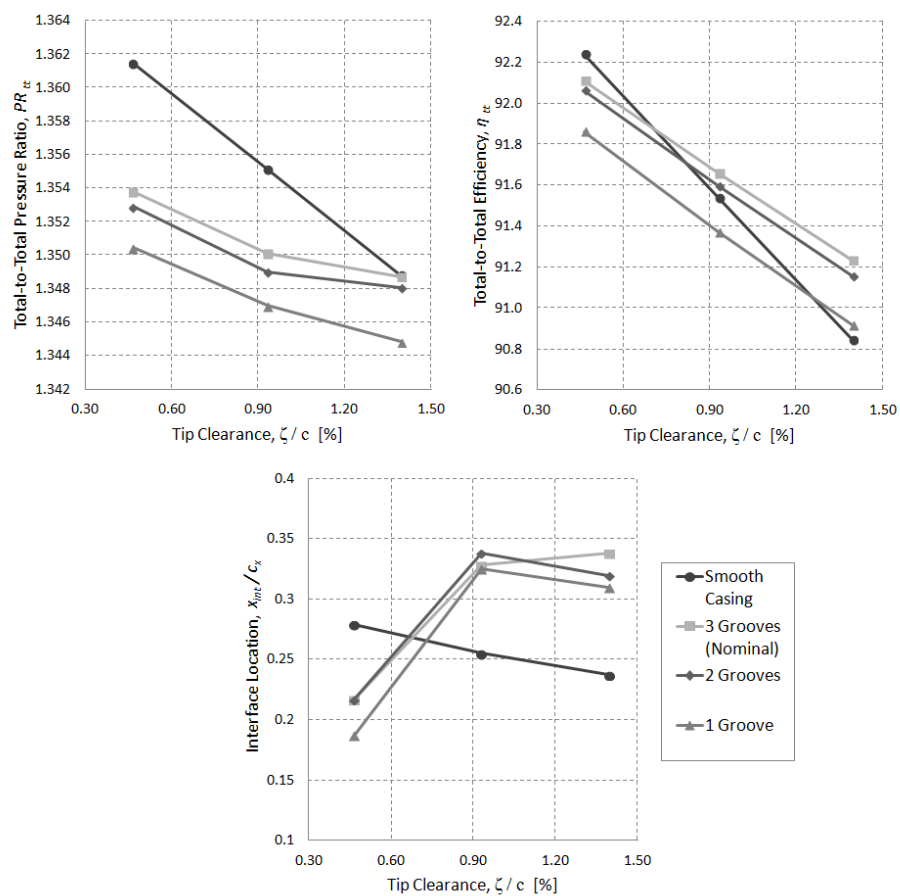
Figure F-4: Change of performance and stability of the groove number configurations with tip clearance size
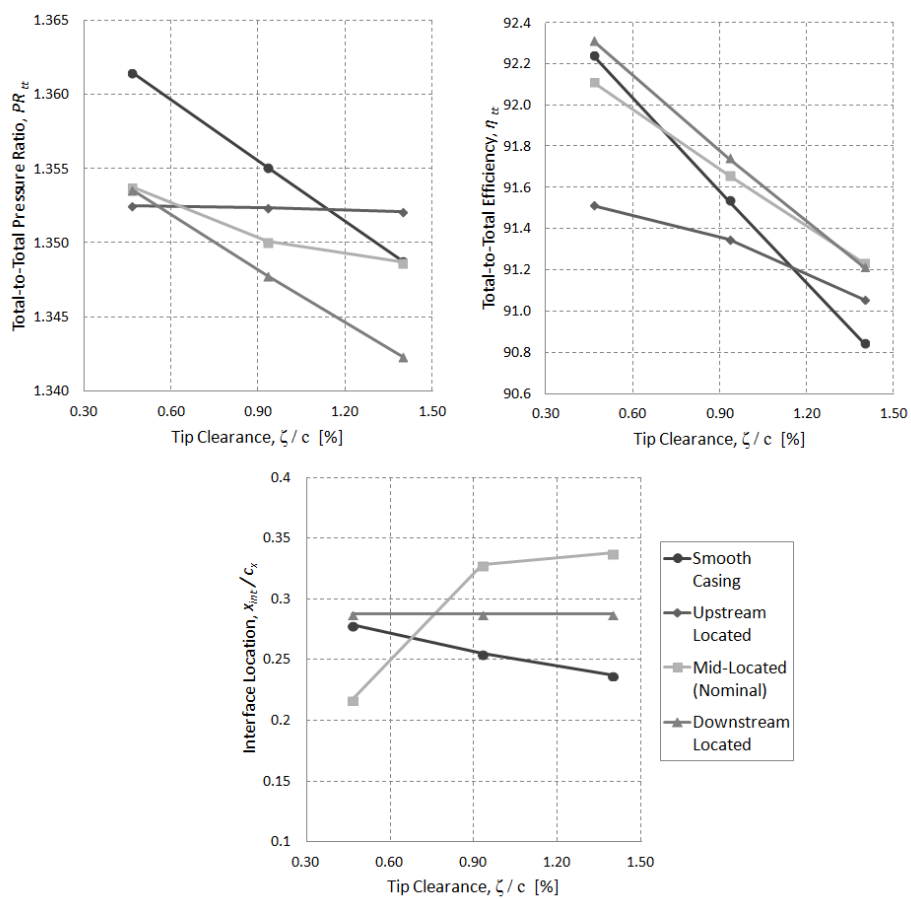
Figure F-5:   Change of performance and stability of the location configurations with tip
clearance size